Instituto de Investigaciones Químicas,
Instituto de Bioquímica Vegetal y Fotosíntesis,
cicCartuja, Universidad de Sevilla - CSIC

Phosphorylation of Cytochrome *c*: Functional and Structural Features

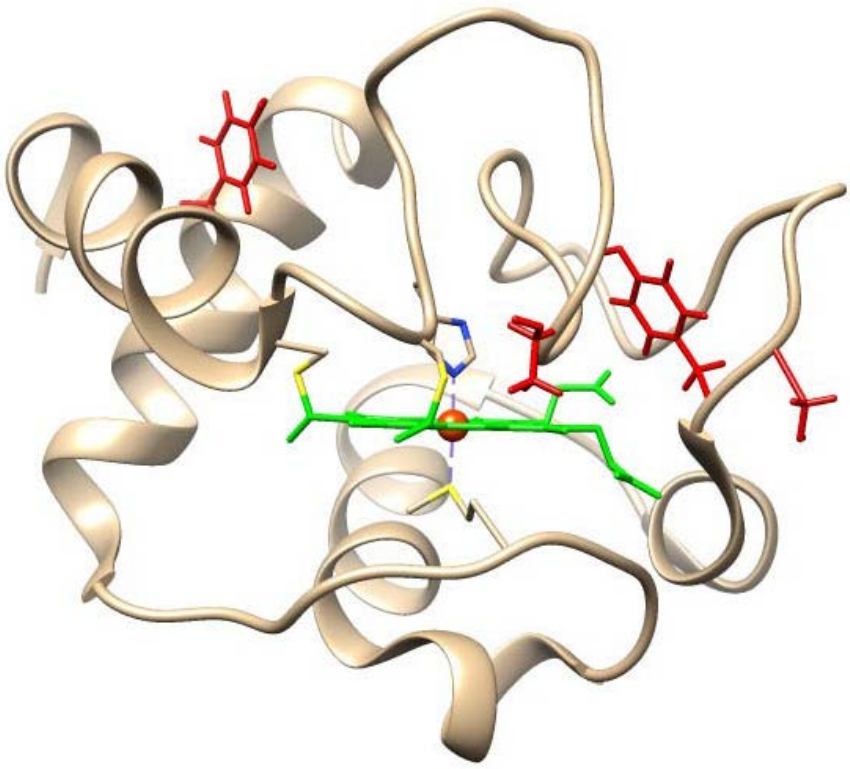

PhD Thesis

Alejandra Guerra Castellano

Instituto de Investigaciones Químicas
Instituto de Bioquímica Vegetal y Fotosíntesis
cicCartuja, Universidad de Sevilla – CSIC

PHOSPHORYLATION OF CYTOCHROME *c*:

FUNCTIONAL AND STRUCTURAL FEATURES

Memoria presentada por la licenciada **Dña. Alejandra Guerra Castellano**

para optar al título de Doctor por la Universidad de Sevilla.

Sevilla, 2016

Directores

Firmado digitalmente por Miguel A. De la Rosa
Nombre de reconocimiento (DN): cn=Miguel A. De la Rosa, o=Universidad de Sevilkla & CSIC, ou=cicCartuja, email=marosa@us.es, c=ES
Fecha: 2016.10.20 11:06:54 +01'00'

Dr. D. Miguel Ángel De la Rosa Acosta
Catedrático, Universidad de Sevilla

Digitally signed by DIAZ QUINTANA ANTONIO - 28712161L
Date: 2016.10.20 18:50:05 +02'00'

Dr. D. Antonio J. Díaz Quintana
Profesor Titular, Universidad de Sevilla

A los que están.

A los que estuvieron.

AGRADECIMIENTOS

En estas líneas me gustaría expresar mi más sincero agradecimiento a todos los que, de una manera u otra, han hecho posible la realización de esta tesis doctoral.

En particular, quiero agradecer a mis directores, Prof. Miguel Ángel De la Rosa y Dr. Antonio J. Díaz Quintana, el tiempo e interés que han dedicado a mi formación. A Miguel Ángel, que me abrió las puertas de su laboratorio y, a pesar de sus innumerables compromisos y obligaciones institucionales, siempre ha encontrado tiempo para comentar y discutir cuestiones científicas. Su organización, eficiencia y rigor científico son un ejemplo para mí. A Antonio, por las horas que ha pasado conmigo en el laboratorio (y en el despacho) dedicándose a sacar adelante este trabajo. Además de algunos de sus conocimientos, espero que me haya transmitido un poco de su amor por la Ciencia y su saber-cómo-tienen-que-ser las cosas.

Agradecer a las siguientes fuentes de financiación, que han permitido la ejecución de este trabajo:

Consejo Superior de Investigaciones Científicas (CSIC) – Beca JaePre017 Convocatoria 2011.

Junta de Andalucía – Proyecto Interactómica del apicoplasto (P11-CVI-7216).

Fundación Ramón Areces – Proyecto Bases moleculares de las enfermedades: Biointeractómica de la muerte celular programada.

Junta de Andalucia – Incentivos al grupo de investigación (BIO-198).

cicCartuja – Servivios generales y Plataforma de Biointeractómica (BIP).

Centro de Investigación Tecnología e Innovación de la Universidad de Sevilla (CITIUS) – Servicio de resonancia magnética nuclear.

Sociedad Española de Bioquímica y Biología Molecular (SEBBM); Grupo de Resonancia Magnética (GERMN) de la Real Sociedad Española de Química – Bolsas de viaje para la asistencia a cursos y congresos.

Gracias al grupo de Biointeractomica, que me acogió como miembro todos estos años. En primer lugar, quiero hacer una mención especial a la Dr. Irene Díaz Moreno porque sin su ayuda no hubiera llegado a esta meta. Agradecer sus palabras de ánimo, su apoyo en cada uno de los experimentos, ideas y tropiezos que he tenido en esta etapa, así como por todas esas horas que dedicó a discutir cada uno de los resultados que obtuve y a elaborar un plan de trabajo para dar respuesta a cada una de las cuestiones que aparecieron en este camino científico. Finalmente, gracias por su capacidad analítica, así como por ver más allá y mantener siempre viva mi avidez por nuevos retos científicos. Gracias a los que comenzaron siendo mis compañeros de laboratorio para pasar a formar parte de mi "familia sevillana". Gracias Isa y Blas por vuestros consejos "tesianos", en estos últimos meses han sido de gran ayuda. Gracias a las doctoras, Kati y Sofía, habéis sido y sois un pilar. Gracias a las dos por bajarme a la tierra cuando mis ideas iban más allá de lo científicamente posible (aunque he de decir que la mayoría dieron sus frutos). A Carlos y a Curro, que a partir de hoy pasáis a ser oficialmente Proto-Doc, disfrutad de cada momento, porque el final está más cerca que lo que imagináis. Tras estos agradecimientos científicamente formales, chicos, sin vosotros, nada hubiera sido igual. Carlos, gracias por tus montajes fotográficos que tantas carcajadas me han producido. Gracias Curro por salvarme del monstruo de la informática, sin ti mi ordenador hace tiempo no existiría. Sofía, gracias por la locura diaria del Lab5, por cada detalle que has tenido para que todos los días tuviera una sonrisa…y una canción que cantar. Y Kati, gracias por todas las charlas, risas, brindis y consejos que me has ido dando a lo largo de estos años, y espero siempre tener.

Gracias a todos los alumnos que han pasado por el laboratorio, no sólo aprendisteis vosotros, también me enseñasteis el duro arte de formar. Rafa, Antonio, Cristina, Paula, Eva y Alejandro: suerte, la ciencia es un mundo

maravilloso que os exigirá dar mucho de vosotros, pero compensa. No me olvido de la gran Claudia Sansone, ver como poco a poco (o más bien rápido) ibas amando cada vez más el trabajo de laboratorio fue muy gratificante. Espero volver a compartir laboratorio contigo.

Este trabajo no habría sido posible sin la colaboración estrecha de los siguientes investigadoes:

A los Dres. Pedro M. Nieto Mesa y Javier López Prados (Instituto de Investigaciones Químicas (IIQ), Universidad de Sevilla – CSIC) por su ayuda en la sístesis del aminoácido no canónico *p*-carboximetil-L-fenilalanina (*p*CMF).

Al Dr. Carlos Santos Ocaña (Centro Andaluz de Biología del Desarrollo (CABD), Universidad Pablo de Olavide – CSIC y CIBERER Instituto de Salud Carlos III), por darme la bienvenida al mundo de las levaduras y formarme en el análisis de los supercomplejos respiratorios.

Al Dr. Adrián Velázquez Campoy (Instituto de Biocomputación y Física de Sistemas Complejos (BIFI), Universidad de Zaragoza – CSIC; Instituto Aragones de Ciencias de la Salud a (IIS Aragon) y Fundacion ARAID, Gobierno de Aragón) y a los Profes. Peter Hildebrant (Technische Universität Berlin, Institut fìr Chemie) y Miguel Teixeira (Instituto de Tecnologia Química e Biológica António Xavier, Universidade Nova de Lisboa) por sus estudios de calorimetría isotérmica de valoración (ITC por su acrónimo en inglés), resonancia de Ramman y resonancia paramagnética electrónica (EPR por su acrónimo en inglés), respectivamente. Así como por sus discusiones científicas en sus respectivos campos.

A los Dres. Manuel Angulo Álvarez y Encarnación Zafra Rodríguez por su soporte en los equipos de resonancia del CITIUS.

Por último, agradecer a mi familia el apoyo incondicional, la confianza y la capacidad de superación que siempre me han transmitido. Gracias por el esfuerzo que habéis hecho por entender mi mundo científico, siendo una familia dedicada a las bellas artes, a la música y a la literatura (siempre seré

vuestra “científica loca”). Por todas las horas que he compartido con vosotros…con los apuntes bajo el brazo. Simplemente, sois quien me habéis hecho ser.

GRACIAS.

CONTENTS

1. FOREWORD

The current document has been prepared according to the guidelines of the University of Seville as regards submitting a PhD thesis as a collection of journal papers. Hence, the scientific statements herein comprise the following sections:

1. Abbreviations.
2. Publications and merits of the PhD candidate.
3. Summary.
4. Introduction and state-of-the-art.
5. Objectives.
6. Brief description of Results and a Discussion, highlighting main achievements and outcomes.
7. Conclusions.
8. References.
9. Appendix I, containing journal articles on which the PhD thesis is based. All were published in scientific journals indexed in Journal Citation reports (JCR) database.
10. Appendix II, containing a manuscript under submission addressing the effects of phosphorylation of cytochrome *c* at position 48.
11. Appendix III, corresponding to another manuscript in preparation that focuses on the characterization of a phosphomimetic mutant of cytochrome *c* at position 97.

2. ABBREVIATIONS

ANP32B	Acidic nuclear phosphoprotein 32B
Apaf-1	Apoptosis Protease Activation Factor-1
ATP	Adenosine triphosphate
BID	BH3-interacting domain death agonist
CARD	Caspase recruitment domain
CL	Cardiolipin
CI	Complex I
CII	Complex II
CII	Complex III
CIV	Complex IV
CV	Complex V
C*c*	Cytochrome *c*
Cc_1	Cytochrome c_1
C*c*O	Cytochrome *c* oxidase
CLT	Cytotoxic T lymphocytes
EPR	Electron paramagnetic resonance
ETC	Electron transport chain
EXAFS	Extended X-ray absorption fine structure
$FADH_2$	Reduced flavin adenine dinucleotide
Hig1	Hypoxia-induced gene 1
HIGD	Hypoxia inducible domain family
HIGD1A	HIG1 hypoxia inducible domain family 1A
HIGD2A	HIG1 hypoxia inducible domain family 2A
IMM	Inner mitochondrial membrane.
ITC	Isothermal titration calorimetry
K_D	Equilibrium dissociation constant
MD	Molecular dynamics
NADH	Reduced nicotinamide adenine dinucleotide
nBID	Amino terminal fragment of BID protein

NMR	Nuclear Magnetic Resonance
*p*CMF	*p*-carboxymethyl-L-phenylalanine
PTMs	Post-translational modifications
PCD	Programmed Cell Death
PDB	Protein Data Bank
PTR	Phosphotyrosine
PTK	Protein tyrosine kinases
Q	Coenzyme Q_{10}
Rcfs	Respiratory supercomplex factors
Rcf1	Respiratory supercomplex factor 1
Rcf2	Respiratory supercomplex factor 2
RIP1	Kinase activity of receptor-interacting protein 1
RIP3	Kinase activity of receptor-interacting protein 3
ROS	Reactive oxygen species
SEP	Phosphoserine
SET	SET nuclear oncogene
tBID	Truncate BID protein
TCA	Tricarboxylic acid
TPO	Phosphothreonine
TNF	Tumour necrosis factor
TNF1	Tumour necrosis factor receptor 1
WT	Wild-type
XAS	X-ray spectra absorption

3. LIST OF PUBLICATIONS

Publications and achievements of the PhD candidate are listed as follows:

1. Journal papers

1. Moreno-Beltrán B*, **Guerra-Castellano A***, Díaz-Quintana A, Del Conte R, M. García-Mauriño S, Díaz-Moreno S, González-Arzola K, Santos-Ocaña C, Velázquez-Campoy A, De la Rosa MA, Turano P and Díaz-Moreno I (2016) Structural basis of mitochondrial dysfunction in response to cytochrome *c* phosphorylation at tyrosine 48. *Submitted*.

2. **Guerra-Castellano A**, Díaz-Moreno I, Velázquez-Campoy A, De la Rosa MA and Díaz-Quintana A (2016) Structural and functional characterization of phosphomimetic mutants of cytochrome *c* at threonine 28 and serine 47. *Biochim Biophys Acta – Bioenerg* **1857**, 387-395.
   Impact Factor 2015: 5.353

3. **Guerra-Castellano A**, Díaz-Quintana A, Moreno-Beltrán B, López-Prados J, Nieto PM, Meister W, Staffa J, Teixeira M, Hildebrandt P, De la Rosa MA and Díaz-Moreno I (2015) Mimicking tyrosine phosphorylation in human cytochrome *c* by the evolved tRNA synthetase technique. *Chem Eur J* **21**, 15004-15012.
   Impact Factor 2014/2015: 5.731

4. Moreno-Beltrán B Díaz-Moreno I, González-Arzola K, **Guerra-Castellano A**, Velázquez-Campoy A, De la Rosa MA and Díaz-Quintana A (2015) Respiratory complexes III and IV can each bind two molecules of cytochrome *c* at low ionic strength. *FEBS Lett* **589**, 476-483.
   Impact Factor 2014/2015: 3.169

2. Proceedings

1. Muñoz García-Mauriño S, Sansone C, Cruz-Gallardo I, **Guerra-Castellano A**, Díaz-Quintana A and Díaz-Moreno I (2015)

Oligomerization and phosphorylation of RNA binding proteins in the assembly of stress granules. *FEBS J* **282**, 211.
Impact Factor: 4.001

2. **Guerra-Castellano A**, Moreno-Beltrán B, López-Prados J, Rivero-Rodríguez F, Nieto PM, Velázquez-Campoy A, Díaz-Quintana A, De la Rosa MA and Díaz-Moreno I (2014) Structure, dynamics and function of phosphomimetic mutants of respiratory cytochrome *c*. *FEBS J* **281**, 362.
Impact Factor: 4.001

3. Díaz-Moreno I, Moreno-Beltrán B, **Guerra-Castellano A**, González-Arzola A, García-Heredia JM, Velázquez A, Nieto PM, Ubbink M, Díaz- Quintana A and De la Rosa MA (2013) How redox proteins form transient complexes in photosynthesis and respiration. *Eur Biophys J* **42**, S37.
Impact Factor: 2.474

4. **Guerra-Castellano A**, García-Heredia JM, Díaz-Quintana A, López-Prado J, Nieto PM, Moreno-Beltrán B, De la Rosa MA and Díaz-Moreno I (2012) Construction of a mimetic mutant of cytochrome *c* phosphorylated at tyrosine 48 to further study its biological role in the transition from cell life to death. *FEBS J* **279**, 413. Impact Factor: 4.25

3. Book chapters

1. Rodríguez Morgado B, Gelabert Ramos D, **Guerra Castellano A**, Montes Ramos P, Rodríguez Lumbreras L, García Martínez AM, Tejada Moral M and Parrado Rubio J (2010) Aplicación de ácido láctico en suelo: Influencia en propiedades bioquímicas y biológicas in Congreso ibérico de la ciencia del suelo. Suelo: Funciones y manejo. p. 1059-1071. Copicentro, Granada (España) ISBN: 978 84-15026-39-6

4. Oral communications

1. Functional and structural implications of phosphorylated cytochrome *c*.
   Guerra-Castellano A, Díaz-Quintana A, Moreno-Beltrán B, Velázquez-Campoy A, López-Prados J, Nieto PM, De la Rosa MA and Díaz-Moreno I.
   41st FEBS Congress. Molecular and Systems Biology for a Better Life. September 3th-8th, 2016. Ephesus/Kusadasi (Turkey). (The Congress was cancelled by FEBS one month ahead.)

2. Structural and functional characterization of phosphomimetic mutants of cytochrome *c* at threonine 28 and serine 47.
   Guerra-Castellano A, Díaz-Moreno I, Velázquez-Campoy A, De la Rosa MA and Díaz-Quintana A.
   FEBS/IUBMB Workshop on Biointeractomics: From Bimolecular Interactions to Networks. May 17th-20th, 2016. Sevilla (Spain).

3. Mimicking tyrosine phosphorylation in human cytochrome *c* by the evolved tRNA synthetase technique.
   Guerra-Castellano A, Díaz-Quintana A, Moreno-Beltrán B, López-Prados J, Nieto PM, Meister W, Staffa J, Teixeira M, Hildebrandt P, De la Rosa MA and Díaz-Moreno I.
   IX Meeting of the Protein Structure and Function Spanish Network. November 11th-13th, 2015. Sevilla (Spain).

4. Effect of phosphorylation of Thr28 and Ser47 residues of cytochrome *c* in its double role in the cell.
   Guerra-Castellano A, Moreno-Beltrán B, Velázquez-Campoy A, Díaz-Quintana A, De la Rosa Acosta MA and Díaz-Moreno I.
   INSTRUCT FRISBI PSB Workshop on Molecular interactions: the complementarity between biophysical methods. June 1st-5th, 2015. Grenoble (France).

5. Structural changes of cytochrome *c* upon phosphorylation explain differences in functional properties.

Guerra-Castellano A, García-Heredia JM, Díaz-Quintana A, López-Prado J, Nieto PM, Moreno-Beltrán B, De la Rosa MA and Díaz-Moreno I.
Summer School: Chemistry of Metals in Biology Systems Systems. May 12th-19th, 2013. Louvain-la-Neuve (Belgium).

5. International research training

1. INSTRUCT FRISBI PSB Workshop on Molecular interactions: the complementarity between biophysical methods. EPN campus Grenoble. Grenoble (France). June 1st-5th, 2015.
   Course tutors and organizers: Dr. Christine Ebel (IBS), Dr. Alain Le Roy (IBS), Prof. Marc Jamin (UVHCI), Dr. Nicole Thielens (IBS), Dr. Jean-Baptiste Reiser (IBS), Dr. Andrés Palencia (ISBG), Dr. Florent Bernaudat (PSB) and Dr. Catherine Birck (IGBMC Strasbourg).

2. Structural studies of X-ray absorption. Diamond Light Source Synchrotron. Campus Harwell Science & Innovation. Oxford (United Kingdom). November 16th-21th, 2012.
   Supervisor: Dr. Sofía Díaz-Moreno.

3. Summer School: Chemistry of Metals in Biology Systems Systems.. Louvain-la-Neuve (Belgium). May 12th-19th, 2013.
   Co-organizers: Prof. Robert R. Crichton, Dr. Ridardo O. Louro, Prof. Roland Sigel.

6. Bursaries and Awards

1. 16th FEBS Young Scientists' Forum Awards 2016.

2. Training school Grant, COST Action CM1003-120513-025785. 2013

3. Graduated Research PhD Fellowship of Spanish Research Council (JAEPre017). 2011.

4. SUMMARY

Post-translational modifications often modulate protein function. Actually, phosphorylation of cytochrome *c* occurs *in vivo* at threonine 28, serine 47 and tyrosines 48 and 97. Phosphorylation of the two latters, in particular, is related to a wide range of human diseases as cytochrome *c* plays a pleiotropic role serving as an electron carrier in the respiratory electron transfer and acting as a cell death signal at the onset of apoptosis. The effect that phosphorylation of threonine 28 and serine 47 bears on the physiological functions of this protein remains concealed.

The low yield of phosphorylated cytochrome *c* purification from cell extracts makes its analysis challenging. Also the specific kinases acting on the protein remain unknown. Hence, it has resorted to mutations to mimic targeted phosphorylation. Here, we have replaced threonine 28 and serine 47 by aspartate. And the analysis of tyrosine 48 and 97 phosphorylation has been performed by using the non-canonical amino acid *p*-carboxymethyl-L-phenylalanine (*p*CMF), which is a close phosphorylation mimic of tyrosine.

Noteworthy, the Y48*p*CMF mutation significantly lowers the value for the alkaline transition pK_a of oxidized cytochrome *c*. The negative charges at positions 28 and 48 cause a decrease in the midpoint redox potential value of 30 mV and 60 mV, respectively, and lower the affinity towards the *distal site* of cytochrome c_1 in complex III. However, the phosphomimic variants at position 28, 47 and 48 are more efficient as electron donors to cytochrome *c* oxidase than the wild-type species. Concerning the role of cytochrome *c* in programmed cell death, negative charges at positions 48 and 97 hinder its ability to triger caspase-3 activation. In addition, any modification of residue 47 affects the pro-apoptotic function of cytochrome *c*.

In summary, phosphorylation of cytochrome *c* modulates its distinct functions depending on the targeted residue, and can thus be the basis to understand an ample set of molecular diseases.

5. INTRODUCTION

5.1 Post-translational modifications

Post-translational modifications (PTMs) constitute an excellent mechanism to increase the functional diversity of proteins. These changes occur after ribosomal RNA translation and include covalent addition of complex molecules, chemical groups, proteins/peptides, cleavage and amino acid modification (**Figure 1**). PTMs are present in both, eukaryotes and prokaryotes. However, they are less common in the last, and mostly being of a different nature (Szymanski and Wren, 2005; Dell *et al*., 2010). PTMs are one of the most important gears for cell metabolism modulation. Indeed, they are involved in the regulation of gene expression, signal transduction, protein-protein interaction, cell-cell interaction and communication between the intracellular and extracellular environment (Deribe *et al*., 2010). Protein PTM flaws are related to several developmental disorders and human diseases (Wang *et al*., 2014).

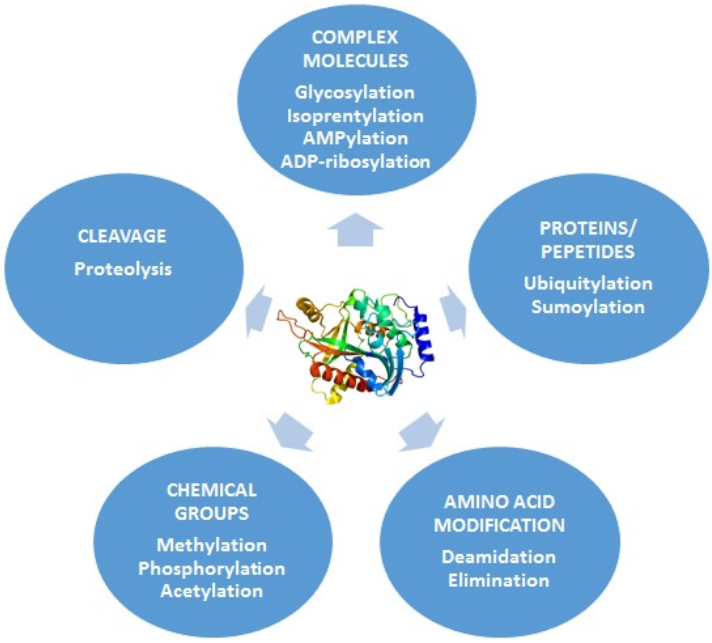

Figure 1. PTMs mechanisms presented in cell.

5.1.1 Phosphorylation

Phosphorylation has been termed 'the PTM of choice' for cell signal transduction systems because it provides a rapid and accurate transmission from cell-surface receptors to the nucleus. Protein phosphorylation consists in the addition of a phosphate group through an ester bond, generally by a kinase.

The residues that are preferably phosphorylated are serine, threonine and tyrosine in a 1000:100:1 ratio, respectively. Tyrosine phosphorylation is the most frequent in intercellular signaling and regulation despite showing the lowest ratio (Hunter, 2009). The reason is the successful evolution of phosphotyrosine (PTR)-binding domains in combination with most protein tyrosine kinases (PTK) substrates having a very low basal level of tyrosine phosphorylation, essential for a signaling system (Liu and Nash, 2012). Furthermore, the aromatic side chain of PTR affords a significantly greater binding energy than the aliphatic side chain of phosphoserine (SEP) or phosphothreonine (TPO) because the phosphate on tyrosine is linked to the O4 position of the phenolic ring, which it lies much further away from the peptide backbone than the phosphate on the β-OH groups of serine and threonine.

Tyrosine kinases are critical mediators of intracellular signaling and intracellular responses to extracellular signaling. Perturbations in tyrosine phosphorylation underlie many human diseases in particular, cancer and neurodegenerative diseases associated with microtubule-associated protein Tau (Sefton *et al*., 1980; Bhaskar *et al*., 2010; Ingley, 2012).

Histidine, arginine and lysine residues also may undergo phosphorylation (Cieśla *et al.*, 2011). In fact, histidine phosphorylation forms a regulatory mechanism in prokaryotes and occurs to the extent of 6% of total in higher eukarya; but it is chemically unstable (Puttick *et al*., 2008).

This work is focused on the regulatory role of SEP, TPO and PTR in the transient interactions mediated by cytochrome *c*, a moonlighting protein.

5.2 Transient protein-protein redox interactions

Protein-protein interactions play an essential role in cell metabolism. These interactions can be classified by their composition (homo- and hetero-oligomeric complexes), affinity (non-obligate and obligate complexes) and life time (transient and permanent complexes) (Nooren and Thornton, 2003).

Transient interactions can be further subdivided into strong and weak complexes. Strong transient interactions are stabilized by binding of an effector molecule and have a dissociation constant (K_D) in the nanomolar range. On the other hand, weak transient interactions are characterized by a K_D in the micromolar range and lifetimes of seconds (Perkins *et al*., 2010).

Electron transfer complexes are excellent examples of weak transient interactions, where high turnover rates is required and the lifetimes are even shorter than seconds (Drepper *et al*., 1997; Czapla *et al*., 2013). In addition, electron carriers display a certain degree of "promiscuity" due to their surfaces being often recognized by multiple partners (Schreiber and Keating 2011; Cruz-Gallardo *et al*., 2012). However, their redox centers are usually close to a hydrophobic patch that optimizes the electron transfer between redox partners (Crowley *et al*., 2001; Nogués *et al*., 2003; Díaz-Moreno *et al*., 2005; Monari *et al.*, 2012). Post-translational modifications can affect the redox centers or the interaction surfaces of proteins (Ly *et al*., 2012).

5.3 Cellular respiration

Cellular respiration encompasses the processes that lead to the production of energy, in form of adenosine 5'-triphosphate (ATP) (**Figure 2a**). Two types of cellular respiration are described according to the

presence of oxygen: aerobic - if oxygen is present - and anaerobic. In eukaryotic cells, respiration is carried out in the cytoplasm and mitochondria. Mitochondria generate most of the chemical energy in aerobic cells using the end product of glycolysis (pyruvate) for the reactions of the tricarboxylic acid (TCA) cycle in their matrix and, later, through the oxidative phosphorylation, which occurs in the inner mitochondrial membrane (**Figure 2b**).

Oxidative phosphorylation relies on the electron transport chain (ETC), and it is the last step in aerobic respiration (Hatefi, 2015). The oxidation of metabolites in TCA cycle yields molecules containing highly energetic electrons, responsible for electron-motive force. In the ETC, the electron-motive force is transduced into the proton-motive force that leads to generation of ATP. The ETC comprises four transmembrane complexes: complex I (CI; NADH-Q oxidoreductase), complex II (CII; succinate-Q reductase), complex III (CIII; Q-cytochrome *c* oxidoreductase), and complex IV (CIV; cytochrome *c* oxidase). In addition, ETC can be complemented with auxiliary enzymes, such as the electron-transferring flavoprotein Q oxidoreductase, glycerophosphate dehydrogenase and dihydroorotate dehydrogenase (Lenaz and Genova, 2010). The electron flow across the ETC is coupled to the transport of protons across the inner mitochondrial membrane, except within complex II, which is not a proton pump. Electrons from reduced nicotinamide adenine dinucleotide (NADH) are transferred to CI, and subsequently to CIII by the reduced form of coenzyme Q_{10} (Q), a hydrophobic quinone that diffuses rapidly within the inner mitochondrial membrane. CII is an auxiliary complex which connects the TCA cycle with ETC, transferring electrons from reduced flavin adenine dinucleotide ($FADH_2$) generated upon succinate oxidation to Q. Cytochrome *c* (C*c*), a small soluble heme protein, shuttles electrons from CIII to CIV, the final component in the chain and the one that catalyzes the reduction of O_2 (**Figure 2**).

The proper working and regulation of the mitochondrial ETC is essential for energy production and cell detoxification. Consequently, its

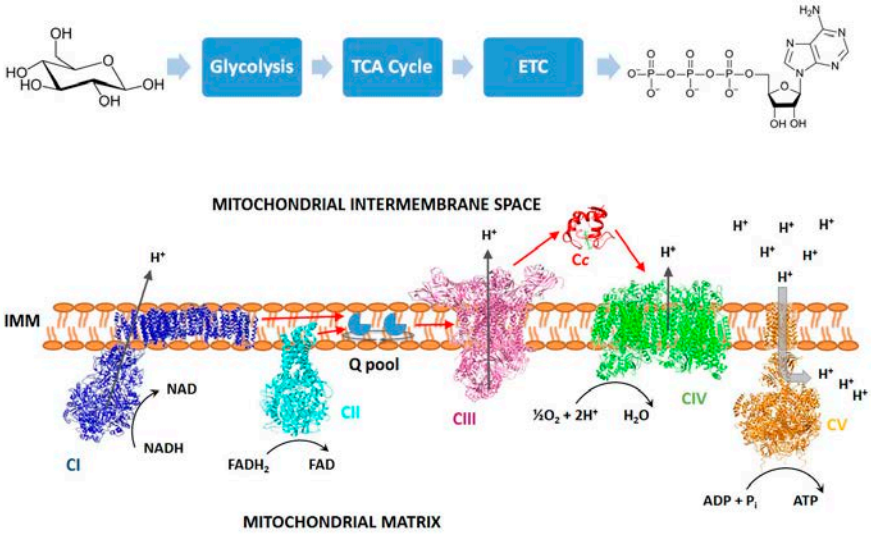

malfunction is related to several mitochondrial diseases and aging (Storz, 2007; Gao *et al*., 2008; Liesa and Shirihai, 2013)

Figure 2. **Cellular respiration and oxidative phosphorylation process**. **a**) Respiration is an important cellular process that uses glucose and oxygen to create adenosine triphosphate (ATP), the cell main energy source. **b**) Oxidative phosphorylation. Five protein transmembrane complexes are involved in this process: The complex I (CI), complex II (CII), complex III (CIII), complex IV (CIV), and complex V (IV). Coenzyme Q_{10} (Q) and cytochrome *c* (C*c*) shuttle electrons from CI to CIII and from CIII to CIV, respectively. IMM: Inner mitochondrial membrane.

5.3.1 Respiratory supercomplexes

The organization and dynamics of the protein components of the ETC is a matter of debate (Genova *et al*., 2008). Three models have been proposed to explain their behaviour in the membrane (**Figure 3**). On one hand, the fluid model proposes that diffusional motions of the distinct membrane protein components are free and independent (Hackenbrock

et al., 1986). In contrast, the solid model claims the existence of mitochondrial supercomplexes, assemblies formed by the stable association between respiratory complexes CI, CII, CIII and CIV (Chance and Williams, 1955; Yu and Yu, 1980; Hochman *et al*., 1985; Lenaz and Genova, 2012; Lapuente-Brun *et al*., 2013). The assemblage of mitochondrial supercomplexes is strictly dependent on metabolic needs (Ramírez-Aguilar *et al*., 2011). Finally, the plasticity model consists on a balanced distribution between free respiratory complexes and supercomplexes (Acín-Pérez *et al*., 2008; Acín-Perez and Enriquez, 2014).

Supercomplex formation occurs in animals, plants, fungi and bacteria (Berry and Trumpower, 1985; Schägger and Pfeiffer, 2000; Eubel *et al*., 2004; Krause *et al*., 2004a). Most supercomplexes comprise CI, CII, CIII and CIV, except in the specific case of *Saccharomyces cerevisiae*, where supercomplexes lack CI (Schägger, 2002; Krause *et al*., 2004b; Acín-Pérez *et al*., 2008). Supercomplexes containing CI to CIV are also named respirasomes, since they can transfer directly electrons from NADH to oxygen (Schägger and Pfeiffer, 2000; Dudkina *et al*., 2011). Respiratory supercomplexes provide efficiency to the electron transport during the oxidative phosphorylation, thereby minimizing the generation of reactive oxygen species (ROS) (Genova and Lenaz, 2014).

Respiratory supercomplex factors (Rcfs), which are proteins that mediate the association of the ETC complexes under hypoxia, have been described in mammals and yeasts. In yeast, these factors are respiratory supercomplex factor 1 (Rcf1, formerly Aim31) and respiratory supercomplex factor 2 (Rcf2, formerly Aim38), both being members of the conserved hypoxia-induced gene 1 (Hig1) protein family. They mediate the formation of the CIII/CIV supercomplex (Strogolova *et al*., 2012; Vukotic *et al*., 2012). Rcf1 has two human orthologous: the HIG1 hypoxia inducible domain family 1A (HIGD1A) and the HIG1 hypoxia inducible domain family 2A (HIGD2A) (Shoubridge, 2012). HIGD2A is necessary for the assembly of the C1/CIII2/CIV supercomplex (Chen *et al*., 2012). HIGD1a is a positively regulator of cytochrome *c* oxidase (C*c*O), and plays a role in the modulation of cell survival and tumor growth

(Ameri *et al*., 2015; Hayashi *et al*., 2015). In addition, some studies suggest a putative stabilization of CI/CIII and CIII/CIV supercomplexes by the mobile carriers Q and C*c*, respectively (Acín-Pérez *et al*., 2008; Enriquez and Lenaz, 2014).

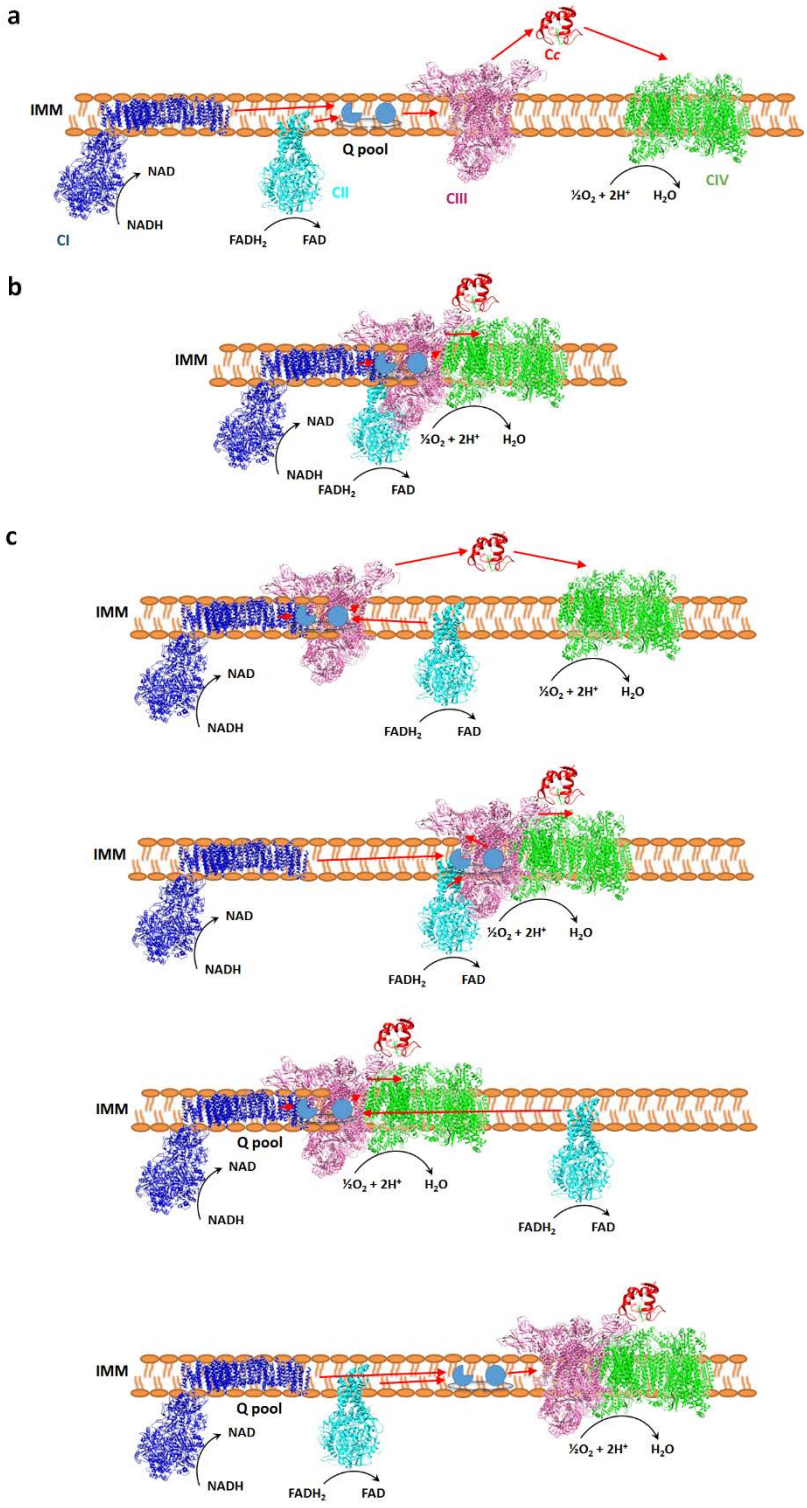
a
IMM
Cc
Q pool
NAD
NADH
CI
CII
CIII
CIV
FADH2
FAD
½O2 + 2H+
H2O
b
IMM
NAD
NADH
FADH2
FAD
½O2 + 2H+
H2O
c
IMM
NAD
NADH
FADH2
FAD
½O2 + 2H+
H2O
IMM
NAD
NADH
FADH2
FAD
½O2 + 2H+
H2O
IMM
Q pool
NAD
NADH
½O2 + 2H+
H2O
FADH2
FAD
IMM
Q pool
NAD
NADH
FADH2
FAD
½O2 + 2H+
H2O

Figure 3. **Schematic representation of models for the organization of respiratory complexes organization**. **a**) Fluid **b**) solid and **c**) plasticity models. For the plasticity model, all supercomplexes that are described in the literature are represented.

5.4 Cytochrome *c*

Cytochrome *c* (C*c*) is a small soluble heme protein (*ca.* 12 kDa, 104 amino acids) located in the mitochondrial intermembrane space under homestotatic conditions (Delivani and Martin, 2006). C*c* has a globular structure with four α-helices and a heme group, which is covalently bound by Cys14 and Cys17 (**Figure 4a**). The heme group is wrapped within a hydrophobic pocket, though part of the cofactor is exposed to the solvent (**Figure 4b**). This conformation allows the electron transfer between C*c* and its redox partners.

The iron ion of heme group is essential for the activity of C*c* and shows two redox forms in the native protein, a ferric (Fe^{III}) oxidized state and a ferrous one (Fe^{II}) (Rackovsky and Goldstein, 1984; Brown and Borutaite, 2008). At physiological pH values, the heme iron ion is hexacoordinated, with His18 and Met80 providing the axial ligands (Banci *et al*., 1997). For the oxidized form, at least five distinct configurations can exist within the range of pH values from 1 to 12. These result from changes in heme axial coordination and/or in protein folding (Boffi *et al*., 2001, Ying *et al*., 2009). The transformation from the physiological state III into state IV upon a pH increase is called the alkaline transition, which involves the replacement of Met80 as an axial ligand by Lys72, Lys73, or Lys79 (Wilson and Greenwood, 1996; Assfalg *et al*., 2003) (**Figure 4a**).

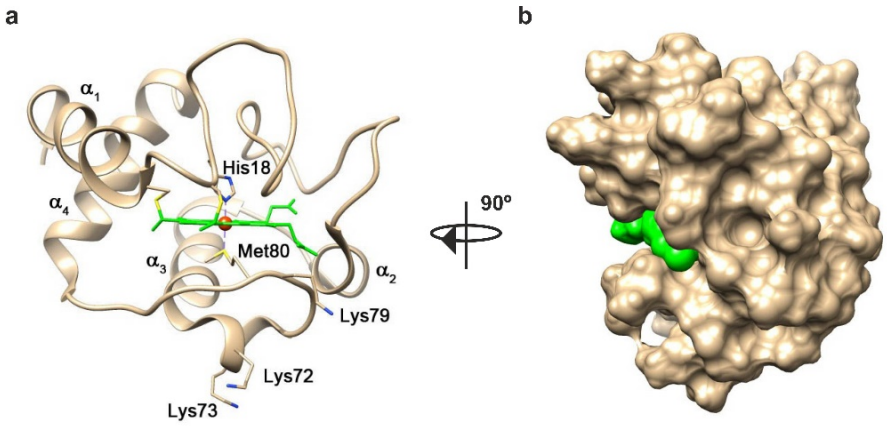

Figure 4. **Tridimensional structure of human C*c***. **a**) Ribbon representation of the solution NMR structure of human C*c* (Protein Data Bank, PDB, code 1J3S (Jeng *et al*., 2002)). The Fe atom of the heme group is colored in red. The two axial ligands of heme group (His18 and Met80), Lys72, 73 and 79 are also shown. The four α-helix are denoted as α1, α2, α3 and α4. **b**) Surface representation of human C*c* showing the portion of heme group (colored in green) exposed to solvent.

C*c* plays a double role in the cellular metabolism. Under homeostasis, C*c* acts as electron carrier between CIII and CIV. The redox reactions between C*c* and its partners cytochrome c_1 (Cc_1), from CIII, and CIV have been characterized by time-resolved spectroscopy and steady-state enzyme kinetic analyses (Yu *et al*., 1973; Speck *et al*., 1984; Esposti and Lenaz, 1991; Konermann *et al*., 1997; Trouillard *et al*., 2011). These studies showed multiphasic kinetic traces that suggested the presence of additional binding sites for C*c* on its partners. Recently, Moreno-Beltrán and co-workers reported two binding sites of C*c* in Cc_1 using nuclear magnetic resonance (NMR) and isothermal titration calorimetry (ITC) (Moreno-Beltrán *et al*., 2014; 2015). The first one, named *proximal site*, is a catalytic site suitable for transfers of electrons between both hemeproteins. It corresponds to the binary complex conformation determined by X-ray diffraction in yeast (Lange and Hunte, 2002). The

second, called *distal site*, locates close to the Rieske subunit and facilitates the turnover and sliding mechanism of C*c* molecules. In its turn, CIV also shows two binding sites: a productive or catalytic site and a non-productive binding site (Osheroff *et al*, 1983; Moreno-Beltrán *et al*, 2015). The presence of secondary binding sites for C*c* in CIII and CIV suggest a "restrained diffusion pathway" for C*c* molecules carrying electrons between the two respiratory complexes (Moreno-Beltrán *et al*., 2014, 2015).

Under stress conditions, C*c* releases to cytosol and nucleus to interact with several targets (Zou *et al*., 1999; Martínez-Fábregas *et al*, 2013, 2014a, 2014b; González-Arzola *et al*., 2015). In the cytosol, C*c* acts as an inducer of programmed cell death (PCD) by activating the caspase cascade (Desagher and Martinou, 2000; Jiang and Wang, 2004; Ow *et al*., 2008) (**Figure 5**). The next section shows an overview of PCD and the role of C*c* in this process.

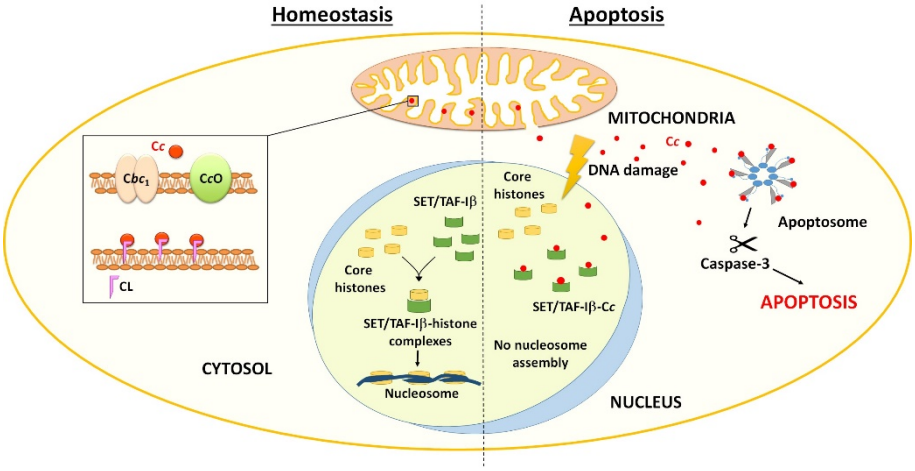

Figure 5. **Roles of C*c* in cell metabolism under homeostatic and stress conditions.** In the square is represented the ETC and the C*c* bound to cardiolipin.

5.4.1 Programmed cell death

A multicellular organism is a highly organized community of cells, where their number is tightly regulated by controlling the rates of cell division and death. Cells that are no longer needed, they "commit suicide" by activating an intracellular death program called programmed cell death (PCD). PCD is a regulated process that occurs under homeostatic conditions and tissue development in all multicellular and some unicellular organisms (Kerr *et al*., 1972; Ameisen, 2002; Debrabant *et al*., 2003; Engelberg-Kulka *et al*., 2006). Alterations in PCD process are related to many diseases (Gilchrist, 1998; Vila and Przedborski, 2003; Fuchs and Steller, 2011). In multicellular organisms, several PCD processes that use different pathways for active cell suicide have been described (Galluzzi *et al*., 2012). PCD shows four main routes that are summarized in **Table 1**:

Apoptosis is a mechanism that implicates the activation of a family of aspartic acid-specific proteases, called caspases. They are synthesized as zymogens, requiring a proteolytic process carried out by other caspases for their activation. This is known as caspase proteolytic cascade and provides a self-protection mechanism to cell, avoiding the start of uncontrolled cell death (Chang and Yang, 2000; Denault and Salvesen, 2002; Logue and Martin, 2008).

Autophagy is a self-degradative process that responds to stress conditions such as starvation, hypoxia, mitochondrial damage, and pathogen infection. This mechanism is independent of caspases activation and is accompanied by a massive cytoplasmic vacuolization. It is an important process for balancing sources of energy at critical times during development (Glick *et al*., 2010).

Necroptosis is a regulated necrosis, which implicates the activation of death receptors (such as tumour necrosis factor receptor 1, TNF1) and requires the kinase activity of receptor-interacting protein 1 and 3 (RIP1

and RIP3, respectively). This programmed necrosis involves the active disintegration of mitochondrial, lysosomal and plasma membranes (Vandenabeele *et al*., 2010).

Finally, **pyroptosis** was described as a peculiar cell death in macrophages induced by certain bacterial infections, such as *Salmonella typhimurium* (Bergsbaken *et al*., 2009). Pyroptosis can also be triggered by non-bacterial pathological stimuli (Kepp *et al*., 2010). The most distinctive biochemical feature of pyroptosis is the early induced, proximity-mediated activation of caspase-1, which leads to the release of pyrogenic interleukins (Franchi *et al*., 2009).

Table 1. Schematic overview of the multiple pathways of PCD.

	Apoptosis (type 1 PCD)	Autophagic cell death (type 2 PCD)	Necroptosis (type 3 PCD)	Pyroptosis
Mode of cell death	Programmed	Programmed	Programmed	Programmed
Initiators	TNF-α, FasL, or TRAIL, infectious pathogens	Nutrient deprivation, HDAC inhibitors, hypoxia, infectious pathogens	TNF-α, FasL, or TRAIL, microbial infections Ischemic injury	DAMPs, microbial infections
Intermediate signalings	Mitochondrial pathway Caspase-3, -6, -7-dependent	Caspase-independent autophagosome formation. Lysosomal protease	TNF receptor signaling JNK activation Caspase-independent RIP1/RIP3 necrosome	Nod-like receptors Caspase 1-dependent pyroptosome Inflammasome
Terminal cellular events	Non-lytic cell shrinkage DNA fragmentation apoptotic bodies	Non-lytic autophagic bodies	Non-lytic, loss of plasma membrane, swollen cellular organelles	Lytic, rapid loss of plasma membrane, cell swelling, pore formation
Inflammation	Non-inflammatory	Non-inflammatory	Proinflammatory	Proinflammatory

TNF-α: tumor necrosis factor-α; FasL: Fas ligand; TRAIL: TNF-related apoptosis-inducing ligand; HDAC: histone deacetylase; DAMPs: Damage-associated molecular pattern molecules; JNK: c-Jun N-terminal kinase. Based on Inoue and Tani, 2014.

5.4.1.1 Apoptotic pathways

Apoptosis has can be induced by three different signaling pathways that converge in the activation of caspase-3, considered one of the central molecules in PCD (Porter and Jänicke RU, 1999; Elmore, 2007): the extrinsic pathway, the perforin/granzyme pathway and the intrinsic pathway.

The extrinsic pathway (or death receptor pathway) is triggered by extracellular stimuli acting on receptors of the tumor necrosis factor (TNF) receptor gene superfamily (Locksley *et al*., 2001). The best-characterized ligands and their corresponding death receptors include FasL/FasR, TNF-α/TNFR1, Apo3L/DR3, Apo2L/DR4 and Apo2L/DR5. Upon ligand binding of to its receptor, the adaptor proteins FADD, TRADD or RIDD transmit the activating signal to effector caspases 2, 8, and 10 (Kruidering and Evan, 2000).

The perforin/granzyme pathway involves the release of perforin/granzyme by cytotoxic T lymphocytes (CTL) (Trapani and Smyth, 2002). CTL secrete perforin over target cells to generate pores in their cell membrane. These pores are the entry for granules that contain granzyme B or granzyme A. Granzyme B is able to activate the intrinsic death pathway by activation of pro-apoptotic members of the BCL-2 family, such as BH3-interacting domain death agonist (BID) (see below). In addition, granzyme B can directly activate procaspase-3. Granzyme A cleaves NDUFS3, a component of CI of the ETC, generating ROS (Martinvalet *et al*., 2005). On the other hand, granzyme A goes to reticulum endoplasmic and interacts with SET complex, which comprises the base excision repair endonuclease Ape1, an endonuclease NM23-H1, and a 5'-3' exonuclease Trex1. The complex SET/granzyme A goes into the nucleus and activates DNase NM23-H1, which cleaves DNA. This results in the accumulation of single stranded DNA and activates a

caspase-independent cell death pathway. (Beresford *et al*., 1999; Fan *et al*., 2003).

Finally, the intrinsic apoptotic pathway (also called mitochondrial pathway) is triggered by stimuli such as DNA damage, stress signals or cytotoxic drugs. These stimuli activate caspase 8, which cleaves the amino terminal fragment of BID protein (nBID), a member of the BH3-only subgroup of Bcl-2 family proteins in the cytosol (Li *et al*., 1998). However, the dissociation of the nBID of the rest of the truncate protein (tBID) occurs in the mitochondria by the interaction betwwen tBID and cardiolipin (Liu *et al*., 2005). tBid promotes the assembly of Bak–Bax oligomers within the mitochondrial outer membrane (Gonzalvez *et al*., 2005). The Bak–Bax oligomers form pores in mitochondria membrane, yielding the release of C*c* to cytosol (Chipuk and Green, 2008). Under DNA damage, C*c* goes to the nucleus where it interacts with SET/TAF-1β (González-Arzola *et al*., 20015).

Remarkably, the PCD is evolutionarily conserved along plants to humans, being C*c* a central axis of this process (Martínez-Fábregas *et al*., 2013; Martínez-Fábregas *et al*., 2014b).

5.4.2 Cytochrome *c* and apoptosis

Under stress conditions, C*c* plays a second role in the cell as intermediate in apoptosis (Cai *et al*., 1998). During apoptosis, C*c* is released from mitochondria to the cytosol to activate the caspases cascade. The release of C*c* from mitochondria is still unknow, but several hypotheses have been proposed, such as the formation of a *permeability transition pore* or a mitochondrial swelling (Green and Reed, 1998; Gao *et al*., 2001).

Although C*c* is a soluble hemeprotein, a substantial population of it is bound to the lipid cardiolipin (CL), which is specific of the inner mitochondrial membrane. It has been suggested that the apoptosis-inducing form of C*c* is the membrane-bound fraction (Jemmerson *et al*., 1999; Iverson and Orrenius, 2004; Kagan *et al*., 2005; Bergstrom *et al*.,

2013). C*c* shows two interaction sites with CL. The first one is called *A-site* (constituted by Asn52) and is responsible for the electrostatic interaction with the deprotonated phospholipids. The second one is the *C-site*, which comprises Lys73, Lys73 and Lys79, and allows the binding of the protonated phospholipids by hydrogen bond and the insertion of two acyl chains of the CL into two hydrophobic pockets of C*c* (**Figure 6**) (Rajagopal *et al*., 2012; Sinibaldi *et al*., 2010, 2013). The hydrophobic pockets of C*c* enable the displacement of water molecules, allowing the formation of hydrogen bonds more freely and increasing their number. The degree of acidic phospholipid protonation was suggested to be a critical factor governing C*c* association with membrane via either *A*- or *C-sites*. Complex formation causes loosening and reversible unfolding of C*c* (Spooner and Watts, 1991). Recently, it has been demonstrated that the binding of C*c* to CL enhances the peroxidase activity of the protein, a property shared by almost all hemeproteins, due to a conformational change that allows the access of hydrogen peroxide to the heme crevice (Radi *et al*., 1991; Lawrence *et al*., 2003; Kim *et al*., 2004; Kagan *et al*. 2009; Pandiscia and Schweitzer-Stenner, 2015).

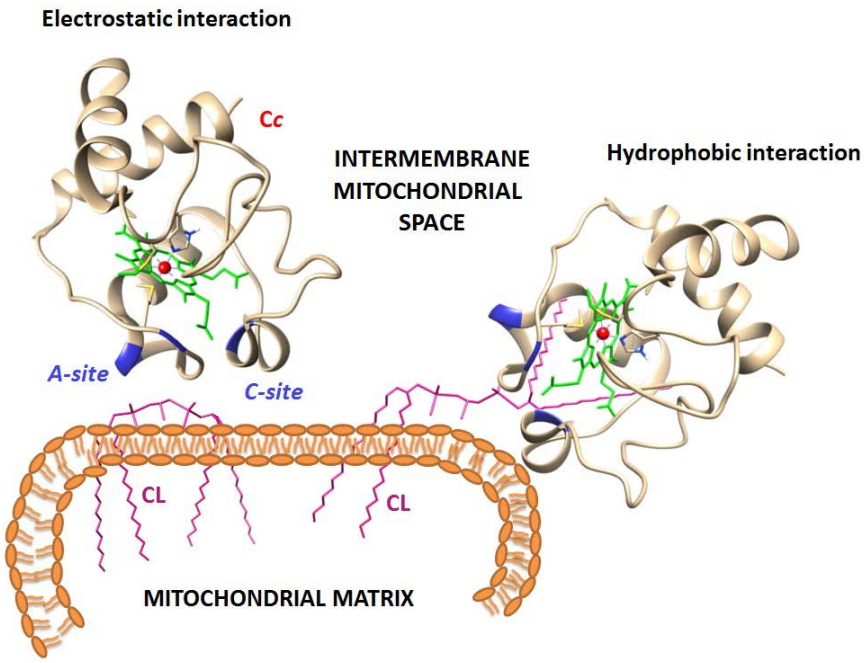

Figure 6. A model of CL-C*c* interaction. A putative 1:1 complex of CL with C*c* showing the two interactions that occurs in the CL-C*c* complex (Sinibaldi *et al*., 2010, 2013). In the hydrophobic interaction, two acyl chains of CL are inserted into two hydrophobic pockets surrounding Met80 of C*c*. The CL moiety is in magenta, *A-site* and *C-site* are in blue. The heme group is in green and the iron ion is shown as a red sphere.

Upon oxidation of cardiolipin, C*c* is released to the cytosol and interacts with the Apoptosis Protease Activation Factor-1 (Apaf-1) to assemble the apoptosome (Li *et al*., 1997). Apaf-1 consists in several copies of WD-40 domains, a caspase recruitment domain (CARD), and an ATPase domain (NB-ARC). dATP binding triggers a set of conformational changes that results in the formation of the active apoptosome, which is formed by seven Apaf-1/C*c* complexes arranged in a wheel form (**Figure 7**) (Zhou *et al*., 2015). This complex cleaves pro-caspase 9, generating its activated shape. Caspase 9 activates caspase 3, which stimulates the subsequent caspase cascade that commits the cell to apoptosis (Li *et al*., 1997).

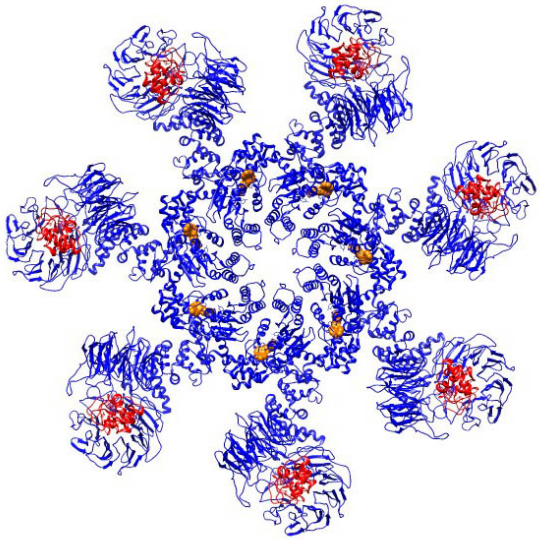

Figure 7. Structure of the heptamer Apaf-1/C*c* apoptosome. Ribbon representation of the solution NMR structure of human apoptosome (Protein Data Bank, PDB, code 3JBT (Zhou *et al*., 2015)). C*c* is colored in red, Apaf-1 in blue and dATP in orange.

Recent proteomic studies have shown that C*c* could also be translocated to the nucleus where it interacts with several targets, such

as SET nuclear oncogene (SET) or acidic nuclear phosphoprotein 32B (ANP32B) (Nur-E-Kamal *et al*., 2004; Martínez-Fábregas *et al.*, 2014a, b). Specifically, C*c* goes to the nucleus upon DNA damage, where it interacts with SET/TAF-Iβ. This interaction blocks the binding of SET/TAF-Iβ to core histones, thereby locking its histone-binding domains and inhibiting its nucleosome assembly activity (González-Arzola *et al*., 2015).

5.5 Post-translational modifications and cytochrome *c* function

Post-translational nitration, phosphorylation and (tri)methylation regulate C*c* function (Kluck *et al*., 2000; Cruthirds *et al*., 2003; Oursler *et al*., 2004; García-Heredia *et al*., 2010; García-Heredia *et al*., 2012). In human C*c*, phosphorylations of Thr28 and Ser47 have been reported recently (Zhao *et al*., 2011). The residues Tyr46, Ser67 and Tyr74 can be nitrated (Cassina *et al*., 2000; MacMillan-Crow *et al*., 2001; Abriata *et al*., 2009; Díaz-Moreno *et al*., 2011). Further, Tyr48 and Tyr97 of mammal C*c* undergo both, phosphorylation and nitration (Lee *et al*., 2006; Yu *et al*., 2008; Abriata *et al*., 2009). In addition, yeast C*c* can be (tri)methylated at Lys72, which abolishes its pro-apoptotic activity (DeLange *et al*., 1970; Polevoda *et al*., 2000; Kluck *et al*., 2000) (**Figure 8**).

The effects of post-translational modificacion of C*c* have been usually studied by nitro- and phosphomimetic variants due the low yield from cell extracts and the difficulty to preserve the post-translational modifications after purification. In addition, C*c*-kinases remain unidentified. Tyrosine nitration of C*c* is implicated in cell metabolism regulation under oxidative stress (Cassina *et al*, 2000; Abriata *et al*, 2009; Su and Groves, 2009; Garcia-Heredia *et al*., 2010, 2012). However, phosphorylation is postulated as the main regulation mechanism of the ETC in higher organisms under homeostatic and stress conditions (Hüttemann *et al*., 2005). The effects of this modification on C*c* function become a particular interest because it relates to several diseases or pathological conditions like cancer, inflammation, sepsis, asthma and ischemia/reperfusion (Hüttemann *et al*., 2012; Sanderson *et al*, 2013; Lee and Hüttemann, 2014; Shay *et al*., 2015).

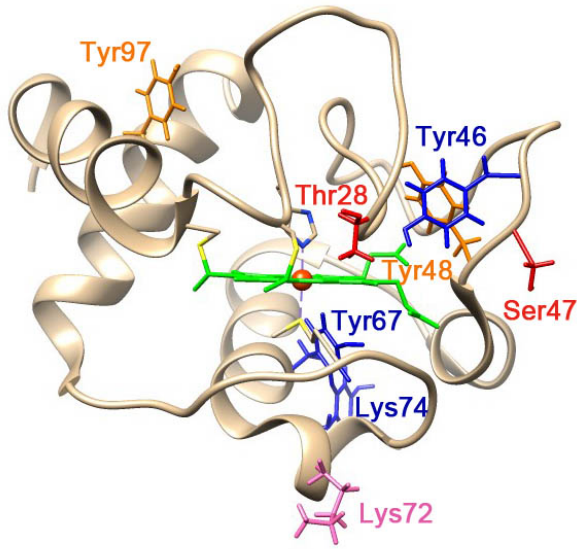

Figure 8. **Residues involved in post-translational modifications of cytochrome *c*.** Ribbon representation of structure of human C*c* (PDB code 1J3S (Jeng *et al*., 2002)). Residues Thr28 and Ser47 (in red) can be phosphorylated. Tyr46, Tyr67 and Tyr 74 (in blue) undergo nitration. Tyr48 and Try97 (in orange) can be nitrated or phosphorylated. Lys72 (in pink) can be (tri)methylated.

In this context, it is known that phosphorylation at either Y48 or Y97 affects the role of C*c* as electron carrier. In relation to the PCD process, a negative charge at position 48 decreases the ability of C*c* to activate the caspase cascade (Lee *et al*., 2006; Yu *et al*., 2008; Pecina *et al*., 2010; Garcia-Heredia *et al*., 2011). However, how the phosphorylation at position 28 and 46 alters the role of C*c* in cell life and death is unknown. Moreover, the use of glutamate or aspartate residue to imitate a PTR is under discussion, because only mimic the charge but not the aromatic ring of the PTR residue (Xie *et al*., 2007; Ge *et al*., 2010).

Hence, the goal of this Thesis is to contribute to a general understanding of the effects of phosphorylation of C*c* in the interaction with its physiological targets. In addition, this work shows a new tool to analyze tyrosine-phosphorylated proteins, whose yield from cell extracts are low or their kinases are unknown.

6. OBJECTIVES

The main goal of this PhD thesis research work is to determine the effects that post-translational phosphorylation of cytochrome *c* bears not only on its 3D structure but also on its double role in controlling cell life and death. Specifically, the work herein reported aims at determining whether such modification in cytochrome *c* induces conformational changes that could alter the interaction with its cellular targets.

The specific objectives are as follows:

1. To characterize the changes in the biophysical and structural properties of cytochrome *c* induced by phosphorylation at position 28, 47, 48 and 97. In particular, to compare the effects of the classical Tyr-by-Glu mimetic mutation with those promoted by replacement of tyrosine 48 with the novel non-canonical amino acid *p*-carboxymethyl-L-phenylalanine, which is introduced by using the evolved tRNA synthetase technique.

2. To understand how phosphorylation of cytochrome *c* affects the interactions with its partners in the electron transport chain, namely complexes bc_1 and cytochrome *c* oxidase, under different physiological contexts.

3. To assess the ability of phosphorylated cytochrome *c* to oxidize cardiolipin – an exclusive inner mitochondrial membrane lipid. In particular, to test whether the phosphorylation of cytochrome *c* affects its affinity by the lipid.

4. To investigate the capacity of phosphorylated cytochrome *c* to trigger apoptosis. Specifically, to understand the effects of phosphorylation on the caspase activation capacity of cytochrome *c*.

In addition, a secondary objective is listed below:

1. To improve the synthesis of the non-canonical amino acid *p*-carboxymethyl-L-phenylalanine.

7. RESULTS AND DISCUSSION

In this section, a quick overview at the Results and Discussion of published and unpublished works is presented. Please, refer to the journal publications in Appendix I and unpublished works in Appendix II and III for further details.

Post-translational modifications of proteins are relevant regulatory mechanisms to control an ample number of processes involved in cell metabolism. One of the most usual modifications is phosphorylation, which is implicated in the control of fundamental cellular processes including the cell cycle, cell adhesion, and cell survival, as well as cell proliferation and differentiation. The purpose of this thesis is to investigate the effect of phosphorylation of C*c* on its structure and function, with a particular focus on interactions with its physiological targets due to the role of phosphorylated C*c* in diseases such as cancer or isquemia.

The ETC is postulated to be primarily regulated by protein phosphorylation in higher organisms (Hüttemann *et al*., 2008). However, the effects of this modification on the dual function of C*c* are partially understood. C*c* is phosphorylated *in vivo* in Tyr48 and Tyr97 (Lee *et al*., 2006; Yu *et al*., 2008). Recently, a proteomic analysis has yielded the discovery of two new phosphorylation sites at positions 28 and 47. These sites are the first residue phosphorylations described in human C*c* (Zhao *et al*., 2011).

The specific C*c*-phosphorylating kinase remains unknown and, due to the difficulty in obtaining enough phosphorylated C*c* for experimental studies, phosphorylation of C*c* is usually studied by phosphomimic C*c* variants (Kadenbach and Urban, 1968; Pecina *et al*., 2010; García-Heredia *et al*., 2011).

Traditionally, tyrosine phosphorylation has been mimicked by glutamate and aspartate residues (García-Heredia *et al*., 2011). However, the volume of these two amino acids is smaller regarding that from a phosphotyrosine and also they exhibit one charge less. The non-canonical amino acid *p*-carboxymethyl-L-phenylalanine (*p*CMF) is a

mimetic of phosphotyrosine residue that emulates better its volume and charge than glutamate or aspartate residues (**Figure 8a**) (Guerra-Castellano *et al*., 2015). Moreover, *p*CMF is more stable than traditional analogues, and it is resistant to protein tyrosine phosphatase hydrolysis. Hence, to mimic the phosphorylations of tyrosines 48 and 97, the evolved tRNA synthetase technique was used to introduce biologically the *p*CMF at the desired position (Ryu and Schultz, 2006; Xie *et al*., 2007) (**Figure 8b**). Thus, the mutants Y48*p*CMF and Y97*p*CMF C*c*, respectively,

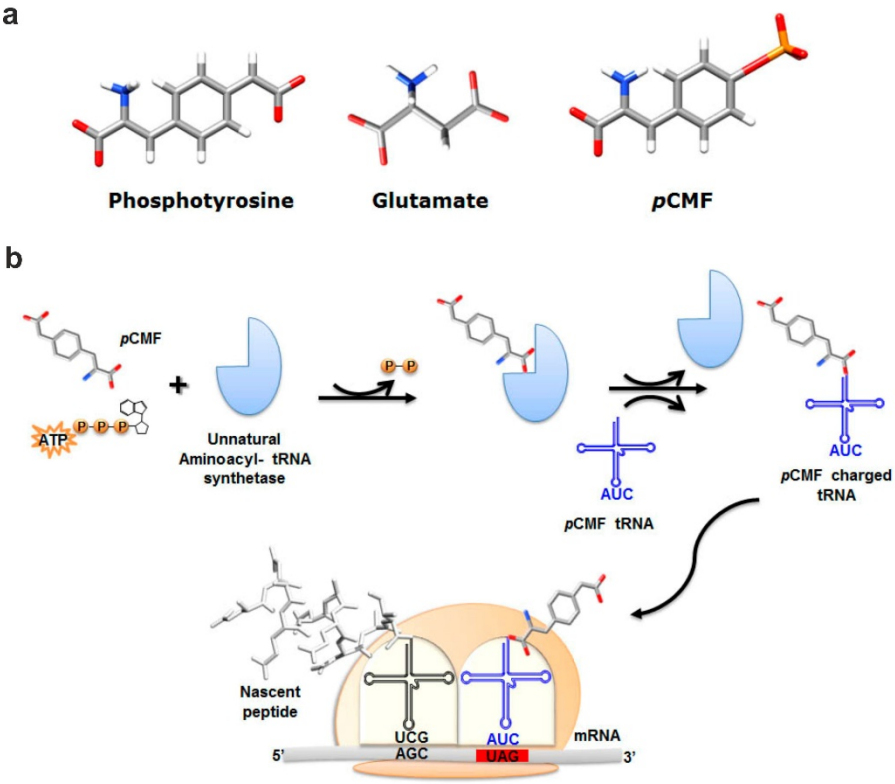

were obtained (Guerra-Castellano *et al*., 2015).

Figure 8. *p*CMF and the evolved tRNA synthetase technique. **a**) Eschematic representation of phosphotyrosine, glutamate and pCMF residues. Atoms are colored by element according to the CPK code. **b**) To introduce the *p*CMF into the protein, the Tyr-encoding triplet of interest - 48 and 97 to produce de Y48*p*CMF and Y97*p*CMF mutants, respectively - was replaced with an amber codon (TAG) in the human C*c* gene. The

latter allows the incorporation of *p*CMF aided by a designed orthogonal tRNA that recognizes the amber codon**.**

It was suggested recently that this approach has the major drawback of affecting the folding pathway of the protein, thereby leading to non-native states (Radi, 2012). Hence, we have tested whether the introduction of *p*CMF affects the structure of C*c* by molecular dynamics (MD) computations, UV CD and ^{15}N, ^{1}H, ^{13}C, ^{1}H- heteronuclear correlation spectra (HSQC) (Guerra-Castellano *et al*., 2015). The results imply that the mutation does not affect the overall folding of the protein during its synthesis and the protein structure remained similar to the wild type species.

To the best of our knowledge, this is the first time that this technique has been applied to hemeproteins. Moreover, the overall yield of the organic synthesis of the *p*CMF has been significantly improved, from 44% to 75%, by modifications of the original synthetic protocol (Ryu and Schultz, 2006; Guerra-Castellano *et al*., 2015). In addition, replacing the initial reactant for the first step of methyl esterification has considerably lowered the cost of the synthesis to 70% of cost per yield (Guerra-Castellano *et al*., 2015).

For positions 28 and 47, the corresponding residue was replaced by the canonical amino acid aspartic acid (T28D and S47D, respectively). As a control, two other mutants were analyzed in the same two positions (S47A and T28A C*c*) in order to differentiate the effects due to the presence of a negatively charged residue (Guerra-Castellano *et al*., 2016).

The heme coordination of phosphomimetic species was analyzed by visible CD spectra. CD is a technique that provides information about the interaction between the heme group and the protein matrix (Dragomir *et al*., 2007). All phosphomimetic species showed the distinctive spectrum for C*c* at state III, with a maximum at 410 nm corresponding to the B-band, which reveals a splitting (Guerra-Castellano *et al*., 2015; Guerra-Castellano *et al*., 2016). This splitting is due to the internal electric field of the protein, and it is usually observed in low-spin cytochromes

(Schweitzer-Stenner, 2008). Surprisingly, such B-band splitting was fully lost in the S47A mutant. To assess this behavior of the mutation by alanine at position 47 and to compare it to the wild-type (WT) protein, MD computations were performed on the native WT and S47A species. Data suggest that a change in the motion modes of C*c*, rather than a substantial structural change, is responsible for the loss of the B-band splitting induced by the S47A mutation (Guerra-Castellano *et al*., 2015).

The alkaline transition of C*c*, which involves the replacement of Met80 as an axial ligand by Lys72, Lys73, or Lys79 at high pH values was only affected in the mutant Y48*p*CMF C*c*, in which the pK_a value for this transition drops to physiological values. To understand how this substitution affected the coordination of heme group, Raman scattering in collaboration with Prof. Peter Hildebrandt (Technische Universität Berlin, Germany), electron paramagnetic resonance (EPR) in collaboration with Prof. Miguel Teixeira (Institute of Biological Chemistry and Technology António Xavier, Portugal) and X-ray spectra absorption (XAS) in collaboration with Dr. Sofia Diaz Moreno (Diamond Light Source, Oxford, UK), were recorded at different pH values. Raman spectroscopy data showed that the alkaline state contribution increased along the pH range from 7.0 to 12.0. However, no change was seen in the range from pH 5.8 to 7.0. In contrast, 1D NMR spectra show that the Met80 H_ε signal fades at neutral pH values; and they indicate a pK_a value of 6.3. The 698-nm band of the visible spectrum shows a similar behavior (pK_a = 6.7). To better understand of the heme environment of Y48*p*CMF mutant, EPR assays were performed at different pH values. At low pH, the phosphomimic mutant showed two resonance sets. The first one corresponded to hexacoordinated low-spin ferric iron, the same as those found for the Y48E mutant (García-Heredia *et al*., 2011). The second was a signal typical of high-spin Fe^{III} population in a tetragonal ligand field, indicative of pentacoordinated iron. Remarkably, the high-spin signal is substantially weaker in the Y48E mutant (García-Heredia *et al*., 2011). This finding is of particular relevance, since loss of the sixth iron ligand promotes translocation of the heme-protein to the cytosol and to the nucleus (Hannibal *et al*., 2016). However, the extended X-ray absorption

fine structure (EXAFS) spectra of WT and Y48*p*CMF Cc species were highly similar. Taking together, data showed an overall intact heme pocket, with the exception of the mutation site due to the presence of the carboxyl group of *p*CMF near the heme propionates (Guerra-Castellano *et al*., 2015)

In the ETC, C*c* carries electrons from its donor protein, Cc_1 of CIII, to CIV. The success in a redox process is that the carrier recognizes the donor and the acceptor proteins and dissociates quickly from them (Bashir *et al*., 2011; Díaz-Quintana *et al*., 2015). The ETC reactions between C*c* and its partners have been characterized by time-resolved spectroscopy and steady-state enzyme kinetic studies (Yu *et al*., 1973; Speck *et al*., 1984; Esposti and Lenaz, 1991; Konermann *et al*., 1997; Trouillard *et al*., 2011). The thermodynamics and stoichiometry of the binding of C*c* mutants – obtained by substitutions at positions 28, 47 and 48 - to the soluble N-terminal domain of *Arabidopsis thaliana* Cc_1 were studied by ITC and compared with previously reported data for WT C*c* (Moreno-Beltrán *et al*., 2015). All mutants maintained the stoichiometry 2:1 (C*c*: Cc_1) described for the WT species. The two binding sites for C*c* in Cc_1 are known as *proximal* and *distal*, according to the corresponding heme-to-heme distances (Moreno-Beltrán *et al*., 2015). All phosphomimetic proteins showed similar affinity by the *proximal site* of Cc_1 (compatible with electron transfer). However, the *distal site*, dependent on electrostatics, was substantially weakened by the presence of negative charges at positions 28 and 48 of C*c* (Guerra-Castellano *et al*., 2016). In addition, the redox potential of the T28D and Y48*p*CMF C*c* species showed a decrease in ca. 30 mV and ca. 60 mV in comparison with WT species, respectively (Guerra-Castellano *et al*., 2015; Guerra-Castellano *et al*., 2016).

To dig into the interaction of phosphovariant Y48*p*CMF C*c* with Cc_1, NMR titrations of ^{15}N labeled reduced Y48*p*CMF C*c* with unlabeled reduced plant Cc_1 were performed as previously described for WT species (Moreno-Beltrán *et al*., 2015). All the perturbed amide signals, excepting those from Lys55 and Ile58, are from residues surrounding the

heme crevice, as described for the interaction between WT C*c* and Cc_1 (Moreno-Beltrán *et al*, 2014; 2015). In fact, this region constitutes a very well-conserved interaction surface patch in *c*-type cytochromes (Díaz-Moreno *et al*., 2005a, b; Volkov *et al*., 2006; Díaz-Quintana *et al.*, 2008, Sakamoto *et al.*, 2011,). The residues Lys55 and Ile58 are located just on the opposite side to the interaction surface and their perturbations only appear in the mutant. A plausible explanation of these perturbations is that the bound to C*c*1 promotes several internal movements which are favored by the more flexibility of the mutant structure.

Aditionally, the binding affinity of the cross-complex between bovine C*c*O, the other C*c* partner in the ETC, and the Y48*p*CMF mutant was analyzed by ITC, as previously described for WT C*c* species (Moreno-Beltrán *et al*., 2015). Y48*p*CMF C*c* bound two sites on C*c*O, as described previously for WT Cc (Moreno-Beltrán *et al*., 2015). However, both sites – *proximal* and *distal* – showed an affinity for Y48*p*CMF Cc substantially lower than that for the WT species.

To better understand how phosphorylation at position 28, 47, 48 and 97 could affect the oxidative phosphorylation process, the ability of C*c* mutants to reduce C*c*O was analyzed using the isolated protein C*c*O with WT and phosphomimetic variants of C*c*. The C*c*O activity was higher when a negative charge was presented at positions above-mentioned, suggesting that phosphorylation enhances electron donor capacity of C*c* towards C*c*O (Guerra-Castellano *et al*., 2016). As noted in the **Introduction** section, three models have been proposed for the organization of the respiratory complexes. The *fluid model*, where all membrane proteins and redox components catalyzing electron transport and ATP synthesis are in constant and independent diffusional motion (Hackenbrock *et al*., 1986). The *solid model*, which shows a supramolecular organization of individual respiratory complexes mediated by specific interactions and where are implicated respiratory factors, such as Rcfs in yeast or HIGDs in mammals (Schagger and Pfeiffer, 2000; Shoubridge, 2012; Strogolova *et al*., 2012; Vukotic *et al*, 2012). Finally, the *plasticity model* conciles these apparently opposite

models. In this model, the supercomplex formation is dynamic and in equilibrium between fixed supercomplexes and independent respiratory complexes (Acín-Pérez *et al*., 2008). For this reason, the effect of supercomplex formation and the role of the respiratory factors over the C*c*O activity were analyzed. The study with the isolated HIGD1A and HIGD2A proteins with the Y48*p*CMF and Y97*p*CMF mutants showed a significant increment in the rate of C*c*O-catalyzed oxidation of both mutants in comparison to WT C*c* species. In addition, data revealed that HIGD2A modulated the kinetics of the reaction more than HIGD1A. Nevertheless, the HIGD-dependent increase in C*c*O activity is slightly smaller for phosphomimic species compared to WT species. This observation was confirmed in the cellular context, using yeast mitochondria that express Rcf1, the orthologous of HIGD1A and HIGD2A (Chen *et al*., 2012). Rcf1 mediates the assembly CIII and CIV to form a supercomplex (Strogolova *et al.*, 2012; Vukotic *et al.*, 2012). Hence, the effects of supercomplex in the OxPhos process were also tested. To do that, wild-type and knockout in Rcfs proteins – in yeast Rcf2 also mediated supercomplex assembly – mitochondria were tested under different growth media because the assembly of mitochondrial supercomplexes is strictly dependent on the metabolic needs (Ramírez-Aguilar *et al.*, 2011). In addition, respiratory supercomplexes can show a certain degree of heterogeneity in their composition due to metabolic transition in yeast, or to tissue-specific isoform variability in mammal (Kennaway *et al*., 1990; Fukuda *et al*., 2007). Under the context of supercomplexes, Y48*p*CMF and Y97*p*CMF Cc species were less efficient than WT as an electron carrier towards C*c*O. Hence, the Rcf-mediated ETC flux increase was lower with phosphomimetic mutants of C*c*. It is known that nitration of C*c* in its tyrosine residues by peroxynitrite increments its peroxidase activity and, concomitantly the impairment of the membrane potential formation (Nakagawa *et al*., 2007). Similarly, the phosphorylation at position 48 and 97 may help to prevent hyperpolarization of the mitochondrial membrane due to ROS/RNS production, which is related to apoptosis process (Rego *et al*., 2001; Perl *et al*, 2004). Thus, data suggests that phosphorylation of C*c* modulates

the mitochondrial ETC, allowing a fast adaptation of the hemeprotein activity to shift in the physiological circumstances.

The role of C*c* as inductor of PCD was also analyzed. Mitochondria contain a pool of C*c* that interacts with CL (Ascenzi *et al*., 2015). During apoptosis, C*c* is able to oxidize CL (Vladimirov *et al*., 2006). This peroxidation allows the release of C*c* to cytosol, where it participates in the formation of apoptosomes and the caspase activation (Puchkov *et al*., 2013; Li *et al*., 1997). The interaction of C*c* mutants with CL was analyzed in liposomes that contained CL in a ratio 1:4 (CL:lipids), which represents the physiological ratio under homeostasis (Vik *et al*., 1981). All phosphomimic mutants showed a decrease in their affinity by CL. However, the CL-C*c* peroxidase activity increased in T28D and Y48*p*CMF mutants (Guerra-Castellano *et al*., 2016). Thus, phosphorylation may produce a structural change allowing greater accessibility to H_2O_2 and affect the insertion of the acyl moiety in the C*c*. Notably, both mutations of Ser 47 decrease the affinity towards CL and peroxidase activity (Guerra-Castellano *et al*., 2016).

Finally, the capacity of phosphomimetic C*c* to activate caspase-3 was tested in cell extract devoid endogenous C*c*. Caspase-3 is a good marker of apoptosis, being considered one of the central molecules in PCD (Porter and Jänicke RU, 1999; Elmore, 2007). The presence of a negative charge at position 48 and 97 decreased the caspase activation capacity in comparison with WT Cc species. This result is particularly relevant for the phosphorylation at position 97, which is strongly induced after insulin treatment in post-ischemia state. In addition, this increase is related to a decrease in neuronal death of 50% (Sanderson *et al*., 2013). Caspase-3 cleavage constitutes a potent neuroprotective strategy, so the study of the phosphomimetic Y97*p*CMF would be a useful tool to design therapeutic applications (Namura *et al*., 1998; Yuan, 2009). Surprisingly, both mutations of Ser47 (S47A and S47D mutans) decreased caspase-3 activation, so this effect is independent of the additional negative charge concomitant to phosphorylation and reveals the importance of position 47 in caspase activation (Guerra-Castellano *et al.*, 2016).

In summary, C*c* is a well-conserved protein along eucaryotic organisms, where participates in electron transport and apoptotic processes. Here, we have tested whether post-translational modificacions, such as phosphorylation, could affect its structure and ability to interact with its physiological partners. Data that presents in this PhD thesis shows that the phosphomimic mutations of residues 28, 47, 48 and 97 hardly affect the overall conformation of C*c*. In relation of the effects on C*c* roles in the cell, a negative charge at position 28 alters the function of C*c* as electron carrier in the ETC. However, the Y48*p*CMF and Y97*p*CMF mutants could prevent the hyperpolarization of mitochondrial membrane and decrease the ability of C*c* to activate the caspase cascade during PCD. So, phosphorylation of these residues could act as "antiapoptotic switch". Moreover, residue 47 of C*c* has been revealed important for caspase-3 activation during apoptosis.

8. CONCLUSIONS

In this PhD thesis, four phosphorylation sites of cytochrome *c* have been analyzed by using biophysical techniques and functional approaches. The following conclusions can be inferred:

1. None of the amino acid substitutions performed at positions 28, 47, 48 and 97 does significantly affect the overall structure of cytochrome *c*.

2. The substitution of tyrosine 48 by the non-canonical amino acid *p*-carboxymethyl-L-phenylalanine mimics the phosphorylation-induced conformational changes of cytochrome *c* much better than the classical glutamate replacement.

3. The presence of a negative charge at position 48 affects the redox properties of cytochrome *c* and lowers the pK_a value of the alkaline transition to physiological pH.

4. The phosphomimetic mutants of cytochrome *c* at position 28, 47 and 48 are able to bind cytochrome c_1 with a stoichiometry of 1:2 (cytochrome c_1 : cytochrome *c*). The *proximal site* of cytochrome c_1 – compatible with electron transfer – shows a similar affinity towards the wild-type and mutant cytochrome *c* species, whereas docking to the *distal site* is weaker when a negative charge is present at either position 28 or 48 of cytochrome *c*. Remarkably, the phosphomimetic species are best electrons donnors than wild-type cytochrome *c*, and so their oxidation rate by cytochrome *c* oxidase is higher.

5. All phosphomimic cytochrome *c* species, except mutant at position 97, have their affinity towards cardiolipin altered. The negative charge at positions 28, 47 and 48 increases the peroxidase activity of cytochrome *c* both in the presence and in the absence of cardiolipin.

6. Phosphomimetic cytochrome *c* species at position 48 and 97 show lower caspase activation ability. Residue 47 seems to be

crucial in cytochrome *c*-dependent triggering of the caspase cascade in apoptosis.

7. Phosphorylation of cytochrome *c* at particular positions does specifically control the different functions of the hemeprotein in cell life and death.

8. The overall yield of organic synthesis of the non-canonical amino acid *p*-carboxymethyl-L-phenylalanine has been significantly improved, from 44% to 75%, over the original synthetic protocol. Replacing the initial reactant for the first step of methyl esterification has considerably lowered the cost of the synthesis.

9. GENERAL REFERENCES

Abriata LA, Cassina A, Tórtora V, Marín M, Souza JM, Castro L, Vila AJ and Radi R (2009) Nitration of solvent-exposed tyrosine 74 on cytochrome *c* triggers heme iron-methionine 80 bond disruption. Nuclear magnetic resonance and optical spectroscopy studies. *J Biol Chem* **284**, 17-26.

Acín-Pérez R, Fernández-Silva P, Peleato ML, Pérez-Martos A and Enriquez JA (2008) Respiratory active mitochondrial supercomplexes. *Mol Cell* **32**, 529-539.

Acin-Perez R and Enriquez JA (2014) The function of the respiratory supercomplexes: the plasticity model. *Biochim Biophys Acta – Bioenerg* **1837**, 444-450.

Ameisen JC (2002) On the origin, evolution, and nature of programmed cell death: a timeline of four billion years. *Cell Death Differ* **9**, 367-393.

Ameri K, Jahangiri A, Rajah AM1, Tormos KV, Nagarajan R, Pekmezci M, Nguyen V, Wheeler ML, Murphy MP, Sanders TA, Jeffrey SS, Yeghiazarians Y, Rinaudo PF, Costello JF, Aghi MK and Maltepe (2015) HIGD1A regulates oxygen consumption, ROS production, and AMPK activity during glucose deprivation to dodulate cell survival and tumor growth. *Cell Rep* **10**, 891-899.

Ascenzi P, Coletta M, Wilson MT, Fiorucci L, Marino M, Polticelli F, Sinibaldi F and Santucci R (2015) Cardiolipin-cytochrome *c* complex: Switching cytochrome *c* from an electron-transfer shuttle to a myoglobin- and a peroxidase-like heme-protein. *IUBMB Life* **67**, 98-109.

Assfalg M, Bertini I, Dolfi A, Turano P, Mauk AG, Rosell FI and Gray HB (2003) Structural model for an alkaline form of ferricytochrome *c. J Am Chem Soc* **125**, 2913-2922.

Banci L, Bertini I, Gray HB, Luchinat C, Reddig T, Rosato A and Turano P (1997) Solution structure of oxidized horse heart cytochrome *c*. *Biochemistry* **36,** 9867-9877.

Bashir Q, Scanu S and Ubbink M (2011) Dynamics in electron transfer protein complexes. *FEBS J* **278**, 1391-1400.

Beresford PJ, Xia Z, Greenberg AH and Lieberman J (1999) Granzyme A loading induces rapid cytolysis and a novel form of DNA damage independently of caspase activation. *Immunity* **10**, 585-594.

Bergsbaken T, Fink SL and Cookson BT (2009) Pyroptosis: host cell death and inflammation. *Nat Rev Microbiol* **7**, 99-109.

Bergstrom CL, Beales PA, Lv Y, Vanderlick TK and Groves JT (2013) Cytochrome *c* causes pore formation in cardiolipin-containing membranes. *Proc Natl Acad Sci USA* **110**, 6269-6274.

Berry EA and Trumpower BL (1985) *J Biol Chem* **260**, 2458-2467.

Bhaskar K, Hobbs GA, Yen SH and Lee G (2010) Tyrosine phosphorylation of tau accompanies disease progression in transgenic mouse models of tauopathy. *Neuropathol Appl Neurobiol* **36**, 462-477.

Boffi F, Bonincontro A, Cinelli S, Congiu Castellano A, De Francesco A, Della Longa S, Girasole M and Onori G (2001) pH-Dependent local structure of ferricytochrome *c* studied by x-ray absorption spectroscopy. *Biophys J* **80**, 1473-149.

Brown GC and Borutaite V (2008) Regulation of apoptosis by the redox state of cytochrome *c*. *Biochim Biophys Acta – Bioenerg* **1777**, 877-881.

Cai J Yang J and Jones DP (1998) Mitochondrial control of apoptosis: the role of cytochrome *c*. *Biochim Biophys Acta – Bioenerg* **1366**, 139-149.

Cassina AM, Hodara R, Souza JM, Thomson L, Castro L, Ischiropoulos H, Freeman BA, Radi R (2000) Cytochrome *c* nitration by peroxynitrite. *J Biol Chem* **275**, 21409-21415.

Chance B and Williams GR (1955) A method for the localization of sites for oxidative phosphorylation. *Nature* **176**, 250-254.

Chang HY and Yang X (2000) Proteases for cell suicide: functions and regulation of caspases. *Microbiol Mol Biol Rev* **64**, 821-846.

Chen YC, Taylor EB, Dephoure N, Heo JM, Tonhato A, Papandreou I, Nath N, Denko NC, Gygi SP and Rutter J (2012) Identification of a protein mediating respiratory supercomplex stability. *Cell Metab* **15**, 348-360.

Chipuk JE and Green DR (2008) How do BCL-2 proteins induce mitochondrial outer membrane permeabilization? *Trends Cell Biol* **18**, 157-164.

Cieśla J, Frączyk T and Rode W (2011) Phosphorylation of basic amino acid residues in proteins: important but easily missed. *Acta Biochim Pol* **58**, 137-148.

Crowley PB, Otting G, Schlarb-Ridley BG, Canters GW and Ubbink M (2001) Hydrophobic interactions in a cyanobacterial plastocyanin-cytochrome *f* complex. *J Am Chem Soc* **123**, 10444-10453.

Cruthirds DL, Novak L, Akhi KM, Sanders PW, Thompson JA and MacMillan-Crowa LA (2003) Mitochondrial targets of oxidative stress during renal ischemia/reperfusion. *Arch Biochem Biophys* **412**, 27-33.

Cruz-Gallardo I, Díaz-Moreno I, Díaz-Quintana A and De la Rosa MA (2012) The cytochrome *f*-plastocyanin complex as a model to study transient interactions between redox proteins. *FEBS Lett* **586**, 646-652.

Czapla M, Cieluch E, Borek A, Sarewicz M and Osyczka A (2013) Catalytically-relevant electron transfer between two hemes b_L in the hybrid cytochrome bc_1-like complex containing a fusion of Rhodobacter sphaeroides and capsulatus cytochromes *b*. *Biochim Biophys Acta – Bioenerg* **1827**, 751-760.

Debrabant A, Lee N, Bertholet S, Duncan R and Nakhasi HL (2003) Programmed cell death in trypanosomatids and other unicellular organisms. *Int J Parasitol* **33**, 257-267.

DeLange RJ, Glazer AN and Smith EL (1970) Identification and location of ε-N-trimethyllysine in yeast cytochromes *c*. *J Biol Chem* **245**, 3325-3327.

Delivani P and Martin SJ (2006) Mitochondrial membrane remodeling in apoptosis: an inside story. *Cell Death Differ* **13**, 2007-2010.

Dell A, Galadari A, Sastre F and Hitchen P (2010) Similarities and differences in the glycosylation mechanisms in prokaryotes and eukaryotes. *Int J Microbiol* **2010,** 148178.

Denault JB and Salvesen GS (2002) Caspases: keys in the ignition of cell death. *Chem Rev* **102**, 4489-4500.

Deribe YL, Pawson T and Dikic I (2010) Post-translational modifications in signal integration. *Nat Struct Mol Biol* **17**, 666-672.

Desagher S and Martinou JC (2000) Mitochondria as the central control point of apoptosis. *Trends Cell Biol* **10**, 369-377.

Díaz-Quintana A, Hervás M, Navarro JA and De la Rosa MA (2008) Plastocyanin and cytochrome c_6: The soluble electron carriers between cytochrome b_6f and photosystem I. In: Photosynthetic protein complexes: A structural approach. Ed. P. Fromme. Wyley-Blackwell.

Díaz-Moreno I, Díaz-Quintana A, Molina-Heredia FP, Nieto PM, Hansson O, De la Rosa MA and Karlsson BG (2005a) NMR analysis of the transient complex between membrane photosystem I and soluble cytochrome c_6. *J Biol Chem* **280**, 7925-7931.

Díaz-Moreno I, Díaz-Quintana A, Ubbink M and De la Rosa MA (2005b) An NMR-based docking model for the physiological transient complex between cytochrome *f* and cytochrome c_6. *FEBS Lett* **579**, 2891-2896.

Díaz-Moreno I, García-Heredia JM, Díaz-Quintana A, Teixeira M and De la Rosa MA (2011) nitration of tyrosines 46 and 48 induces the specific degradation of cytochrome *c* upon change of the heme iron state to high-spin. *Biochim Biophys Acta – Bioenerg* **1807**, 1616-1623.

Díaz-Quintana A, Cruz-gallardo I, De la Rosa MA and Díaz-Moreno I (2015) Diversity of interactions of redox systems: from short-lived to

long-lived complexes. In *Redox proteins in supercomplexes and signalosomes*. Taylor and Francis Group (Boca Raton). p. 35-60.

Dragomir I, Hagarman A, Wallace C and Schweitzer-Stenner R (2007) Optical band splitting and electronic perturbations of the heme chromophore in cytochrome *c* at room temperature probed by visible electronic circular dichroism spectroscopy. *Biophys J* **92**, 989-998.

Drepper F, Dorlet P and Mathis P (1997) Cross-linked electron transfer complex between cytochrome c_2 and the photosynthetic reaction center of Rhodobacter sphaeroides. *Biochemistry* **36**, 1418-1427.

Dudkina NV, Kudryashev M, Stahlberg H and Boekema EJ (2011) Interaction of complexes I, III, and IV within the bovine respirasome by single particle cryoelectron tomography. *Proc Natl Acad Sci U S A* **108**, 15196-15200.

Elmore S (2007) Apoptosis: A Review of Programmed Cell Death. *Toxicol Pathol* **35**, 495-516.

Engelberg-Kulka H, Amitai S, Kolodkin-Gal I and Hazan R (2006) Bacterial programmed cell death and multicellular behavior in bacteria. *PLoS Genet* **2**, e135.

Enriquez JA and Lenaz G (2014) Coenzyme q and the respiratory chain: coenzyme q pool and mitochondrial supercomplexes. *Mol Syndromol* **5**, 119-140.

Esposti MD and Lenaz G (1991) The kinetic mechanism of ubiquinol: cytochrome c reductase at steady state. *Arch Biochem Biophys* **289**, 303-312.

Eubel H, Heinemeyer J and Braun HP (2004) Identification and characterization of respirasomes in potato mitochondria. *Plant Physiol* **134**, 1450-1459.

Fan Z, Beresford PJ, Oh DY, Zhang D and Lieberman J (2003) Tumor suppressor NM23-H1 is a granzyme A-activated DNase during CTL-

mediated apoptosis, and the nucleosome assembly protein SET is its inhibitor. *Cell* **112**, 659-672.

Franchi L, Eigenbrod T, Munoz-Planillo R and Nunez G (2009) The inflammasome: a caspase-1- activation platform that regulates immune responses and disease pathogenesis. *Nat Immunol* **10**, 241-247.

Fuchs Y and Steller H (2011) Programmed cell death in animal development and disease. *Cell* **147**, 742-758.

Fukuda R, Zhang H, Kim JW, Shimoda L, Dang CV and Semenza GL (2007) HIF-1 regulates cytochrome oxidase subunits to optimize efficiency of respiration in hypoxic cells. *Cell* **129**, 111-122.

Galluzzi L, Vitale I, Abrams JM, Alnemri ES, Baehrecke EH, Blagosklonny MV, Dawson TM, Dawson VL, El-Deiry WS, Fulda S, Gottlieb E, Green DR, Hengartner MO, Kepp O, Knight RA, Kumar S, Lipton SA, Lu X, Madeo F, Malorni W, Mehlen P, Nuñez G, Peter ME, Piacentini M, Rubinsztein DC, Shi Y, Simon HU, Vandenabeele P, White E, Yuan J, Zhivotovsky B, Melino G and Kroemer G (2012) Molecular definitions of cell death subroutines: recommendations of the Nomenclature Committee on Cell Death 2012. *Cell Death Differ* **19**, 107-120.

García-Heredia JM, Díaz-Moreno I, Nieto PM, Orzáez M, Kocanis S, Teixeira M, Pérez-Payá M, Díaz-Quintana A and De la Rosa MA (2010) Nitration of tyrosine 74 prevents human cytochrome *c* to play a key role in apoptosis signaling by blocking caspase-9 activation. *Biochim Biophys Acta – Bioenerg* **1797**, 981-993.

García-Heredia JM, Díaz-Quintana A, Salzano M, Orzáez M, Pérez-Payá E, Texeira M, De la Rosa MA and Díaz-Moreno I (2011) Tyrosine phosphorylation turns alkaline transition into a biologically relevant process and makes human cytochrome *c* behave as an anti-apoptotic switch. *J Biol Inorg Chem* **16**, 1155-1156.

García-Heredia JM, Díaz-Moreno I, Díaz-Quintana A, Orzáez M, Navarro JA, Hervás, M and De la Rosa MA (2012) Specific nitration of tyrosines 46

and 48 makes cytochrome *c* assemble a non-functional apoptosome. *FEBS Lett* **586**, 154-158.

Gao W, Pu Y, Luo KQ and Chang DC (2001) Temporal relationship between cytochrome *c* release and mitochondrial swelling during UV-induced apoptosis in living HeLa cells. *J Cell Sci* **114**, 2855-2862.

Gao L, Laude K and Cai H (2008) Mitochondrial pathophysiology, reactive oxygen species, and cardiovascular diseases. *Vet Clin North Am Small Anim Pract* **38**, 137-155.

Ge J, Wu H and Yao SQ (2010) An unnatural amino acid that mimics phosphotyrosine. *Chem Commun (Camb)* **46**, 2980-2982.

Genova ML, Baracca A, Biondi A, Casalena G, Faccioli M, Falasca AI, Formiggini G, Sgarbi G, Solaini G and Lenaz G (2008) Is supercomplex organization of the respiratory chain required for optimal electron transfer activity? *Biochim Biophys Acta – Bioenerg* **1777**, 740-746.

Genova ML and Lenaz G (2014) Functional role of mitochondrial respiratory supercomplexes. *Biochim Biophys Acta – Bioenerg* **1837**, 427-443.

Gilchrist DG (1998) Programmed cell death in plant disease: the purpose and promise of cellular suicide. *Annu Rev Phytopathol* **36**, 393-414.

González-Arzola K, Díaz-Moreno I, Cano-González A, Díaz-Quintana A, Velázquez-Campoy A, Moreno-Beltrán B, López-Rivas A and De la Rosa MA (2015) Structural basis for inhibition of the histone chaperone activity of SET/TAF-Iβ by cytochrome *c*. *Proc Natl Acad Sci USA* **112**, 9908-9913.

Gonzalvez F, Bessoule JJ, Rocchiccioli F, Manon S and Petit PX (2005) Role of cardiolipin on tBid and tBid/Bax synergistic effects on yeast mitochondria. *Cell Death Differ* **12**, 659-667.

Glick D, Barth S and Macleod KF (2020) Autophagy: cellular and molecular mechanisms. *J Pathol* **221**, 3-12.

Green DR and Reed JC (1998) Mitochondria and apoptosis. *Science* **281,** 1309-1312.

Hackenbrock CR, Chazotte B and Gupte SS (1986) The random collision model and a critical assessment of diffusion and collision in mitochondrial electron transport. *J Bioenerg Biomembr* **18**, 331-368.

Hannibal L, Tomasina F, Capdevila DA, Demicheli V, Tórtora V, Alvarez-Paggi D, Jemmerson R, Murgida DH and Radi R (2016) Alternative conformations of cytochrome *c*: Structure, function, and detection. *Biochemistry* **55**, 407-428.

Hatefi Y (1985) The mitochondrial electron transport and oxidative phosphorylation system. *Annu Rev Biochem* **54**, 1015-1069.

Hayashi T, Asano Y, Shintani Y, Aoyama H, Kioka H, Tsukamoto O, Hikita M, Shinzawa-Itoh K, Takafuji K, Higo S, Kato H, Yamazaki S, Matsuoka K, Nakano A, Asanuma H, Asakura M, Minamino T, Goto Y, Ogura T, Kitakaze M, Komuro I, Sakata Y, Tsukihara T, Yoshikawa S and Takashima S (2015) Higd1a is a positive regulator of cytochrome *c* oxidase. *Proc Natl Acad Sci USA* **112**, 1553-1558.

Hochman J, Ferguson-Miller S and Schindler M (1985) Mobility in the mitochondrial electron transport chain. *Biochemistry* **24**, 2509-2516.

Hunter T (2009) Tyrosine phosphorylation: thirty years and counting. *Curr Opin Cell Biol* **21**, 140-146.

Hüttemann M, Lee I, Pecinova A, Pecina P, Przyklenk K and Doan JW (2008) Regulation of oxidative phosphorylation, the mitochondrial membrane potential, and their role in human disease. *J Bioenerg Biomembr* **40**, 445-456.

Hüttemann M, Pecina P, Rainbolt M, Sanderson TH, Kagan VE, Samavati L, Doan JW and Lee I (2011) The multiple functions of cytochrome *c* and their regulation in life and death decisions of the mammalian cell: From respiration to apoptosis. *Mitochondrion* **11,** 369-381.

Hüttemann M, Lee I, Grossman LI, Doan JW and Sanderson TH (2012) Phosphorylation of mammalian cytochrome *c* and cytochrome *c* oxidase in the regulation of cell destiny: respiration, apoptosis, and human disease. *Adv. Exp. Med. Biol*. **748**, 237-264.

Ingley E (2012) Functions of the Lyn tyrosine kinase in health and disease. *Cell Commun Signal* **10**, 21.

Inoue H and Tani K (2014) Multimodal immunogenic cancer cell death as a consequence of anticancer cytotoxic treatments. *Cell Death Differ* **21**, 39-49.

Iverson SL and Orrenius (2004) The cardiolipin-cytochrome c interaction and the mitochondrial regulation of apoptosis. *Arch Biochem Biophys* **423**, 37-46.

Jemmerson R, Liu J, Hausauer D, Lam KP, Mondino A and Nelson RDA (1999) Conformational change in cytochrome *c* of apoptotic and necrotic cells is detected by monoclonal antibody binding and mimicked by association of the native antigen with synthetic phospholipid vesicles. *Biochemistry* **38**, 3599-3609.

Jeng, WY, Chen CY, Chang HC, Chuang WJ (2002) Expression and characterization of recombinant human cytochrome *c* in *E. coli*. *J Bioenerg Biomembr* **34**, 423-431.

Jiang X and Wang X (2004) Cytochrome-*c*-mediated apoptosis. *Annu Rev Biochem* **9**, 205-219.

Kagan VE, Tyurin VA, Jiang J, Tyurina YY, Ritov VB, Amoscato AA, Osipov AN, Belikova NA, Kapralov AA, Kini V, Vlasova II, Zhao Q, Zou M, Di P, Svistunenko DA, Kurnikov IV and Borisenko GG (2005) Cytochrome *c* acts as a cardiolipin oxygenase required for release of proapoptotic factors. *Nat Chem Biol* **1**, 223-232.

Kennaway NG, Carrero-Valenzuela RD, Ewart G, Balan VK, Lightowlers R, Zhang YZ, Powell BR, Capaldi RA and Buist NR (1990) Isoforms of

mammalian cytochrome c oxidase: correlation with human cytochrome c oxidase deficiency. *Pediatr Res* **28**, 529-535.

Kepp O, Galluzzi L, Zitvogel L and Kroemer G (2010) Pyroptosis - a cell death modality of its kind? *Eur J Immunol* **40**, 627-630.

Kerr JF, Wyllie AH and Currie AR (1972) Apoptosis: a basic biological phenomenon with wide-ranging implications in tissue kinetics. *Br J Cancer* **26**, 239-257.

Kim NH, Jeong MS, Choi SY and Kang JH (2004) Peroxidase activity of cytochrome *c*. *Bull Korean Chem Soc* **25**, 1889-1892.

Konermann L, Collings BA and Douglas DJ (1997) Cytochrome *c* folding kinetics studied by time-resolved electrospray ionization mass spectrometry. *Biochemistry* **36**, 5554-5559.

Kluck RM, Ellerby LM, Ellerby HM, Naiem S, Yaffe MP, Margoliash E, Bredesen D, Mauk AG, Sherman F and Newmeyer DD (2000) Determinants of cytochrome *c* pro-apoptotic activity. The role of lysine 72 trimethylation. *J Biol Chem* **275**, 16127-16133.

Krause F, Scheckhuber CQ, Werner A, Rexroth S, Reifschneider NH, Dencher NA and Osiewacz HD (2004a) Supramolecular organization of cytochrome *c* oxidase- and alternative oxidase-dependent respiratory chains in the filamentous fungus *Podospora anserine*. *J Biol Chem* **279**, 26453-26461.

Krause F, Reifschneider NH, Vocke D, Seelert H, Rexroth S and Dencher NA (2004b) “Respirasome”-like supercomplexes in green leaf mitochondria of spinach. *J Biol Chem* **279**, 48369-48375.

Kruidering M and Evan GI (2000) Caspase-8 in apoptosis: the beginning of "the end"? *IUBMB Life* **50**, 85-90.

Lange C and Hunte C (2002) Crystal structure of the yeast cytochrome bc_1 complex with its bound substrate cytochrome *c*. *Proc Natl Acad Sci USA* **99**, 2800-2805.

Lapuente-Brun E, Moreno-Loshuertos R, Acín-Pérez R, Latorre-Pellicer A, Colás C, Balsa E, Perales-Clemente E, Quirós PM, Calvo E, Rodríguez-Hernández MA, Navas P, Cruz R, Carracedo Á, López-Otín C, Pérez-Martos A, Fernández-Silva P, Fernández-Vizarra E and Enríquez JA (2013) Supercomplex assembly determines electron flux in the mitochondrial electron transport chain. *Science* **340**, 1567-1570.

Lawrence A, Jones CM, Wardman P and Burkitt MJ (2003) Evidence for the role of a peroxidase compound I-type intermediate in the oxidation of glutathione, NADH, ascorbate, and dichlorofluorescin by cytochrome *c*/H_2O_2 implications for oxidative stress during apoptosis. *J Biol Chem* **278**, 29410-29419.

Lee I, Salomon AR, Yu K, Doan JW, Grossma LI and Hüttemann M (2006) New prospects for an old enzyme: mammalian cytochrome *c* is tyrosine-phosphorylated *in vivo*. *Biochemistry* **45**, 9121-912.

Lee I and Hüttemann M (2014) Energy crisis: the role of oxidative phosphorylation in acute inflammation and sepsis. *Biochim Biophys Acta – Mol Basis Dis* **1842**, 1579-1586.

Lenaz G and Genova ML (2010) Structure and organization of mitochondrial respiratory complexes: a new understanding of an old subject. *Antioxid Redox Signal* **12**, 961-1008.

Lenaz G and Genova ML (2012) Supramolecular organisation of the mitochondrial respiratory chain: a new challenge for the mechanism and control of oxidative phosphorylation. *Adv Exp Med Biol* 748 107-144

Li P, Nijhawan D, Budihardjo I, Srinivasula SM, Ahmad M, Alnemri ES and Wang X (1997) Cytochrome *c* and dATP-dependent formation of Apaf-1/caspase-9 complex initiates an apoptotic protease cascade. *Cell* **91**, 479-489.

Li H, Zhu H, Xu CJ and Yuan J (1998) Cleavage of BID by caspase 8 mediates the mitochondrial damage in the Fas pathway of apoptosis. *Cell* **94**, 491-501.

Liesa M and Shirihai OS (2013) Mitochondrial dynamics in the regulation of nutrient utilization and energy expenditure. *Cell Metab* **17**, 491-506.

Liu J, Durrant D, Yang HS, He Y, Whitby FG, Myszka DG and Lee RM (2005) The interaction between tBid and cardiolipin or monolysocardiolipin. *Biochem Biophys Res Commun* **330**,865-870.

Liu BA and Nash PD (2012) Evolution of SH2 domains and phosphotyrosine signalling networks. *Philos Trans R Soc Lond B Biol Sci* **367**, 2556-2573.

Locksley RM, Killeen N and Lenardo MJ (2001) The TNF and TNF receptor superfamilies: integrating mammalian biology. *Cell* **104**, 487-501.

Logue SE and Martin SJ (2008) Caspase activation cascades in apoptosis. *Biochem Soc Trans* **36**, 1-9.

Ly HK, Utesch T, Díaz-Moreno I, García-Heredia JM, De La Rosa MA and Hildebrandt P (2012) Perturbation of the redox site structure of cytochrome *c* variants upon tyrosine nitration. *J. Phys. Chem. B* **116**, 5694-5702.

MacMillan-Crow LA, Cruthirds DL, Ahki KM, Sanders PW and Thompson JA (2001) Mitochondrial tyrosine nitration precedes chronic allograft nephropathy. *Free Radic Biol Med* **31**, 1603-1608.

Martinvalet D, Zhu P and Lieberman J (2005) Granzyme A induces caspase-independent mitochondrial damage, a required first step for apoptosis. *Immunity* **22**, 355-370.

Martínez-Fábregas J, Díaz-Moreno I, González-Arzola K, Janocha S, Navarro JA, Hervás M, Bernhardt R, Díaz-Quintana A and De la Rosa MA (2013) New Arabidopsis thaliana cytochrome *c* partners: a look into the elusive role of cytochrome c in programmed cell death in plants. *Mol Cell Proteomics* **12**, 3666-3676.

Martínez-Fábregas J, Díaz-Moreno I, González-Arzola K, Janocha S, Navarro JA, Hervás M, Bernhardt R, Díaz-Quintana A and De la Rosa MA

(2014a) Structural and functional analysis of novel human cytochrome c targets in apoptosis. *Mol Cell Proteomics* **13**, 1439-1456.

Martínez-Fábregas J, Díaz-Moreno I, González-Arzola K, Díaz-Quintana A and De la Rosa MA (2014b) A common signalosome for programmed cell death in humans and plants. *Cell Death Dis* **5**, e1314.

Monari S, Battistuzzi G, Bortolotti CA, Yanagisawa S, Sato K, Li C, Salard I, Kostrz D, Borsari M, Ranieri A, Dennison C and Sola M (2012) Understanding the mechanism of short-range electron transfer using an immobilized cupredoxin. *J Am Chem Soc* **134**, 11848-11851.

Nakagawa H, Komai N, Takusagawa M, Miura Y, Toda T, Miyata N, Ozawa T and Ikota N (2007) Nitration of specific tyrosine residues of cytochrome C is associated with caspase-cascade inactivation. *Biol Pharm Bull* **30**, 15-20.

Namura S, Zhu J, Fink K, Endres M, Srinivasan A, Tomaselli KJ, Yuan J and Moskowitz MA (1998) Activation and cleavage of caspase-3 in apoptosis induced by experimental cerebral ischemia. *J Neurosci* **18**, 3659-3668.

Nogués I, Martínez-Júlvez M, Navarro JA, Hervás M, Armenteros L, de la Rosa MA, Brodie TB, Hurley JK, Tollin G, Gómez-Moreno C and Medina M (2003) Role of hydrophobic interactions in the flavodoxin mediated electron transfer from photosystem I to ferredoxin-NADP+ reductase in Anabaena PCC 7119. *Biochemistry* **42**, 2036-2045.

Nooren IM and Thornton JM (2003) Diversity of protein-protein interactions. *EMBO J*. **22**, 3486-3492.

Nur-E-Kamal A, Gross SR, Pan Z, Balklava Z, Ma J and Liu LF (2004) Nuclear translocation of cytochrome c during apoptosis. *J Biol Chem* **279**, 24911-24914.

Oursler MJ, Bradley EW, Elfering SL and Giulivi C (2004) Native, not nitrated, cytochrome *c* and mitochondria-derived hydrogen peroxide drive osteoclast apoptosis. *Am J Physiol - Cell Physiol* **288**, C156-C168.

Ow YP, Green DR, Hao Z and Mak TW (2008) Cytochrome *c*: functions beyond respiration. *Nature* **9**, 532-542

Pandiscia LA and Schweitzer-Stenner R (2015) Coexistence of native-like and non-native cytochrome *c* on anionic liposomes with different cardiolipin content. *J Phys Chem B* **119**, 1334-1349.

Pecina P, Borisenko GG, Belikova NA, Tyurina YY, Pecinova A, Lee I, Samhan-Arias AK, Przyklenk K, Kagan VE and Hüttemann M (2010) Phosphomimetic substitution of cytochrome *c* tyrosine 48 decreases respiration and binding to cardiolipin and abolishes ability to trigger downstream caspase activation. *Biochemistry* **49**, 6705-6714.

Perl A, Gergely P Jr, Nagy G, Koncz A and Banki K (2004) Mitochondrial hyperpolarization: a checkpoint of T-cell life, death and autoimmunity. *Trends Immunol* **25**, 360-367.

Polevoda B, Martzen MR, Das B, Phizicky EM and Sherman F (2000) Cytochrome *c* methyltransferase, Ctm1p, of yeast. *J Biol Chem* **275**, 20508-20513.

Porter AG and Jänicke RU (1999) Emerging roles of caspase-3 in apoptosis. *Cell Death Differ* **6**, 99-104.

Puchkov MN, Vassarais RA, Korepanova EA and Osipov AN (2015) Cytochrome *c* produces pores in cardiolipin-containing planar bilayer lipid membranes in the presence of hydrogen peroxide. *Biochim Biophys Acta* – Biomembr **1828**, 208-201.

Puttick J, Baker EN and Delbaere LT (2008) Histidine phosphorylation in biological systems. *Biochim Biophys Acta – Proteins Proteomics* **1784**, 100-105.

Rackovsky S and Goldstein DA (1984) On the redox conformational change in cytochrome *c*. *Proc Natl Acad Sci U S A*. **81**, 5901-5905.

Radi R, Thomson L, Rubbo H and Prodanov E (1991) Cytochrome *c*-catalyzed oxidation of organic molecules by hydrogen peroxide. *Arch Biochem Biophys* **288**, 112-117.

Radi R (2012) Protein tyrosine nitration: Biochemical mechanisms and Structural Basis of its Functional Effects. *Acc Chem Res*, **45**, 550–559.

Rajagopal BS, Silkstone GG, Nicholls P, Wilson MT and Worrall JA (2012) An investigation into a cardiolipin acyl chain insertion site in cytochrome *c*. *Biochim Biophys Acta – Bioenerg* **1817**, 780-791.

Ramírez-Aguilar SJ, Keuthe M, Rocha M, Fedyaev VV, Kramp K, Gupta KJ, Rasmusson AG, Schulze WX and van Dongen JT (2011) The composition of plant mitochondrial supercomplexes changes with oxygen availability. *J Biol Chem* **286,** 43045-43053.

Rego AC, Vesce S and Nicholls DG (2001) The mechanism of mitochondrial membrane potential retention following release of cytochrome *c* in apoptotic GT1-7 neural cells. *Cell Death Differ*. **8**, 995-1003.

Riedl SJ and Shi Y (2004) Molecular mechanisms of caspase regulation during apoptosis. Nature reviews. *Nat Rev Mol Cell Biol* **5**, 897-907.

Sanderson TH, Mahapatra G, Pecina P, Ji Q, Yu K, Sinkler C, Varughese A, Kumar R, Bukowski MJ, Tousignant RN *et al*. (2013) Cytochrome *c* is tyrosine 97 phosphorylated by neuroprotective insulin treatment. *PLoS One* **8**, e78627.

Sakamoto K, Kamiya M, Imai M, Shinzawa-Itoh K, Uchida T, Kawano K, Yoshikawa S and Ishimori K (2011) NMR basis for interprotein electron transfer gating between cytochrome c and cytochrome *c* oxidase. *Proc Natl Acad Sci USA* **108**, 12271-12276.

Schägger H and Pfeiffer K (2000) Supercomplexes in the respiratory chains of yeast and mammalian mitochondria. *EMBO J* **19**, 1777-1783.

Schägger H (2002) Respiratory chain supercomplexes of mitochondria and bacteria. *Biochim Biophys Acta – Bioenerg* **1555**, 154-159.

Schreiber G and Keating AE (2011) Protein binding specificity *versus* promiscuity. *Curr Opin Struct Biol* **21**, 50-61.

Sefton BM, Hunter T, Beemon K, Eckhart W (1980) Evidence that the phosphorylation of tyrosine is essential for cellular transformation by Rous sarcoma virus. *Cell* **20**, 807-816.

Shay J, Elbaz HA, Lee I, Zielske SP, Malek MH and Hüttemann M (2015) Molecular mechanisms and therapeutic effects of (−)-epicatechin and other polyphenols in cancer, inflammation, diabetes, and neurodegeneration. *Oxid Med Cell Longev* **2015**, 181260.

Shoubridge EA (2012) Supersizing the mitochondrial respiratory chain. *Cell Metab* **15**, 271-272.

Sinibaldi F, Howes BD, Piro MC, Polticelli F, Bombelli C, Ferri T, Coletta M, Smulevich G, Santucci R (2010) Extended cardiolipin anchorage to cytochrome c: a model for protein-mitochondrial membrane binding. *J Biol Inorg Chem* **15**, 689-700.

Sinibaldi F, Howes BD, Droghetti E, Polticelli F, Piro MC, Di Pierro D, Fiorucci L, Coletta M, Smulevich G and Santucci R (2013) Role of lysines in cytochrome *c*-cardiolipin interaction. *Biochemistry* **52**, 4578-4588.

Spooner PJ and Watts A (1991) Reversible unfolding of cytochrome *c* upon interaction with cardiolipin bilayers. Evidence from deuterium NMR measurements. *Biochemistry* **30**, 3871-3879.

Speck SH, Dye D and Margoliash E (1984) Single catalytic site model for the oxidation of ferrocytochrome *c* by mitochondrial cytochrome *c* oxidase. *Proc Natl Acad Sci USA* **81**, 347-351.

Storz P (2007) Mitochondrial ROS--radical detoxification, mediated by protein kinase D. *Trends Cell Biol* **17**, 13-18.

Strogolova V, Furness A, Robb-McGrath M, Garlich J and Stuart RA (2012) Rcf1 and Rcf2, members of the hypoxia-induced gene 1 protein family, are critical components of the mitochondrial cytochrome bc_1-cytochrome *c* oxidase supercomplex. *Mol Cell Biol* **32**, 1363-1373.

Su J and Groves JT (2010) Mechanisms of peroxynitrite interactions with heme proteins. *Inorg Chem* **49**, 6317-6329.

Szymanski CM and Wren BW (2005) Protein glycosylation in bacterial mucosal pathogens. *Nat. Rev. Microbiol.* **3**, 225-237.

Trapani JA and Smyth MJ (2002) Functional significance of the perforin/granzyme cell death pathway. *Nat Rev Immunol* **2**, 735-747.

Trouillard M, Meunier B, Rappaport F (2011) Questioning the functional relevance of mitochondrial supercomplexes by time-resolved analysis of the respiratory chain. *Proc Natl Acad Sci USA* **108**, E1027- E1034.

Vandenabeele P, Galluzzi L, Vanden Berghe T and Kroemer G (2010) Molecular mechanisms of necroptosis: an ordered cellular explosion. *Nat Rev Mol Cell Biol* **11**, 700-714.

Vik SB, Georgevich G and Capaldi RA (1981) Diphosphatidylglycerol is required for optimal activity of beef heart cytochrome *c* oxidase. *Proc Natl Acad Sci US* **78**, 1456-1460.

Vila M and Przedborski S (2003) Targeting programmed cell death in neurodegenerative diseases. *Nat Rev Neurosci* **4**, 365-375.

Volkov AN, Worrall JA, Holtzmann E and Ubbink M (2006) Solution structure and dynamics of the complex between cytochrome *c* and cytochrome *c* peroxidase determined by paramagnetic NMR. *Proc Natl Acad Sci USA* **103**, 18945-18950.

Vukotic M, Oeljeklaus S, Wiese S, Vögtle FN, Meisinger C, Meyer HE, Zieseniss A, Katschinski DM, Jans DC, Jakobs S, Warscheid B, Rehling P and Deckers M (2012) Rcf1 mediates cytochrome oxidase assembly and

respirasome formation, revealing heterogeneity of the enzyme complex. *Cell Metab* **15**, 336-347.

Wang YC, Peterson SE and Loring JF (2004) Protein post-translational modifications and regulation of pluripotency in human stem cells. *Cell Res* **24**, 143-160.

Wilson MT and Greenwood C (1996) *Cytochrome c: a multidisciplinary approach* (Eds: Scott RA and Mauk AG) University Science Books, Sausilito, pp. 611-634.

Xie J, Supekova L and Schultz PG (2007) A genetically encoded metabolically stable analogue of phosphotyrosine in *Escherichia coli*. *J Am Chem Soc* **2**, 474-478.

Yin T, Zhong F, Xie J, Feng Y, Wang Z-H, Huang Z-X and Tan X (2009) Evolutionary alkaline transition in human cytochrome *c*. *J Bioenerg Biomembr* **41**, 251-257.

Ying T, Zhong F, Xie J, Feng Y, Wang ZH, Huang ZX and Tan X (2009) Evolutionary alkaline transition in human cytochrome *c*. *J Bioenerg Biomembr* **41**, 251-257.

Yu CA, Yu L and King TE (1973) Kinetics of electron transfer between cardiac cytochrome c_1 and *c*. *J Biol Chem* **248**, 528-533.

Yu A and Yu L (1980) Resolution and reconstitution of succinate-cytochrome *c* reductase: preparations and properties of high purity succinate dehydrogenase and ubiquinol-cytochrome *c* reductase. *Biochim Biophys Acta – Bioenerg* **591**, 409-420.

Yu H, Lee I, Salomon AR, Yu K and Hüttemann M (2008) Mammalian liver cytochrome *c* is tyrosine-48 phosphorylated *in vivo*, inhibiting mitochondrial respiration. *Biochim Biophys Acta – Bioenerg* **1777**, 1066-1071.

Yuan J (2009) Neuroprotective strategies targeting apoptotic and necrotic cell death for stroke. *Apoptosis* **14**, 469-477.

Zhou M, Li Y, Hu Q, Bai XC, Huang W, Yan C, Scheres SH and Shi Y (2015) Atomic structure of the apoptosome: mechanism of cytochrome *c* and dATP-mediated activation of Apaf-1. *Genes Dev* **29**, 2349-2361.

Zou H, Li Y, Liu X and Wang X. (1999) An APAF-1·cytochrome *c* multimeric complex is a functional apoptosome that activates procaspase-9. *J Biol Chem* **274**, 11549-11556.

10. APPENDIX I

Journal papers

1. **Guerra-Castellano A**, Díaz-Moreno I, Velázquez-Campoy A, De la Rosa MA, Díaz-Quintana A (2016) Structural and functional characterization of phosphomimetic mutants of cytochrome *c* at threonine 28 and serine 47. *Biochim Biophys Acta – Bioenerg* **1857**, 387-395.
   Impact Factor 2015: 5.353

2. **Guerra-Castellano A**, Díaz-Quintana A, Moreno-Beltrán B, López-Prados J, Nieto PM, Meister W, Staffa J, Teixeira M, Hildebrandt P, De la Rosa MA, Díaz-Moreno I (2015) Mimicking tyrosine phosphorylation in human cytochrome *c* by the evolved tRNA synthetase technique. *Chem Eur J* **21**, 15004-15012. Impact Factor 2014/2015: 5.731

11. APPENDIX II

PhD candidate contribution:

Performed cloning, expression and purification of the Y48*p*CMF and WT C*c* species and plant Cc_1. Performed NMR titrations. Recorded XAS spectra. Recorded ITC experiments. Measured C*c*O activity and analyzed supercomplexes assembly. Performed peroxidase and caspase activity assays. Wrote the paper and was involved in planning the experiments and in the discussion of results.

Structural Basis of Mitochondrial Dysfunction in Response to Cytochrome *c* Phosphorylation at position 48

Blas Moreno-Beltrán[1,6], Alejandra Guerra-Castellano[1,6], Antonio Díaz-Quintana[1],
Rebecca Del Conte[2], Sofía M. García-Mauriño[1], Sofía Díaz-Moreno[3], Katiuska González-Arzola[1], Carlos Santos-Ocaña[4], Adrián Velázquez-Campoy[5], Miguel A. De la Rosa[1], Paola Turano[2] & Irene Díaz-Moreno[1]

[1]Instituto de Investigaciones Químicas, cicCartuja, Universidad de Sevilla – CSIC, Avda. Américo Vespucio 49, 41092 Seville (Spain).
[2]Magnetic Resonance Center (CERM) – Department of Chemistry, University of Florence, Via Luigi Sacconi 6, 50019 Sesto Fiorentino, Florence (Italy).
[3]Diamond Light Source Ltd., Harwell Science and Innovation Campus, Didcot, Oxfordshire OX11 0DE (United Kingdom).
[4]Centro Andaluz de Biología del Desarrollo, Universidad Pablo de Olavide – CSIC, and CIBERER Instituto de Salud Carlos III, Carretera de Utrera km. 1, 41013 Seville (Spain).
[5]Institute of Biocomputation and Physics of Complex Systems (BIFI), Joint Unit BIFI-IQFR (CSIC), Universidad de Zaragoza, Mariano Esquillor s/n, 50018 Zaragoza (Spain); Aragon Institute for Health Research (IIS Aragon), Avda. San Juan Bosco 13, 50009 Zaragoza, Spain; Fundacion ARAID, Government of Aragon, Maria de Luna 11, 50018 Zaragoza (Spain).
[6]These authors contribute equally to this work.

Correspondence should be addressed to I. D.-M. (idiazmoreno@us.es)
Telephone number: +34 954489513; Fax number: +34 954460065

ABSTRACT

Regulation of mitochondrial activity allows cells to adapt to changing conditions and to control oxidative stress, and its dysfunction can lead to hypoxia-dependent pathologies, such as ischemia and cancer. Although cytochrome *c* phosphorylation—in particular, at tyrosine 48—is a key modulator of mitochondrial signaling, its action and molecular basis remain unknown. Here, we mimic phosphorylation of cytochrome *c* by replacing tyrosine 48 with *p*-carboxy-methyl-L-phenylalanine (*p*CMF). The NMR structure of the resulting mutant reveals significant conformational shifts and enhanced dynamics around *p*CMF that could explain changes observed in its functionality: the phosphomimetic mutation impairs cytochrome *c* diffusion between respiratory complexes, enhances hemeprotein peroxidase and cardiolipin oxidation activities and hinders caspase-dependent apoptosis. Our findings provide a framework to further investigate the modulation of mitochondrial activity by phosphorylated cytochrome *c* and to develop novel therapeutic approaches based on its pro-survival effects.

INTRODUCTION

Oxidative phosphorylation (OxPhos) relies on the electron transport chain (ETC) to generate the membrane potential that drives ATP synthesis (Papa, 1982). Components of the ETC oxidize substrates to reduce molecular oxygen, thereby producing water. Nevertheless, around 2% of the electrons flowing across the ETC yield reactive oxygen species (ROS) (Turrens, 2003). ROS are a source of oxidative stress and act as signaling molecules at low concentrations (Ray *et al*., 2012; Lenaz and Genova, 2010; Hou *et al*., 2014). Hindering redox reactions within the distinct ETC membrane complexes (complexes I to V) leads to enhanced ROS production (Solaini *et al*., 2010). The activity of the ETC is tightly regulated by posttranslational modifications of its components, isoform swapping and modulation of the equilibria for the association of the membrane protein complexes into supercomplexes (Lenaz and Genova, 2010; Lezan *et al*., 2010). Such associations allow substrate channeling while modulating ROS production (Lenaz and Genova, 2010; Lezan et al., 2010).

Oxidative stress response involves redox signals modulating protein phosphorylation (Corcoran and Cotter, 2013). In the ETC, the major phosphorylation targets are NADH:UQ oxidoreductase, cytochrome *c* (C*c*) and cytochrome *c* oxidase (C*c*O) (Helling *et al*., 2012). Besides being essential for oxidative respiration (**Figure 1a**), C*c* acts as a redox regulatory protein within the mitochondrial intermembrane space (Díaz-Moreno *et al.*, 2011a). In addition, C*c* aids to control ROS levels by oxidizing superoxide anions (Wegerich et al., 2009) and exhibiting peroxidase activity (Florence, 2009); the latter, however, also yields lipid peroxidation (Radi *et al*., 2009; Radi *et al*., 1991). Furthermore, C*c* plays a crucial role in programmed cell death, a process that is only in partially understood (Martinou *et al.*, 2000; Basova *et al.*, 2007; Kagan *et al*., 2009; Bertini *et al*., 2011; Martínez-Fábregas *et al.*, 2013; Martínez-Fábregas *et al.*, 2014; González-Arzola *et al*., 2015). In this context, a fraction of C*c* binds and oxidizes cardiolipin (CL) at the internal mitochondrial membrane, thereby facilitating the release of unbound C*c* to the

cytoplasm (Basova *et al.*, 2007; Kagan *et al.*, 2009). In mammalian cells, extramitochondrial C*c* interacts with apoptosis activating factor-1 (Apaf-1) in the cytoplasm to spark the caspase proteolytic cascade (Martinou *et al*., 2000). It has recently been shown that C*c* can interact with several other proteins outside the mitochondria in humans and plants (Bertini *et al*., 2011; Martínez-Fábregas *et al.*, 2013; Martínez-Fábregas *et al.*, 2014a; González-Arzola *et al*., 2015).. The similarities between the C*c* signaling networks in both organisms suggest that key programmed cell death pathways are conserved along evolution (Martínez-Fábregas *et al.*, 2014b).

C*c* phosphorylation is an alleged modulator of the mitochondrial cell death pathway (Hüttemann *et al*., 2008; Hüttemann *et al*., 2012). Its deregulation is believed to be related to the onset of neurological disorders and cancer (Hüttemann *et al*., 2012). Phosphorylation of C*c* is easily reversed by phosphatases, hampering the isolation of the modified protein from tissues (Kadenbach, 1968). Tyr-to-Glu substitutions of C*c* designed to emulate Tyr48 phosphorylation impair both electron transport to C*c*O and triggering of caspase-9 mediated by Apaf-1 under *in vitro* conditions (Pecina *et al*., 2010; García-Heredia *et al*., 2011). Notably, nitration of this residue also hinders the ability of C*c* to activate Apaf-1 (Díaz-Moreno *et al.*, 2011b; García-Heredia *et al*., 2012; Ly *et al*., 2012). Thus, these posttranslational modifications alter both mitochondrial and cytoplasmic functions of C*c*. Tyr48 phosphorylation also affects the spectroscopic and other physical-chemical properties of C*c* (García-Heredia *et al*., 2011; Díaz-Moreno *et al.*, 2011b; García-Heredia *et al*., 2012; Ly *et al*., 2012; Guerra-Castellano *et al*., 2015). Understanding the origin of these effects and how they help modulate C*c* activity requires the 3D conformation of the phosphorylated species. However, deciphering the effects of Tyr48 phosphorylation on the structure and dynamics of C*c* is highly challenging. Indeed, no atomic resolution structure has been reported for either phosphorylated C*c* or any reliable mimic mutant.

Here, we have elucidated the structure of a phosphomimetic C*c* variant in which Tyr48 is replaced by the synthetic, non-canonical amino-acid *p*-carboxy-methyl-L-phenylalanine (*p*CMF). We show that such a replacement induces local perturbations of the C*c* structure and enhanced internal dynamics of the mutation surroundings. We used biochemical assays to show that the Y48*p*CMF mutation impairs C*c* channeling between cytochrome bc_1 (Cbc_1) and C*c*O, enhances the peroxidase activity and CL oxidation capability of C*c* and induces an anti-apoptotic function of C*c*.

RESULTS

Phosphorylation of Tyr48 induces local structural changes in cytochrome *c*

To understand how phosphorylation affects the structure of human C*c*, we tackled the challenge of fully characterizing the phosphomimetic mutant Y48*p*CMF C*c* in its reduced form, which is the redox state of C*c* donating electrons to C*c*O in homeostasis and is essential for the apoptotic activity. Y48*p*CMF C*c* maintains the overall secondary structure and global fold of wild-type (WT) C*c,* as inferred from circular dichroism (CD) (**Figure 1b**) and ^{1}H-^{15}N heteronuclear single-quantum correlation (HSQC) nuclear magnetic resonance (NMR) spectra (**Figure 1c**), respectively. Also, the heme axial coordination was preserved, as indicated by 1D ^{1}H NMR data (**Figure 1d**). The NMR spectra of reduced Y48*p*CMF C*c* were extensively assigned: triple-resonance experiments (**Table supplement 1**) allowed us to detect and assign 91 backbone amide signals and the sequential connectivities for most residues of the protein. Aliphatic side-chain signals were assigned using 3D HBHA(CO)NH and 3D HCCH-TOCSY experiments, leading to the assignment of most (96.4%) of the side-chain proton resonances. The ^{15}N-H resonance of *p*CMF48 was undetectable because the residue was not ^{15}N-enriched. Four proline residues (Pro30, Pro44, Pro71 and Pro76) interrupt the sequential HN-HN connectivity. Additionally, in contrast to WT C*c*, we could not detect the amide protons of the Thr49, Ala51, Gly56 and Ile57

residues. However, the WT spectra also only had four amide protons that could not be detected (Gly1, Glu21, Thr28 and Gly84) under similar experimental conditions. Further, in contrast to WT C*c*, the signals from Asn31, Gly45 and Ser47 in *p*CMF48 C*c* were significantly weaker than the rest. The largest chemical shift perturbations for backbone amides induced by the modified residue at position 48 are confined to nearby residues (**Figure1—Figure supplement 1**).

Assigning ^{1}H resonances to the heme substituents and ^{1}H (and ^{13}C) signals to the aromatic side chains was required for analyzing additional 2D maps (*i.e.* COSY and ^{1}H-^{15}N NOESY) (**Table supplement 1**). Assignment of the Cδ_1, Cδ_2, Cε_1 and Cε_2 aromatic signals from the *p*CMF48 side-chain required the acquisition of an aromatic ^{1}H-^{13}C HSQC spectrum recorded in a natural abundance of ^{13}C (**Figure 1e**). The assignment strategy for the *p*CMF48 side-chain also included the full assignment of the 2D ^{1}H-^{15}N NOESY.

Numerous residues (Val20–Asn31, Thr40–Trp59 and Ile75–Glu90) displayed signals attributable to a second, minor protein conformation, which had a 1:10 ratio in intensity. Hereafter, only the major form was considered for structure calculations.

We were able to assign 96% of all the ^{1}H signals for the major form. Structural information derived from 2D and 3D NOESY maps supported the presence of 5 α-helical regions (labelled α_1 to α_5) with typically strong HN-HN (*i, i*+1), and medium-range Hα-HN (*i, i*+3) and Hα-HN (*i, i*+4), interresidual NOEs. These regions spanned the sequence stretches Val3–Lys13, Ala50–Asn54, Glu61–Glu69, Pro71–Tyr74 and Lys88–Thr102, resembling those in the NMR structure of reduced WT C*c* (Jeng *et al.*, 2002). In total, we observed and assigned 2,176 meaningful NOEs, which corresponded to an average number of meaningful restraints per residue of 20.8 (**Figure 2—Figure supplement 2**). The 71 ϕ and 71 ψ dihedral angle constraints were derived from ^{15}N, ^{13}C', ^{13}Cα, ^{13}Cβ and Hα chemical shifts, using TALOS+ (Cornilescu *et al*., 1999). The heme moiety was included in the calculations, following a procedure previously reported

for WT cytochromes (Banci *et al*, 1999; Baistrocchi *et al*., 1996), which assumes an intact heme iron coordination as supported by the XAS spectroscopic data (see next section).

Two-hundred structures were calculated by CYANA, and the twenty structures with the lowest target-function (TF) value were selected to form a representative family. The range of TF values was 0.38–0.98 $Å^2$, highlighting the high accuracy between calculated and experimental distances. Further refinement of the 20 lowest TF structures involved restrained energy minimization and restrained molecular dynamics (RMD) computations. A final restrained energy minimization carried out on the structure with the lowest root-mean square deviation (RMSD) to the average for each of the 20 trajectories. The overall quality of the 20 lowest TF ensemble was good, according to PROCHECK G-factor (Laskowski *et al*., 1996) MolProbity clash-scores (Word *et al*., 1999) and other structural quality indicators (**Table 1**). Most residues were in the favored regions, whereas Cys14, Cys17, His18, Val20, Lys37 and Asn70 were in the generously allowed Ramachandran plot regions, as also observed for the solution structure of WT C*c* (Cornilescu *et al*., 1999; Rajagopal *et al.*, 2013). Cys14, Cys17 and His18 are covalently bonded to the heme moiety, thereby straining their backbone conformation, as already described for *c*-type cytochromes (Banci *et al.*, 1999; Baistrocchi *et al*., 1996). As an additional control, we performed 20 ns unrestrained molecular dynamics (MD) simulations of the final minimized conformers without applying any geometrical restraints. The RMSD for the main-chain atoms was about 1.55 Å at the plateau, and it hardly drifted (0.122 pm ns^{-1}), as expected for a stable structure (**Figure 2—Figure supplement 3a**).

The overall fold of Y48*p*CMF C*c* is very similar to that of the WT species, with RMSD values for the backbone nuclei of 1.67 ± 1.01 Å (**Figure 2a,b)**. However, the two structures differ in the mutation-containing loop Ω_{NY} (residues 40–57; **Figure 2b**), according to the chemical-shift differences (**Figure 2—Figure supplement 1**) and RMSD variations between the first conformer of the NMR solution structures of WT C*c* (PDB ID: 1J3S) (Jeng

et al., 2002) and the refined lowest-TF Y48*p*CMF C*c* (**Figure 2—figure supplement 4a**). This dynamism in the loop Ω_{NY} is also observed in the mutant G41S C*c* (Karsisiotis *et al*., 2016). The Ω_{NY} loop (also known as foldon V) and helix α_2 constitute the less-stable folding unit of C*c* (Maity *et al*., 2004). Unlike Tyr48 in the WT species, the *p*CMF48 residue presents a very low number of ^{1}H-^{1}H NOEs (**Figure 3—Figure supplement 2**) and a high RMSD value within the family (**Figure 2c** and **Figure 2—figure supplement 4b**). A decrease in the number of detectable NOEs can generally be attributed to either a partial assignment of the residue or an increased internal mobility. In our case, the observed effect can be ascribed to the highly dynamic behavior of the *p*CMF48 residue, in agreement with the presence of internal motions within the ns-ps time scale (see below).

Other regions of the Y48*p*CMF C*c* structure that differed from that of WT C*c* belong to the 19–36 Ω_G-loop (part of foldon II) and the 71–85 Ω_R-loop (foldon IV) comprising Met80 and helix α_4. The former loop (Val20–Gly29) of Y48*p*CMF C*c* shows high RMSD values for the backbone nuclei with respect to WT C*c* (2.75 ± 1.50 Å, **Figure 2—figure supplement 4a**). In the latter loop, the observed differences are mainly restricted to side chains. In fact, the RMSD values for backbone and heavy atoms are 1.18 ± 0.37 Å and 1.77 ± 0.71 Å, respectively. Residues included in the Ω_R loop indeed displayed double conformation, suggesting the presence of conformational equilibria (**Figure 2—figure supplement 4a**).

The ensemble of structures for Y48*p*CMF C*c* is very precise, except for residues surrounding the mutation. The backbone RMSD to the mean is 0.89 ± 0.01 Å for the whole protein and drops to 0.53 ± 0.12 Å when the mutation surroundings are excluded (residues 40–57) (**Figure 2—figure supplement 4b**). As expected, the highest RMSD values correspond to the 40–57 Ω_{NY} loop and the nearby residues Val20–Gly29 in loop Ω_G, with corresponding global RMSD values for backbone atoms of 1.79 ± 0.53 Å and 0.78 ± 0.23 Å, respectively. These segments also exhibited a larger conformational variability in their secondary structure elements along the MD trajectory (**Figure 3—Figure supplement 3b,c**). High RMSD values

along the Val20–Gly29 stretch are typical in C*c* homologs (Banci *et al*., 1999; Baistrocchi *et al*., 1996). They are also consistent with our detection of NMR signals revealing secondary conformations for the His26–Pro30 stretch. Moreover, the nearby Asn31 amide signal is weak, suggesting a high mobility. Notably, all these residues contact the Ω_{NY} loop, comprising the Y48*p*CMF mutation.

Further, the highest RMSD values mapped to the Ω_{NY} loop. Consistently, signals from this region undergo a drastic reduction of their ^{1}H-^{1}H NOE cross-peaks. The intensities of the amide signals of Gly45 and Ser47 in Y48*p*CMF C*c* were severely decreased, while those from Thr49, Ala51, Gly56 and Ile57 were undetectable. The Ω_{R} loop also contains some residues with high RMSD values (**Figure 2—Figure supplement 4b**). The global RMSD value for backbone atoms of the 71–85 Ω_{R} loop is equal to 0.76 ± 0.20 Å. Notably, the end of the Ω_{R} loop shows high RMSD values in WT cytochromes (Banci *et al*., 1999; Baistrocchi *et al*., 1996).

The heme iron coordination is insensitive to Tyr48 phosphorylation

At physiological pH values, the Y48*p*CMF mutation lowers the B-band splitting in the CD spectra (Guerra-Castellano *et al*., 2015). We tested the effects of the mutation on the heme iron coordination environment and the axial coordination restraints used in our structure computations by using X-ray absorption spectroscopy (XAS), studying both WT and Y48*p*CMF species (**Figure 2d–g** and **Figure 2—figure supplement 4c,d**). The absorption spectra of the two proteins are almost identical. The X-ray absorption near-edge structure (XANES) region of the absorption spectra for both proteins are superimposed (**Figure 2e**). The absence of any shift in the energy position of the absorption edge indicates that the mutation did not affect the electron density at the Fe center.

Likewise, the extracted extended X-ray absorption fine structure (EXAFS) signals of the WT and Y48*p*CMF C*c* species were highly similar. However, small differences in high wave vector (*k*) values can be observed (**Figure 2—Figure supplement 4d**), as well as in the slightly lower amplitude of the Y48*p*CMF protein. While the corresponding

Fourier transforms are also very similar (**Figure 2f**), the amplitude of the first peak is lower and broader in the Y48*p*CMF C*c* species, suggesting a larger degree of disorder. The dynamic disorder for the two proteins should be similar, as the measurements were performed at cryogenic temperatures in both cases. Hence, the differences in disorder are due to a larger static disorder in Y48*p*CMF C*c*. The main scattering paths contributing to this peak originate from the four nitrogen atoms of the porphyrin ring, although contributions of the nitrogen and sulphur axial ligands have also been included. The fit to the data requires the addition of the paths involving the eight porphyrin carbons closest to the iron atom, beyond the first coordination sphere. In addition, the multiple scattering paths involving these atoms were also included. Fits were performed in R space but also reproduced well the spectra in *q* space (**Figure 2g**). The parameters obtained from the best fit to the data revealed that the distances between the iron atom and its first coordinating ligands are insensitive to the Y48*p*CMF mutation (**Table 2)**. Specifically, the distances from the iron center to the axial S ligand are 2.26 ± 0.001 Å and 2.25 ± 0.001 Å in the WT and phosphomimetic mutant species, respectively (**Figure 2d**). Data analyses also showed that the value for the Debye-Waller factor corresponding to the path involving the four porphyrin nitrogen atoms increased from 0.0012 ± 0.0006 $Å^2$ in the WT species to 0.003 ± 0.001 in the Y48*p*CMF mutant. These data are consistent with the preserved chemical-shift pattern of the iron axial ligands and heme substituents observed in 1D ^{1}H NMR (**Figure 1d**), which have been reported to be sensitive indicators of the heme iron electronic structures (Banci *et al*., 1999; Baistrocchi *et al*., 1996). The pattern of the observed NOEs for the heme substituents also supports an overall intact heme pocket, with the exception of the mutation site.

Phosphorylation of Tyr48 enhances internal mobility in cytochrome *c*

NMR relaxation measurements were performed to evaluate the dynamics of WT and Y48*p*CMF C*c*. The Y48*p*CMF substitution slightly affected both relaxation rate (R_1 and R_2) parameters (**Table supplement 2**). The rotational correlation time of the phosphomimetic mutant

(6.96 ± 0.02 ns) was higher than that of the WT form (6.33 ± 0.02 ns), in agreement with the small increase (p_{nul} values of approximately 10^{-251}) in the average gyration radius, from 12.95 ± 0.07 Å to 13.04 ± 0.06 Å, as calculated by MD. Indeed, phosphorylation can alter protein dynamics at different timescales and cause conformational rearrangements, such as the formation of secondary conformations (Deshmukh *et al*., 2011; Xiao *et al*., 2014; Wauer *et al*., 2015).

Comparing R_1, R_2 and heteronuclear NOE (HetNOE) relaxation measurements recorded on the two proteins revealed that the Ω_{NY} loop of Y48*p*CMF C*c* exhibits a high mobility in the ps-ns time scale (**Figure 3**). Indeed, the Gly41–Lys55 segment showed a drastic drop of HetNOE values in the mutant species (**Figure 3a**). Further, the amide R_1 rates for the sequence stretch of Tyr46–Lys55 in Y48*p*CMF C*c* differ from those in WT C*c* (**Figure 3b**). In addition, R_2 analyses reveals three regions undergoing conformational exchange in the μs-ms time scale: His26–Thr28, Thr40–Trp59 and Ile75–Thr78 (**Figure 3c**). This behavior agrees with the reduced intensity or lack of detection of the amide signals belonging to these stretches, as compared to the WT form. Furthermore, some regions within the protein displayed signals corresponding to double conformations in the 2D ^{1}H NOESY spectra—namely, Val20–Asn31, Thr40–Trp59 and Ile75–Glu90, indicating the presence of conformational equilibria between two different structures occurring on a slow-time scale with respect to the NMR chemical shift. This dynamics involves residues located in a defined region surrounding the non-canonical amino acid (**Figure 3d**). Altogether, the NMR relaxation measurements of Y48*p*CMF C*c* agree with the per-residue S^2 order parameter values computed with TENSOR (Dosset *et al*., 2000) (**Figure 3e**).

Hydrogen-deuterium exchange experiments showed that a common core region is protected from solvent amide-hydrogen exchange in both C*c* species. Nevertheless, a substantial number of amides become unprotected in *p*CMF48 C*c* (**Figure 3—figure supplement 5a–c**). The newly accessible amide protons in the phosphomimetic mutant (Gly29,

Gly37, Arg38, Thr40, Gln42 and Trp59) are located in the surroundings of *p*CMF48 and the nearby Ω_G loop, in agreement with their high mobility in the μs-ms time scale.

Tyr48 phosphorylation modulates the interaction of cytochrome *c* with its mitochondrial partners in the electron transfer chain

C*c* carries electrons from C*bc*$_1$ to C*c*O within the ETC. To elucidate more details about the process, we analyzed the molecular recognition between the soluble N-terminal domain of plant cytochrome c_1 (Cc_1) and the phosphomimetic human Y48*p*CMF C*c.* The human and plant N-terminal domains of Cc_1 have a 62% overall sequence identity and similar charge distributions on their molecular surfaces (Moreno-Beltrán *et al*., 2015). Two binding sites for human and plant C*c* on plant Cc_1 have been recently reported (Moreno-Beltrán *et al*., 2014; (Moreno-Beltrán *et al*., 2015). The proximal site is located near the heme moiety and is compatible with electron transfer, while the distal site lies far from the heme group and probably constitutes a local energy minimum of the encounter ensemble.

To test how Tyr48 phosphorylation affects the conformation of the Cc_1-C*c* complex, we recorded ^{1}H-^{15}N HSQC spectra upon titration of ^{15}N-labeled reduced C*c* with unlabeled reduced Cc_1. Several amide signals exhibited significant chemical-shift perturbations (CSPs), thus indicating a fast exchange rate within the NMR time scale (**Figure 4a,b**). Average amide CSPs ($\Delta\delta_{Avg}$) were larger than 0.075 ppm for eleven residues: Gln16, Lys27, Gly29, Ala50, Lys55, Ile58, Lys72, Gly77, Met80, Ile81 and Val83 (**Figure 4b,c**). All the perturbed residues, except Lys55 and Ile58, surround the heme crevice, as previously described for the interaction between WT C*c* and Cc_1 (Moreno-Beltrán *et al*., 2014; (Moreno-Beltrán *et al*., 2015) (**Figure 4c**). In fact, this region constitutes a very well-conserved interaction surface in *c*-type cytochromes (Díaz-Moreno *et al*., 2005a; Díaz-Moreno *et al*., 2005b; Volkov *et al*., 2006; Sakamoto *et al*., 2011). Lys55 and Ile58, in turn, are located in the Ω_{NY} loop, which undergoes a conformational exchange in free Y48*p*CMF C*c* (**Figure 4c**). In addition, significant CSPs ($\Delta\delta_{Avg} \geq 0.05$ ppm) were detected for Lys7,

Lys13, His26, Lys39, Ala43, Thr78, Lys86, Lys88 and Glu89. Interestingly, Lys8, Lys13, Lys27, Lys72 and Lys86 also experienced large CSPs, as previously reported for the interaction between WT C*c* and Cc_1 (Moreno-Beltrán *et al*, 2014; 2015).

To obtain accurate data on the binding affinity and stoichiometry of the interaction between the two redox proteins, isothermal titration calorimetry (ITC) experiments were performed on both redox states. The isotherms obtained by titrating reduced Y48*p*CMF C*c* with reduced Cc_1 are displayed (**Figure 4d**, left panel). All data fit a model with two independent binding sites in the corresponding C*c* partner (**Table supplement 3**). The interaction between Y48*p*CMF C*c* and Cc_1 was entropy-driven. At pH 7.4, the dissociation constant (K_D) value at the proximal site was half that observed for WT C*c*, whereas that at the distal site was four times higher (**Table supplement 3**). This could be ascribed to the extra negative charge at position 48, which alters the surface electrostatic potential of the hemeprotein (**Figure 4—figure supplement 6**). Both Cc_1–Y48*p*CMF C*c* and Cc_1-C*c* complexes in their oxidized states showed similar thermodynamic and equilibrium parameters at both acidic and basic pH values. The only exception was the K_D value for the oxidized Cc_1–Y48*p*CMF C*c* complex, at the proximal site of Cc_1, that was approximately four times lower than that for the oxidized Cc_1-WT C*c* adduct at pH 8.5. ITC measurements of the oxidized Cc_1–Y48*p*CMF C*c* complex were not run at neutral pH because the alkaline transition pK_a shifts to this pH value upon Tyr48 phosphorylation (Guerra-Castellano *et al*., 2015); thus, WT and phosphomimic C*c* are expected to have different axial ligands at pH 7.4 (**Table supplement 3**).

In addition, we analyzed the binding affinity of the cross-complex between the reduced species of bovine C*c*O and human Y48*p*CMF C*c* by ITC. Bovine and human C*c*O are evolutionarily-related proteins, with 91% and 96% of sequence identity and homology, respectively. Y48*p*CMF C*c* can bind at two sites on C*c*O, similar to WT C*c* (Moreno-Beltrán *et al.*, 2015; Osheroff *et al.*, 1983). The resulting isotherms likewise fit a model with two independent binding sites, different K_D values (**Figure 4d,** *right*

panel, and **Table supplement 4**) and enthalpy-driven interactions. Both the C*c*O proximal and distal sites had lower affinities for Y48*p*CMF C*c* than the WT species (**Table supplement 4**).

To assess the functional ability of Y48*p*CMF C*c* to reduce respiratory complex IV, we tested the C*c*O activity of isolated complex IV or C*c*-free mitochondria (ΔC*c*) from yeast cells grown with glucose as a carbon source (**Figure 5a**). In both cases, the C*c* oxidation rate was at least two-fold higher with Y48*p*CMF C*c* than with WT C*c*, thereby suggesting that Tyr48 phosphorylation enhances the ability of C*c* to donate electrons to complex IV. Interestingly, the C*c*O activity was positively regulated by the human membrane proteins hypoxia-inducible domain family members 1A and 2A (HIGD1A and HIGD2A), which promote cell survival under hypoxia. HIGD2A was successfully expressed in cell-free expression systems combined with n-dodecyl-β-D-maltoside, as previously reported for HIGD1A (Klammt *et al*., 2012) (**Figure 5—figure supplement 7a–c**). HIGD1A significantly increased the rate of C*c*O-catalyzed oxidation of Y48*p*CMF C*c* (**Figure 5b**), as reported for WT C*c* (Hayasi *et al*., 2015). Strikingly, HIGD2A induced an even a stronger positive effect than HIGD1A (**Figure 5b**). Nevertheless, the HIGD-dependent increase in C*c*O activity was slightly lower with Y48*p*CMF C*c* (**Figure 5b**). This may be due to HIGD-dependent changes in either the complex IV affinity towards C*c* or in the restraints of C*c* diffusion (channeling) from Cc_1 to complex IV. A direct C*c*-HIGD interaction can also not be excluded.

To confirm the HIGD-mediated regulation of the C*c*O activity in a cellular context, we isolated mitochondria from different yeast strains grown either with glucose (YPD medium), which supports fermentation and respiration, or with the non-fermentable carbon sources lactate and galactose (YP-Gal) (Strogolova *et al*., 2012). Under both metabolic conditions, the isoformic respiratory supercomplex factors 1 (Rcf1, formerly Aim31) and 2 (Rcf2, formerly Aim38) are constitutively expressed (**Figure 5c**, *inset*), in agreement with their role in C*c*O activity and supercomplex stability (Strogolova *et al*., 2012; Chen *et al*., 2012; Vukotic *et al*., 2012). Rcf1 is a yeast orthologue of the human HIGD1A

and HIGD2A proteins, whereas Rcf2 is specific to yeast. The external membranes of isolated mitochondria were then permeabilized to allow the entry of exogenous WT or Y48*p*CMF C*c*. Under these conditions, mitochondria isolated from a yeast strain deficient of both Rcf1 and Rcf2 (ΔRcf1/2), as verified by western blot, displayed an endogenous C*c*O activity lower than those isolated from WT yeast (WT_{Rcf}), no matter which type of exogenous hemeprotein—WT or Y48*p*CMF C*c*—was used for supplementing (**Figure 5c**). This indicates that Rcf1 and Rcf2 act as positive modulators of C*c*O activity, similar to human HIGD proteins. In mitochondria isolated from yeast grown with non-fermentable carbon sources, the Rcf-mediated increase in C*c*O activity was less prominent when Y48*p*CMF C*c* rather than WT C*c* was added as an exogenous electron donor, in agreement with the *in vitro* behavior of isolated proteins (**Figure 5b**). This suggests that Tyr48 phosphorylation makes C*c* less sensitive to the enhancer mechanism of the Rcf proteins and/or to the ability of Rcfs to stabilize the Cbc_1-C*c*O supercomplexes (**Figure 5c)**. In fact, Rcf1 and Rcf2 promote the supercomplex assembly, preferably in mitochondria from yeasts grown in a respiratory-based medium (**Figure 5d** and **Figure 5—figure supplement 7d**). This is especially remarkable when comparing the band intensities in an anti–COX-2 immunoblot (**Figure 5d**). Note that such OxPhos supercomplexes could show a certain degree of heterogeneity in their composition, since the gene transcription of COX5a and COX5b—which encode for two C*c*O isoforms—are repressed and active, respectively, in the aerobic-to-anaerobic metabolic transition (Fukuda *et al*., 2007). Moreover, the faint band pattern of ΔRcf1/2 strains grown in YPD medium in the BN-PAGE corresponds to supercomplexes, thus suggesting that other factors may contribute to their assembly (**Figure 5d** and **Figure 5—figure supplement 7d**).

Altogether, our data suggest that phosphorylation of C*c* at Tyr48 modulates the mitochondrial ETC (**Figure 5e**). Such a posttranslational modification allows a fast adaptation of the hemeprotein function to changing cell conditions. The population of Cbc_1-C*c*O supercomplexes is less prominent in the presence than in the absence of glucose, although

Rcf proteins are still expressed. In any case, C*c* channeling from Cbc_1 towards C*c*O is impaired. At a physiological pH, Tyr48 phosphorylation thus favors binding of C*c* to the proximal rather than to the distal site of Cc_1. Under respiration-based growth, the Rcf proteins preferably associate directly with the OxPhos supercomplex, bridging Cbc_1 and C*c*O. However, the weaker Y48*p*CMF C*c*-C*c*O binding, along with the loss of the distal site on Cc_1 due to phosphorylated C*c*, impairs the channeling of C*c* molecules that functionally connects Cbc_1 with C*c*O, which has been proposed to occur with WT C*c*[45,46]. As a consequence, Y48*p*CMF C*c* is less efficient than WT C*c* as an electron carrier towards C*c*O in the context of OxPhos supercomplexes.

Tyr48-phosphorylated cytochrome *c* acts as an improved peroxidase-like enzyme, in particular when bound to cardiolipin-containing liposomes

Assembly of the mitochondrial protein membrane complexes Cbc_1 and C*c*O into OxPhos supercomplexes enables more efficient electron flow and decreases ROS levels generated by the ETC (Louro and Díaz-Moreno, 2015). The phospholipid CL, located in the inner mitochondrial membrane, also stabilizes the resulting supercomplexes (Zhang *et al*., 2002) in a HIGD/Rcf-independent manner (Strogolova *et al*., 2012). In addition, CL interacts with C*c* in a two-step binding reaction (Belikova *et al*., 2006): in the first step, the so-called A-site at the C*c* surface makes transient electrostatic contacts with the membrane; in the second step, hydrophobic forces drive the formation of a tight and stable C*c*-CL complex, with one of the CL acyl chains entering the hydrophobic groove of C*c* (termed the C-site) (Sinibaldi *et al*., 2008; Sinibaldi *et al*., 2010). C-site binding then triggers C*c*-regulated CL peroxidation under oxidative stress and induces early apoptosis (Rajagopal *et al*., 2013).

Within this frame, we analyzed how tyrosine phosphorylation can fine-tune the affinity of C*c* towards CL-containing liposomes, analyzing binding of C*c* species to liposomes in electrophoretic mobility shift assays (EMSA) in native agarose gels (**Figure 6a,b**). To compare the binding properties of C*c* species to the CL-containing liposomes of 4:1

DOPC:TOCL (1,2-dioleoyl-*sn*-glycero-3-phosphocholine:1,1'2,2'-tetraoleoylcardiolipin) or to the liposome DOPC alone, we measured the mobility profiles of C*c* at different C*c*:lipid ratios. While both WT and Y48*p*CMF C*c* bound to DOPC:TOCL and DOPC vesicles, their binding affinity for the CL-free DOPC liposomes seemed to be lower (**Figure 6a,b**). Notably, the presence of free hemeprotein at high lipid concentrations suggested that Y48*p*CMF C*c* has a lower affinity than WT towards DOPC:TOCL liposomes (**Figure 6b**), as recently observed for the phosphomimetic mutant S47D C*c* (Guerra-Castellano *et al.*, 2016).

ITC measurements corroborated these EMSA data and yielded apparent K_D values for the first binding event of 427 μM (WT C*c*) and 780 μM (Y48*p*CMF C*c*) (**Figure 6c**). The interaction with CL resulted in apparent ΔH values equal to 2.75 kcal mol^{-1} for WT C*c* and 38.97 kcal mol^{-1} for Y48*p*CMF C*c*. The differences in K_D indicate a small change in binding energies (of approximately 6 kcal mol^{-1}). Hence, the changes in ΔH are indicative of enthalpy-entropy compensation effects, which are compatible with the electrostatic change resulting from the extra carboxylate group of the Y48*p*CMF species. Further, at least one other, slower exothermic process occurs as the lipid concentrations rose along the titrations. In this case, the apparent ΔH values with the WT and Y48*p*CMF C*c* species were equal to –6.97 kcal mol^{-1} and –47.84 kcal mol^{-1}, respectively, but the apparent K_D value (of approximately 1 mM) was practically the same with the two C*c* species. Altogether, our EMSA and ITC assays indicate that Y48*p*CMF C*c* binds to CL-containing liposomes with a slightly lower affinity than WT C*c*.

WT C*c* undergoes CL-dependent conformational changes that allow H_2O_2 to access the heme crevice (Pandiscia *et al*., 2015). Hence, we addressed whether the affinity differences between WT and Y48*p*CMF C*c* for CL could affect their peroxidase activity. In the absence of CL-containing liposomes, Y48*p*CMF C*c* exhibited a three-fold higher peroxidase activity than WT C*c* (**Figure 6d**). However, the presence of TOCL/DOPC vesicles, at a 1:100 C*c*:lipid ratio, increased the enzymatic activity of both WT and Y48*p*CMF C*c*, similar to that observed for other

phosphomimetic C*c* mutants (Guerra-Castellano *et al.*, 2016). Note that the slightly lower peroxidase activity increment observed for Y48*p*CMF C*c* is likely due to its higher population of free protein as compared to WT C*c* (**Figure 6b,d**).

Tyr48 phosphorylation is an anti-apoptotic posttranslational modification

Phosphorylated C*c* may be more easily released from mitochondria because of its lower affinity towards CL, as inferred from EMSA and ITC assays. Translocation to the cytosol could thus enable phosphorylated C*c* to interact with Apaf-1 and to assemble the caspase-activating apoptosome. However, cytosolic caspase-3 activation was decreased by about 60% in the presence of the Y48*p*CMF C*c* mutant (**Figure 6e**). This is in agreement with the behavior previously reported for the Y48E C*c* mutant, which exhibits a lower ability than WT C*c* to activate not only caspase-3[26] but also procaspase-9 by non-functional apoptosome assembly[27]. These results could thus be indicative of an anti-apoptotic function of C*c* when phosphorylated at position 48.

DISCUSSION

Here we tackle the structural and functional characterization of the Y48*p*CMF variant of human C*c.* This mutation mimics protein phosphorylation at Tyr48 by adding a negative charge and slightly increasing the side-chain size while keeping the aromatic ring. A recent spectroscopic analysis of Y48*p*CMF C*c* showed a singular shift of the typical alkaline transition pK_a to physiological pH values[31], as is the case with the Y48E C*c* mutant[26,27]. Here, we report NMR-based structure computations that indicate that Tyr48 phosphorylation maintains the core foldon of C*c* but increases internal motions in the loops Ω_{NY}, Ω_R and Ω_G. Specifically, the Ω_{NY} loop, the most unstable folding unit of the hemeprotein, becomes looser and reaches conformational equilibria in Y48*p*CMF C*c*. Enhanced motions at the Ω_G and Ω_R loops could be associated to the shift in the alkaline transition pK_a. Indeed, these two loops hold the residues that provide the iron axial ligands, which are

observed to at least partially lose their metal coordination in the alkaline form (Assfalg *et al*., 2003). This is in contrast to XAS data that suggest that axial coordination remains untouched. However, the cryogenic temperatures at which the XAS spectra were recorded may amplify the most stable structures and reduce contributions from minority species with a high disorder, which are undetectable.

The local but substantial changes in conformation and dynamics of the regions surrounding the Y48*p*CMF mutation increased the solvent accessibility of the porphyrin ring, thereby enhancing cytochrome peroxidase activity. Thus, Y48*p*CMF C*c* proficiently scavenges ROS and avoids damage of cellular components (**Figure 7**). Our findings also indicate that Y48*p*CMF C*c* binds to mitochondrial CL with a lower affinity than WT C*c*, an interaction that may facilitate C*c* translocation into the cytoplasm during apoptosis. However, phosphorylation at Tyr48 hinders the proapoptotic activity of extramitochondrial C*c*, similar to the function of HIGD1A protein in ischemia and tumorigenesis (Ameri *et al*., 2013; Ameri *et al*., 2015). Indeed, both HIGD1A and Y48*p*CMF C*c* act as pro-survival proteins by preventing apoptotic caspase activation (**Figure 7**) (An *et al*., 2011).

As expected, the Y48*p*CMF mutation affects the binding mode of C*c* to its well-known respiratory partners C*bc*$_1$ and C*c*O. Not surprisingly, the enhanced internal motions of the loops Ω_{NY} and Ω_R and the electrostatic change at the interaction patch resulting from the additional carboxyl group affect the interaction of Y48*p*CMF C*c* with the two membrane complexes. Indeed, the binding of Y48*p*CMF C*c* on the C*c*$_1$ surface is weak and functionally irrelevant at the distal site but is favored at the proximal site. In addition, the decrease in both the association constant (K_A) between Y48*p*CMF C*c* and C*c*O (as reported here) and the Michaelis constant (K_M) of phosphorylated C*c* with C*c*O (Yu *et al*., 2008) indicates that K_M is governed by the catalytic step, which becomes smaller upon Tyr48 phosphorylation at saturating hemeprotein concentrations (Yu *et al*., 2008). This contrasts with the approximately 60 mV decrease in midpoint reduction potential (E_0) of Y48*p*CMF C*c*[31], which should

facilitate the electron flow from C*c* to C*c*O. It is well known that the catalytic step can be tuned by conformational changes of C*c* upon binding to C*c*O[50]; strikingly, these changes resemble the prominent internal dynamics of Y48*p*CMF C*c*. Therefore, such conformational changes might be the limiting step for Y48*p*CMF C*c* oxidation inside the complex. In contrast, the C*c*O-driven oxidation rate of Y48*p*CMF C*c* is larger than that of WT C*c* at the limiting protein concentrations in the enzymatic activity assays used here, in agreement with the K_M decrease in the reaction between phosphorylated C*c* and C*c*O (Yu *et al*., 2008).

Under nutrient and oxygen depletion, a dysfunctional mitochondrial ETC and OxPhos can lead to many human diseases, including pathologies like ischemia and cancer[23]. The nexus in both disorders could be the rate-control mechanisms based on cellular signaling regulation of the ETC components, such as phosphorylation of C*c*. Indeed, C*c* phosphorylation efficiently fine-tunes respiratory rates. Even though HIGD-mediated assembly of C*bc*$_1$ and C*c*O into OxPhos supercomplexes preferably occurs under low glucose conditions, C*c* channeling is disrupted by its phosphorylation, thus slowing down the ETC flow (**Figure 7**). Intriguingly, not only respiratory supercomplex formation (Strogolova *et al*., 2012;Chen *et al*., 2012)–whose structure has been recently solved (Gu *et al*., 2016; Lets *et al*., 2016)–but also C*c* phosphorylation, and the resulting decrease in the ETC rate, could help to keep ROS levels low and to guarantee cell survival.

Tyr48-phosphorylated C*c* could be targeted as a biomarker of mitochondrial dysfunction with associated pathological states, such as ischemia/reperfusion and cancer. Deciphering the details of the phosphorylated C*c*–controlled complex network requires accurate structural and dynamic analyses, to eventually develop robust therapeutic approaches to foster or silence—as required—the pro-survival action of phosphorylated C*c* reported here.

MATERIAL AND METHODS

Methods and any associated references are available in the Supplementary methods.

Accession codes. Coordinates and structure factors for Y48*p*CMF C*c* have been deposited in the Protein Data Bank under accession code 2N3Y.

ACKNOWLEDGMENTS

Financial support was provided by the Spanish Ministry of Economy and Competitiveness (Grants BFU2015-71017-P/BMC and BFU2015-19451/BMC, co-founded by FEDER EU), European Union (Bio-NMR-00130 and CALIPSO-312284), Ramon Areces Foundation and Andalusian Government (BIO198). BMB was awarded with a PhD fellowship from the Spanish Ministry of Education (AP2009-4092), co-funded by the European Social Fund-ERDF, and with a short-term travelling fellowship from the European Bio-NMR Project. AGC was awarded a PhD fellowship from CSIC (JaePre-2011-01248, co-funded by European Social Fund-ERDF). Experimental work was performed in part at the Grenoble Instruct center (ISBG, UMS 3518 CNRS-CEA-UJF-EMBL) with support from FRISBI (ANR-10-INSB-05-02) and GRAL (ANR-10-LABX-49-01) within the Grenoble Partnership for Structural Biology (PSB). The authors thank Dr. Lionel Imbert and Dr. Jérôme Boisbouvier for assistance and access to the Cell Free platform, as part of the INSTRUCT program. We also thank Diamond Light Source for access to beamline I20-scanning (proposal number SP-6011). We acknowledge the NMR services at the Centro di Ricerca di Risonanze Magnetiche (CERM, Florence), the Centro de Investigación, Tecnología e Investigación (CITIUS, Seville) and the Biointeractomics Platform (BIP-cicCartuja, Seville), as well as TA Instruments for assistance with ITC experiments.

COMPETING FINANCIAL INTERESTS

The authors declare no competing financial interests.

REFERENCES

Ameri K, Rajah AM, Nguyen V, Sanders TA, Jahangiri A, DeLay M, Donne M, Choi HJ, Tormos KV, Yeghiazarians Y, Jeffrey SS, Rinaudo PF, Rowitch DH, Aghi, MK, Maltepe E. 2013. Nuclear localization of the mitochondrial factor HIGD1A during metabolic stress. Plos One 8: e62758. doi:10.1371/journal.pone.0062758.

Ameri K, Jahangiri A, Rajah AM, Tormos KV, Nagarajan R, Pekmezci M, Nguyen V, Wheeler ML, Murphy MP, Sanders TA, Jeffrey SS, Yeghiazarians Y, Rinaudo PF, Costello JF, Aghi MK, Maltepe E. 2015. HIGD1A regulates oxygen consumption, ROS production, and AMPK activity during glucose deprivation to modulate cell survival and tumor growth. *Cell Rep* **10**: 891-9. doi:10.1016/j.celrep.2015.01.020.

An HJ, Shin H, Jo SG, Kim YJ, Lee JO, Paik SG, Lee H. 2011. The survival effect of mitochondrial *Higd-1a* is associated with suppression of cytochrome *c* release and prevention of caspase activation. *Biochim Biophys Acta – Mol Cell Res* **1813**: 2088-98. doi:10.1016/j.bbamcr.2011.07.017.

Assfalg M, Bertini I, Dolfi,A, Turano P, Mauk AG, Rosell FI, Gray HB. 2003. Structural model for an alkaline form of ferricytochrome *c*. *J Am Chem Soc* **125**: 2913-22. doi:10.1021/ja027180s.

Basova LV, Kurnikov IV, Wang L, Ritov VB, Belikova NA, Vlasova II, Pacheco AA, Winnica DE, Peterson J, Bayir H, Waldeck DH¸ Kagan VE. 2007. Cardiolipin switch in mitochondria: shutting off the reduction of cytochrome *c* and turning on the peroxidase activity. *Biochemistry* **46**: 3423-34. doi:10.1021/bi061854k.

Bertini I, Chevance S, Del Conte R, Lalli D, Turano, P. 2011. The anti-apoptotic Bcl-x(L) protein, a new piece in the puzzle of cytochrome *c* interactome. *PLoS One* **6**: e18329. doi:10.1371/journal.pone.0018329.

Chen YC, Taylor EB, Dephoure N, Heo JM, Tonhato A, Papandreou I, Nath N, Denko NC, Gygi SP, Rutter J. 2012. Identification of a protein

mediating respiratory supercomplex stability. *Cell Metab* **15**: 348-60. doi:10.1016/j.cmet.2012.02.006.

Corcoran A, Cotter, TG. 2013. Redox regulation of protein kinases. *FEBS J* **280**: 1944-65. doi:10.1111/febs.12224.

Cornilescu G, Delaglio F, Bax A. 1999. Protein backbone angle restraints from searching a database for chemical shift and sequence homology. *J Biomol NMR* **13**: 289-02. doi:10.1023/A:1008392405740.

Belikova NA, Osipov AN, Kapralov AA, Tyurin VA, Potapovich MV, Basova LV, Peterson J, Kurnikov IV, Kagan VE. 2006. Peroxidase activity and structural transitions of cytochrome *c* bound to cardiolipin-containing membranes. *Biochemistry* **45**: 4998-09. doi:10.1021/bi0525573.

Deshmukh L, Meller N, Alder N, Byzova T, Vinogradova O. 2011. Tyrosine phosphorylation as a conformational switch: a case study of integrin β_3 cytoplasmic tail. *J Biol Chem* **286**: 40943-53. doi:10.1074/jbc.M111.231951.

Díaz-Moreno I, Díaz-Quintana A, Molina-Heredia FP, Nieto PM, Hansson O, De la Rosa MA, Karlsson BG. 2005a. NMR analysis of the transient complex between membrane photosystem I and soluble cytochrome c_6. *J Biol Chem* **280**: 7925-31. doi:10.1074/jbc.M412422200.

Díaz-Moreno I, Díaz-Quintana A, Ubbink M, De la Rosa MA. 2005b. An NMR-based docking model for the physiological transient complex between cytochrome f and cytochrome c_6. *FEBS Lett* **579**: 2891-96. doi:10.1016/j.febslet.2005.04.031.

Díaz-Moreno I, García-Heredia JM, Díaz-Quintana A, De la Rosa MA. 2011a. Cytochrome *c* signalosome in mitochondria. *Eur Biophys J* **40**: 1301-15. doi:10.1007/s00249-011-0774-4

Díaz-Moreno I, García-Heredia JM, Díaz-Quintana A, Teixeira M, De la Rosa MA. 2011b. Nitration of tyrosines 46 and 48 induces the specific degradation of cytochrome *c* upon change of the heme iron state to high-

spin. *Biochim Biophys Acta – Bioenerg* **1807**: 1616-23. doi:10.1016/j.bbabio.2011.09.012.

Dosset P, Hus JC, Blackledge M, Marion D. 2000. Efficient analysis of macromolecular rotational diffusion from heteronuclear relaxation data. *J Biomol NMR* **16**: 23-8. doi:10.1023/A:1008305808620.

Florence TM. 1985. The degradation of cytochrome *c* by hydrogen peroxide. *J Inorg Biochem* **23**: 131-41. doi:10.1016/0162-0134(85)83017-8.

Fukuda R, Zhang H, Kim JW, Shimoda L, Dang CV, Semenza GL. 2007. HIF-1 regulates cytochrome oxidase subunits to optimize efficiency of respiration in hypoxic cells. *Cell* **129**: 111-22. doi:10.1016/j.cell.2007.01.047.

García-Heredia JM, Díaz-Quintana A, Salzano M, Orzáez M, Pérez-Payá E, Teixeira M, De la Rosa MA, Díaz-Moreno I. 2011. Tyrosine phosphorylation turns alkaline transition into a biologically relevant process and makes human cytochrome *c* behave as an anti-apoptotic switch. *J Biol Inorg Chem* **16**: 1155-68. doi:10.1007/s00775-011-0804-9.

García-Heredia JM, Díaz-Moreno I, Díaz-Quintana A, Orzáez M, Navarro JA, Hervás M, De la Rosa MA. 2012. Specific nitration of tyrosines 46 and 48 makes cytochrome *c* assemble a non-functional apoptosome. *FEBS Lett* **586**: 154-8. doi:10.1016/j.febslet.2011.12.007.

González-Arzola K, Díaz-Moreno I, Cano-González A, Díaz-Quintana A, Velázquez-Campoy A, Moreno-Beltrán B, López-Rivas A, De la Rosa MA. 2015. Structural basis for inhibition of the histone chaperone activity of SET/TAF-Iβ by cytochrome *c*. *Proc Natl Acad Sci USA* **112**: 9908-13. doi:10.1073/pnas.1508040112.

Gu J, Wu M, Guo R, Yan K, Lei J, Gao N, Yang M. 2016. The architecture of the mammalian respirasome. *Nature* **537**: 639-43. doi:10.1038/nature19359.

Guerra-Castellano A, Díaz-Quintana A, Moreno-Beltrán B, López-Prados J, Nieto PM, Meister W, Staffa J, Teixeira M, Hildebrandt P, De la Rosa MA, Díaz-Moreno I. 2015. Mimicking tyrosine phosphorylation in human cytochrome *c* by the evolved tRNA synthetase technique. *Chem Eur J* **21**: 15004-12. doi:10.1002/chem.201502019.

Guerra-Castellano A, Díaz-Moreno I, Velázquez-Campoy A, De la Rosa MA, Díaz-Quintana A. 2016. Structural and functional characterization of phosphomimetic mutants of cytochrome *c* at threonine 28 and serine 47. *Biochim Biophys Acta – Bioenerg* **1857**: 387-95. doi:10.1016/j.bbabio.2016.01.011.

Hayashi T, Asano Y, Shintani Y, Aoyama H, Kioka H, Tsukamoto O, Hikita M, Shinzawa-Itoh K, Takafuji K, Higo S, Kato H, Yamazaki S, Matsuoka K, Nakano A, Asanuma H, Asakura M, Minamino T, Goto Y-I, Ogura T, Kitakaze M, Komuro I, Sakata Y, Tsukihara,T, Yoshikawa S, Takashima, S. 2015. Higd1a is a positive regulator of cytochrome *c* oxidase. *Proc Natl Acad Sci USA* **112**: 1553-8. doi:10.1073/pnas.1419767112.

Helling S, Hüttemann M, Ramzan R, Kim SH, Lee I, Müller T, Langenfeld E, Meyer HE, Kadenbach B, Vogt S, Marcus K. 2012. Multiple phosphorylations of cytochrome *c* oxidase and their functions. *Proteomics* **12**: 950-9. doi:10.1002/pmic.201100618.

Hou T, Wang X, Ma Q, Cheng H. 2014. Mitochondrial flashes: new insights into mitochondrial ROS signalling and beyond. *J Physiol* **592**: 3703-13. doi:10.1113/jphysiol.2014.275735.

Hüttemann M, Lee I, Pecinova A, Pecina P, Przyklenk K, Doan JW. 2008. Regulation of oxidative phosphorylation, the mitochondrial membrane potential, and their role in human disease. *J Bioenerg Biomemb* **40**: 445-56. doi:10.1007/s10863-008-9169-3.

Hüttemann M, Lee I, Grossman LI, Doan JW, Sanderson TH. 2012. Phosphorylation of mammalian cytochrome *c* and cytochrome *c* oxidase in the regulation of cell destiny: respiration, apoptosis, and human

disease. *Adv Exp Med Biol* **748**: 237-64. doi:10.1007/978-1-4614-3573-0_10.

Jeng WY, Chen CY, Chang HC, Chuang WJ. 2002. Expression and characterization of recombinant human cytochrome *c* in *E. coli*. *J Bioenerg Biomembr* **34**: 423-31. doi:10.1023/A:1022561924392.

Kadenbach B. 1968. Incorporation of ^{32}P-phosphate into phosphatides of rat liver mitochondria *in vivo* and *in vitro*. *FEBS Lett* **2**: 118-20. doi:10.1016/0014-5793(68)80118-8.

Kagan VE, Bayir HA, Belikova NA, Kapralov O, Tyurina YY, Tyurin VA, Jiang J, Stoyanovsky DA, Wipf P, Kochanek PM, Greenberger JS, Pitt B, Shvedova AA, Borisenko G. 2009. Cytochrome *c*/cardiolipin relations in mitochondria: a kiss of death. *Free Radic Biol Med* **46**: 1439-53. doi:10.1016/j.freeradbiomed.2009.03.004.

Karsisiotis AI, Deacon OM, Wilson MT, Macdonald C, Blumenschein TM, Moore GR, Worrall JA. 2016. Increased dynamics in the 40-57 Ω-loop of the G41S variant of human cytochrome *c* promote its pro-apoptotic conformation. *Sci Rep* **6**: 30447. doi:10.1038/srep30447.

Klammt C, Maslennikov I, Bayrhuber M, Eichmann C, Vajpai N, Chiu EJ, Blain KY, Esquivies L, Kwon JH, Balana B, Pieper U Sali A, Slesinger PA, Kwiatkowski W, Riek R, Choe S. 2012. Facile backbone structure determination of human membrane proteins by NMR spectroscopy. *Nat Methods* **9**: 834-9. doi:10.1038/nmeth.2033.

Lenaz G, Genova ML. 2010. Structure and organization of mitochondrial respiratory complexes: a new understanding of an old subject. *Antioxid Redox Signal* **12**: 961-1008. doi:10.1089/ars.2009.2704.

Lenaz G, Baracca A, Barbero G, Bergamini C, Dalmonte ME, Del Sole M, Faccioli M, Falasca A, Fato R, Genova ML, Sgarbi G, Solaini, G. 2010. Mitochondrial respiratory chain super-complex I-III in physiology and pathology. *Biochim Biophys Acta – Bioenerg* **1797**: 633-40. doi:10.1016/j.bbabio.2010.01.025.

Laskowski RA, Rullmannn JA, MacArthur MW, Kaptein R, Thornton JM. 1996. AQUA and PROCHECK-NMR: programs for checking the quality of protein structures solved by NMR. *J Biomol NMR* **8**: 477-86. doi:10.1007/BF00228148.

Letts JA, Fiedorczuk K, Sazanov LA. 2016. The architecture of respiratory supercomplexes. *Nature* **537***,* 644-48. doi:10.1038/nature19774.

Louro RO, Díaz-Moreno I. 2015. Redox Proteins in Supercomplexes and Signalosomes. CRC Press, Taylor , Francis Group, Oxfordshire, UK.

Ly HK, Utesch T, Díaz-Moreno I, García-Heredia JM, De La Rosa MA, Hildebrandt P. 2012. Perturbation of the redox site structure of cytochrome *c* variants upon tyrosine nitration. *J Phys Chem B* **116**: 5694-02. doi:10.1021/jp302301m.

Maity H, Maity,M, Englander SW. 2004. How cytochrome *c* folds, and why: submolecular foldon units and their stepwise sequential stabilization. *J Mol Biol* **34**: 223-33. doi:10.1016/j.jmb.2004.08.005.

Martínez-Fábregas J, Díaz-Moreno I, González-Arzola K, Janocha S, Navarro JA, Hervás M, Bernhardt R, Díaz-Quintana A, De la Rosa MA. 2013. New *Arabidopsis thaliana* cytochrome *c* partners: a look into the elusive role of cytochrome *c* in programmed cell death in plants. *Mol Cell Proteomics* **12**: 3666-76. doi:10.1074/mcp.M113.030692.

Martínez-Fábregas J, Díaz-Moreno I, González-Arzola K, Janocha S, Navarro JA, Hervás M, Bernhardt R, Velázquez-Campoy A, Díaz-Quintana A, De la Rosa MA. 2014a. Structural and functional analysis of novel human cytochrome *c* targets in apoptosis. *Mol Cell Proteomics* **13**: 1439-56. doi:10.1074/mcp.M113.034322.

Martínez-Fábregas J, Díaz-Moreno I, González-Arzola K, Díaz-Quintana A, De la Rosa MA. 2014b. A common signalosome for programmed cell death in humans and plants. *Cell Death Dis.* **5**: e1314. doi:10.1038/cddis.2014.280.

Martinou JC, Desagher S, Antonsson B. 2000. Cytochrome *c* release from mitochondria: all or nothing. *Nat Cell Biol* **2**: E41-3. doi:10.1038/35004069.

Moreno-Beltrán B, Díaz-Quintana A, González-Arzola K, Velázquez-Campoy A, De la Rosa MA, Díaz-Moreno I. 2014. Cytochrome c_1 exhibits two binding sites for cytochrome *c* in plants. *Biochim Biophys Acta – Bioenerg* **1837**: 1717-29. doi:10.1016/j.bbabio.2014.07.017.

Moreno-Beltrán B, Díaz-Moreno I, González-Arzola K, Guerra-Castellano A, Velázquez-Campoy A, De la Rosa MA, Díaz-Quintana A. 2015. Respiratory complexes III and IV can each bind two molecules of cytochrome *c* at low ionic strength. *FEBS Lett* **589**: 476-83. doi:10.1016/j.febslet.2015.01.004.

Osheroff N, Speck SH, Margoliash E, Veerman EC, Wilms J, König BW, Muijsers AO. 1983. The reaction of primate cytochromes *c* with cytochrome *c* oxidase. Analysis of the polarographic assay. *J Biol Chem* **258**: 5731-8.

Pandiscia LA, Schweitzer-Stenner R. 2015. Coexistence of native-like and non-native cytochrome *c* on anionic liposomes with different cardiolipin content. *J Phys Chem B* **119**: 12846-59. doi:10.1021/acs.jpcb.5b07328.

Papa S. 1982. Molecular mechanism of proton translocation by the cytochrome system and the ATPase of mitochondria. Role of proteins. *J Bioenerg Biomembr* **14**: 69-86.

Pecina P, Borisenko GG, Belikova NA, Tyurina YY, Pecinova A, Lee I, Samhan-Arias AK, Przyklenk K, Kagan VE, Hüttemann M. 2010. Phosphomimetic substitution of cytochrome *c* tyrosine 48 decreases respiration and binding to cardiolipin and abolishes ability to trigger downstream caspase activation. *Biochemistry* **49**: 6705-14. doi:10.1021/bi100486s.

Pettersen EF, Goddard TD, Huang CC, Couch GS, Greenblatt DM, Meng EC, Ferrin TE. 2004. UCSF Chimera - A visualization system for exploratory

research and analysis. *J Comput Chem* **25**: 1605-12. doi:10.1002/jcc.20084.

Radi R, Thomson L, Rubbo H, Prodanov E. 1991a. Cytochrome *c*-catalyzed oxidation of organic molecules by hydrogen peroxide. *Arch Biochem Biophys* **288**: 112-7. doi:10.1016/0003-9861(91)90171-E.

Radi R, Turrens JF, Freeman BA. 1991b. Cytochrome c-catalyzed membrane lipid peroxidation by hydrogen peroxide. *Arch Biochem Biophys* **288**: 118-25. doi:10.1016/0003-9861(91)90172-F.

Rajagopal BS, Edzuma AN, Hough MA, Blundell KL, Kagan VE, Kapralov AA, Fraser LA, Butt JN, Silkstone GG, Wilson MT, Svistunenko DA, Worrall JA. 2013. The hydrogen-peroxide-induced radical behaviour in human cytochrome *c*-phospholipid complexes: implications for the enhanced pro-apoptotic activity of the G41S mutant. *Biochem J* **456**: 441-52. doi:10.1042/BJ20130758.

Ray PD, Huang BW, Tsuji Y. 2012. Reactive oxygen species (ROS) homeostasis and redox regulation in cellular signaling. *Cell Signal* **24**: 981-90. doi:10.1016/j.cellsig.2012.01.008.

Sakamoto K, Kamiya M, Imai M, Shinzawa-Itoh K, Uchida T, Kawano K, Yoshikawa, S, Ishimori K. 2011. NMR basis for interprotein electron transfer gating between cytochrome *c* and cytochrome *c* oxidase. *Proc Natl Acad Sci USA* **108**: 12271-6. doi:10.1073/pnas.1108320108.

Sinibaldi F, Fiorucci L, Patriarca A, Lauceri R, Ferri T, Coletta M,Santucci R. 2008. Insights into cytochrome *c*-cardiolipin interaction. Role played by ionic strength. *Biochemistry* **47**: 6928-35. doi:10.1021/bi800048v.

Sinibaldi F, Howes BD, Piro MC, Polticelli F, Bombelli C, Ferri T, Coletta M, Smulevich G, Santucci R. 2010. Extended cardiolipin anchorage to cytochrome *c*: a model for protein-mitochondrial membrane binding. *J Biol Inorg Chem* **15**: 689-00. doi:10.1007/s00775-010-0636-z.

Solaini G, Baracca A, Lenaz G, Sgarbi G. 2010. Hypoxia and mitochondrial oxidative metabolism. *Biochim Biophys Acta – Bioenerg* **1797**: 1171-7. doi:10.1016/j.bbabio.2010.02.011.

Strogolova V, Furness A, Robb-McGrath M, Garlich J,Stuart RA. 2012. Rcf1 and Rcf2, members of the hypoxia-induced gene 1 protein family, are critical components of the mitochondrial cytochrome bc_1-cytochrome *c* oxidase supercomplex. *Mol Cell Biol* **32**: 1363-73. doi:10.1128/MCB.06369-11.

Turrens JF. 2003. Mitochondrial formation of reactive oxygen species. *J Physiol* **552**: 335-44. doi:10.1111/j.1469-7793.2003.00335.x.

Volkov AN, Worrall JA, Holtzmann E, Ubbink M. 2006. Solution structure and dynamics of the complex between cytochrome *c* and cytochrome *c* peroxidase determined by paramagnetic NMR. *Proc Natl Acad Sci USA* **103**: 18945-50. doi: 10.1073/pnas.0603551103.

Vukotic M, Oeljeklaus S, Wiese S, Vögtle FN, Meisinger C, Meyer HE, Zieseniss A, Katschinski DM, Jans DC, Jakobs S, Warscheid B, Rehling P, Deckers M. 2012. Rcf1 mediates cytochrome oxidase assembly and respirasome formation, revealing heterogeneity of the enzyme complex. *Cell Metab* **15**: 336-47. doi:10.1016/j.cmet.2012.01.016.

Wegerich F, Turano P, Allegrozzi M, Möhwald H, Lisdat F. 2009. Cytochrome *c* mutants for superoxide biosensors. *Anal Chem* **81**: 2976-84. doi:10.1021/ac802571h.

Word JM, Lovell SC, LaBean TH, Taylor HC, Zalis ME, Presley BK, Richardson JS, Richardson DC. 1999. Visualizing and quantifying molecular goodness-of-fit: small-probe contact dots with explicit hydrogen atoms. *J Mol Biol* **285**: 1711-33. doi: http://dx.doi.org/10.1006/jmbi.1998.2400

Xiao Y, Lee T, Latham MP, Warner LR, Tanimoto A, Pardi A, Ahn NG. 2014. Phosphorylation releases constrains to domain motion in ERK2. *Proc Natl Acad Sci USA* **111**: 2506-11. doi:10.1073/pnas.1318899111.

Yu H, Lee I, Salomon AR, Yu K, Hüttemann M. Mammalian liver cytochrome *c* is tyrosine-48 phosphorylated *in vivo*, inhibiting mitochondrial respiration. 2008. *Biochim Biophys Acta – Biomemb* **1777**: 1066-71. doi:10.1016/j.bbabio.2008.04.023.

Zhang M, Mileykovskaya E, Dowhan W. 2002. Gluing the respiratory chain together. Cardiolipin is required for supercomplex formation in the inner mitochondrial membrane. *J. Biol. Chem* **277**: 43553-6. doi:10.1074/jbc.C200551200

TABLES, FIGURES AND LEGENDS

Table 1. NMR statistics of the Y48*p*CMF C*c* structure

NMR distance and dihedral constraints	
Distance constraints	
Total meaningful NOE	2,176
Intra-residue	360
Inter-residue	1,816
Sequential ($\|i-j\| = 1$)	763
Medium-range ($\|i-j\| \leq 5$)	539
Long-range ($\|i-j\| > 5$)	514
Total dihedral angle restraints	
ϕ	71
ψ	71
Structure statistics	
Violations	
Average target function	0.73 ± 0.18
Distance constraints (Å)	0.0059 ± 0.0014
Dihedral angle constraints (º)	0.3336 ± 0.0973
Max. distance constraint violation (Å)	0.29
Max. dihedral angle violation (º)	3.79
RMSD of minimized 20 conformers to the mean (Å)	
Backbone	0.89 ± 0.01
Heavy atoms	1.33 ± 0.24
Global RMSD of minimized 20 conformers (Å)	
Backbone	1.28 ± 0.30
Heavy atoms	1.91 ± 0.38
Ramachandram plot statistics from Procheck	
Residues in favoured regions (%)	98.80 ± 0.10
Residues in generously allowed regions (%)	1.00 ± 0.10
Residues in disallowed regions (%)	0.20 ± 0.10
Global quality	
Procheck G-factor (all dihedrals, raw score)	-0.436 ± 0.046
Verify 3D	0.432 ± 0.030
Prosall	0.578 ± 0.047
MolProbity Clashscore	2.564 ± 1.263
Number of close contacts	0
Deviations from ideal bond distance (Å)	0.013 ± 0.001

Table 2. EXAFS data of the Y48*p*CMF C*c* structure

EXAFS Fits*				
	Paths	**σ^2_{path} (Å^2)**	**R (Å)**	**ΔE_0 (eV)**
WT	N_{Pi}	0.0012 ± 0.0006	1.983 ± 0.008	0.5 ± 1.0
	N_{Iz}	0.0011	2.214	
	S	0.002 ± 0.002	2.26 ± 0.01	
	C_{Pi}	0.002 ± 0.001	2.98	
			3.02 ± 0.01	
			3.06	
	Pi Multiple	0.002		
Y48*p*CMF	N_{Pi}	0.003 ± 0.001	1.990 ± 0.001	0.4 ± 1.3
	N_{Iz}	0.0011	2.21	
	S	0.003 ± 0.002	2.25 ± 0.01	
	C_{Pi}	0.002 ± 0.001	2.99	
			3.03 ± 0.02	
			3.06	
	Pi Multiple	0.003		
*The amplitude reduction factor, S_0^2, was set to 1.0 for all fits. Δk_{WT} = 1.389 – 11.885 Å^{-1}; $\Delta k_{Y48pCMF}$ = 1.358 – 11.685 Å^{-1}; ΔR_{WT} = 1.15 – 2.95 Å; $\Delta R_{Y48pCMF}$ = 1.18 – 2.95 Å. Fit *R* factors: R_{WT} = 0.0043; $R_{Y48pCMF}$ = 0.0097.				

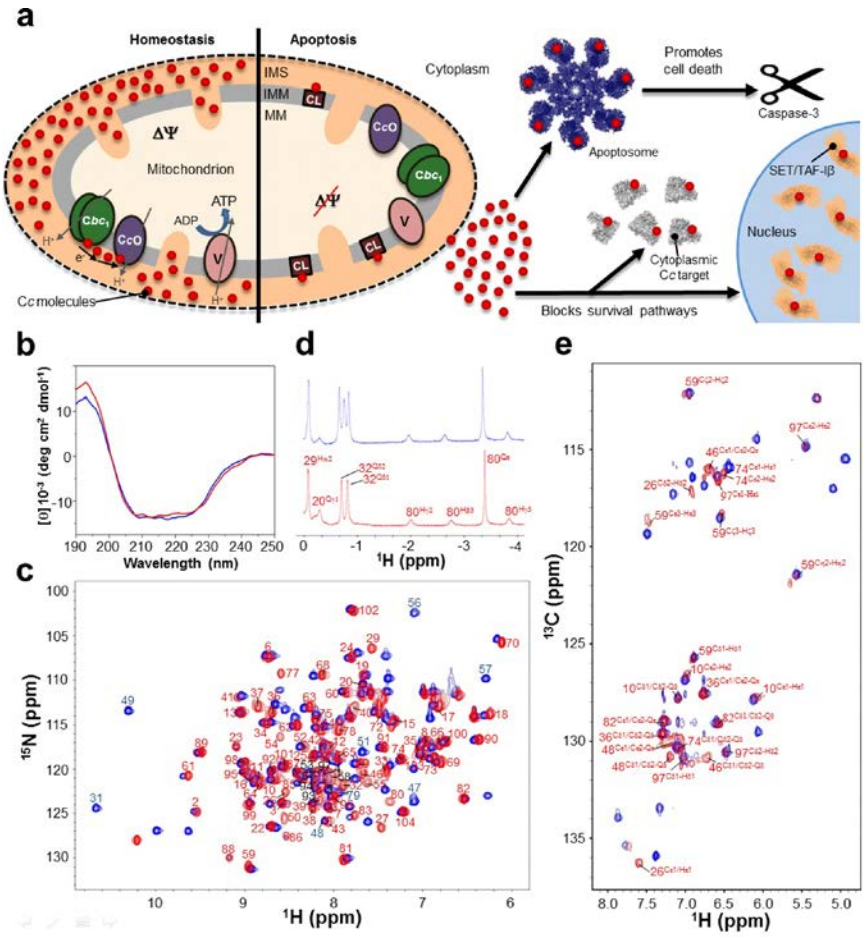

Figure 1. Control of human cell fate by C*c*-based signalosome, and biophysical and structural characterization of the Y48*p*CMF variant of human C*c*. **(a)** Diagram of the role of C*c* in homeostasis and apoptosis. *Left*, C*c* molecules are located in the intermembrane mitochondrial space (IMS) under homeostatic conditions, transferring electrons from cytochrome bc_1 complex (Cbc_1) to cytochrome *c* oxidase complex (C*c*O). Cbc_1 and C*c*O are embedded in the inner mitochondrial membrane (IMM). Such electron transfer reactions are coupled to proton translocations that originate the mitochondrial membrane potential ($\Delta\Psi$) necessary for ATP production in the mitochondrial matrix (MM) via ATP synthase (V). C*c* molecules are represented as small red circles. *Right*, C*c* is released from the mitochondria to the cytosol upon apoptotic stimuli.

Under such conditions, C*c* is involved not only in inducing cell death via apoptosome formation and activation of the caspases pathway, but also in blocking specific pro-survival pathways via inter-protein interactions, including formation of nuclear complexes (for instance, the SET/C*c* complex). Mitochondrial membrane potential ($\Delta\Psi$) is impaired under apoptotic conditions, and a portion of C*c* is retained in the IMM upon binding to cardiolipin (CL). **(b)** Far-UV CD spectra of the reduced forms of WT and Y48*p*CMF C*c*. The spectra of the WT and mutant proteins are displayed in blue and red, respectively. The same color-code is maintained in the following panels. **(c)** Superimposition of the $^{1}H–^{15}N$ HSQC spectra of uniformly ^{15}N-labeled forms of WT and Y48*p*CMF C*c*. Backbone amide resonances of Y48*p*CMF C*c* are labelled in red and black. Particular amide resonances of WT C*c* are labelled in blue. **(d)** Detailed view of the ^{1}H NMR spectra of WT and Y48*p*CMF C*c* at negative ppm values. Resonances for Met80 side-chain protons are shown for both C*c* species. Assigned signals of all residues within this region are displayed for Y48*p*CMF C*c*. The extra signal of WT C*c* corresponds to the $Q\delta_1$ protons of Ile53. **(e)** Superimposition of the aromatic region of the $^{1}H–^{13}C$ HSQC spectra of WT and Y48*p*CMF C*c* acquired in ^{13}C natural abundance. Assigned aromatic resonances of Y48*p*CMF C*c* are displayed in red.

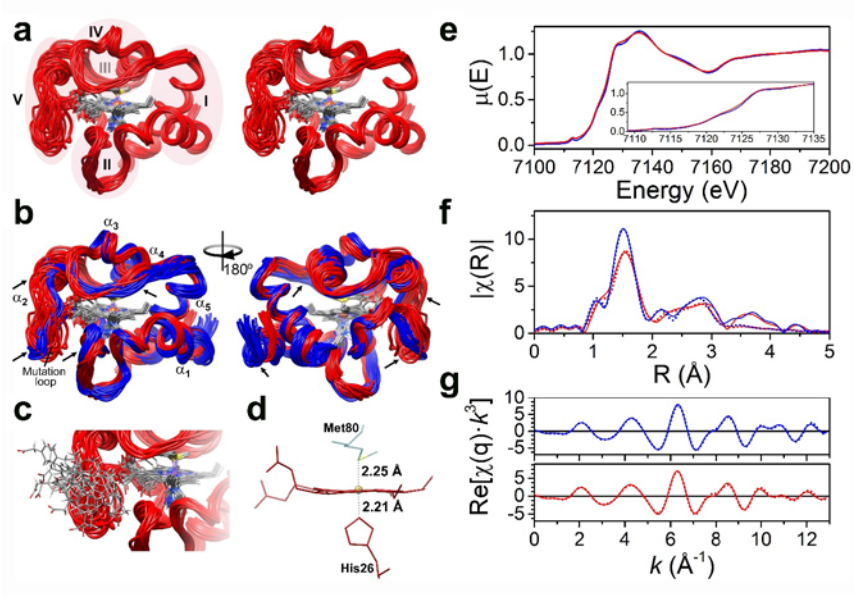

Figure 2. NMR solution structure of the Y48*p*CMF variant of C*c*. **(a)** Stereo-view ribbon representation of the 20 best conformers of Y48*p*CMF C*c*. Heme group atoms are displayed for all conformers. Ribbons are colored in red, whereas atoms from the heme group are colored following the CPK color scheme. Foldons of Y48*p*CMF C*c* are shadowed and marked with Roman numerals, except for foldon III, which is located behind foldon IV. **(b)** Comparison between the NMR solution structures of WT C*c* (PDB ID: 1J3S) (Jeng *et al.*, 2002) and Y48*p*CMF C*c* (this work). The ribbon for WT C*c* is in blue. The five α-helices of both C*c* species, as well as the mutation-containing loop of Y48*p*CMF C*c*, are marked. Arrows point to the regions on the Y48*p*CMF C*c* ribbon with substantial structural changes as compared to the WT form. **(c)** Detailed view of the loop harboring the *p*CMF48 residue. *p*CMF48 atoms follow the CPK color scheme. Protein structures were represented with the UCSF Chimera software (Pettersen *et al*., 2004). **(d)** Detail of the heme group and axial ligands. Labels display iron-to-axial ligand distances for the Y48*p*CMF mutant obtained from the EXAFS analysis. (**e**) Overlay of the XANES regions of the XAS spectra of reduced WT (blue) and Y48*p*CMF (red) C*c*. The inset displays an enlargement of the absorption edge. **(f)** Modulus of the Fourier transforms of the EXAFS signals for the reduced WT

(continuous line, blue) and Y48*p*CMF (continuous line, red) C*c* species. Dotted curves are the best fits of the experimental data carried out within the interval ΔR = 1.38–2.95 Å. Fits in k space are shown in Figure S4d. (**g)** *q*-space, reverse Fourier transform of the experimental data (continuous lines) and best fits (dotted lines), following the same color-code as for (**f**).

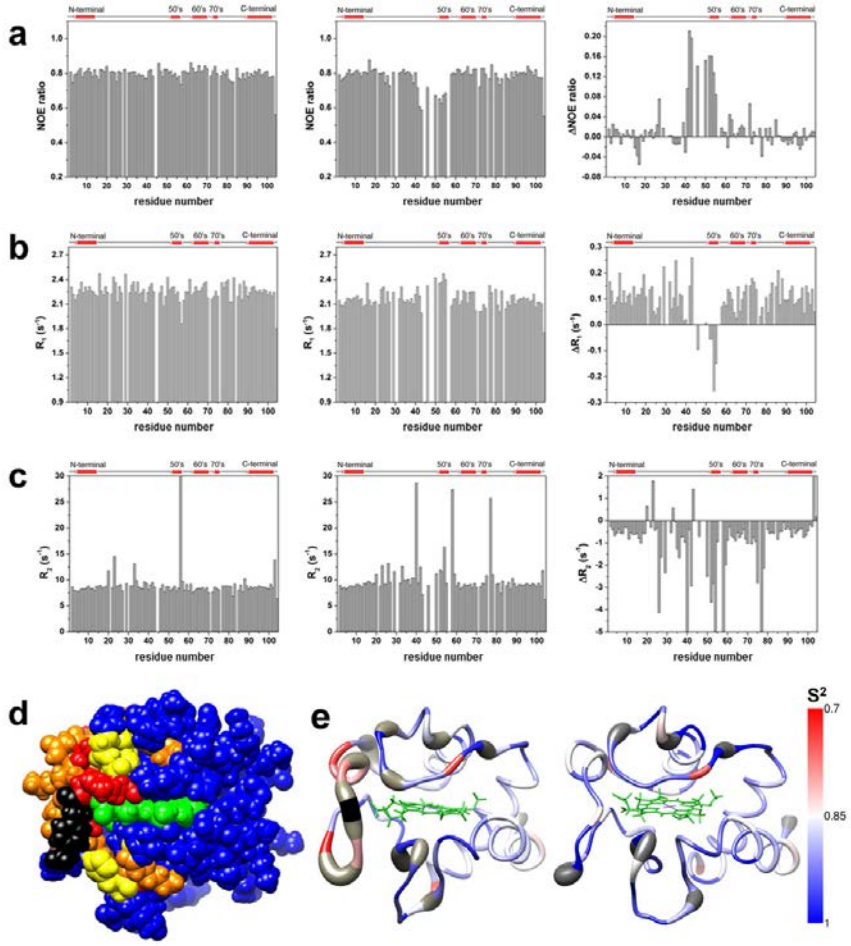

Figure 3. Relaxation NMR measurements and dynamic properties of WT and Y48*p*CMF C*c*. **(a–c)** Heteronuclear NOE (**a**), relaxation rate R_1 (**b**) and relaxation rate R_2 (**c**) for the reduced forms of WT (*left*) and Y48*p*CMF (*middle*) C*c*, plotted as a function of the residue number. The differences between the respective experimental values are also presented (*right*). Gaps in data result from overlapping resonances, broadened resonances beyond the detection limit and unassigned resonances. A scheme of the secondary structure elements is included at the top of each plot. **(d)** Map of the Y48*p*CMF C*c* residues colored according to their dynamic properties. Affected residues in the heteronuclear NOE and relaxation rate R_2 parameters are colored in yellow and orange, respectively. Residues with backbone amide with resonances that are undetectable in the $^{1}H–^{15}N$ HSQC spectrum of Y48*p*CMF C*c* but detectable in the $^{1}H–^{15}N$

HSQC spectrum of WT C*c* are colored in red. *p*CMF48 is shown in black and the heme group, in green. Unaffected, unassigned and proline residues are in blue. **(e)** Internal mobility comparison between Y48*p*CMF and WT C*c*. S^2 order parameter values per residue for Y48*p*CMF (*left*) and WT (*right*) C*c* are represented on the respective NMR ribbon structures using a blue-red scale. Color key is shown. Undetectable backbone resonances are in gray. Heme atoms are in green. Internal mobility was calculated by Tensor 2 software (Dosset *et al*., 2000).

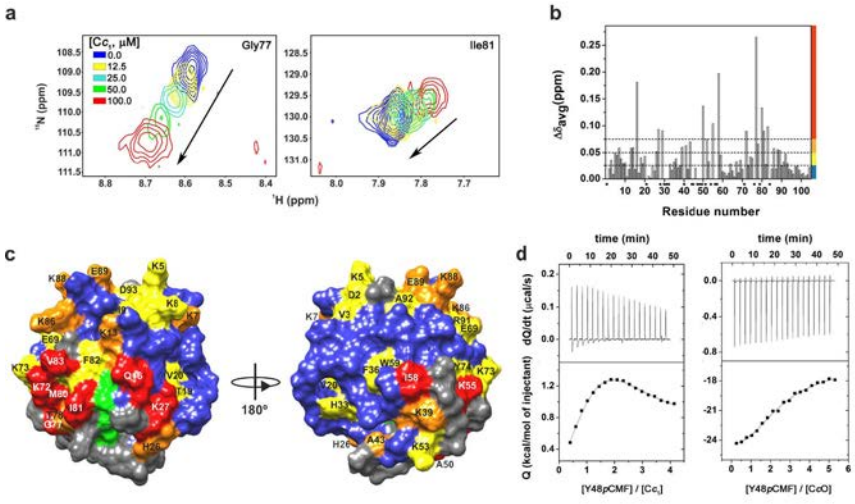

Figure 4. Binding assays between Y48*p*CMF C*c* and its respiratory partners. **(a)** Overlay of selected residues of $^{1}H–^{15}N$ HSQC spectra of ^{15}N-labeled Y48*p*CMF C*c* along with titration with Cc_1. Signals corresponding to different titration steps are colored according to the code indicated in the panel. **(b)** Plot of chemical-shift perturbations (CSPs) of ^{15}N-labeled Y48*p*CMF C*c* as a function of residue number. Proline and non-assigned residues are marked by asterisks. Color bars stand for the $\Delta\delta$avg categories, as follows: insignificant $\Delta\delta$avg < 0.025 ppm, blue; small 0.025 ≤ $\Delta\delta$avg < 0.050 ppm, yellow; medium 0.050 ≤ $\Delta\delta$avg < 0.075 ppm, orange; and large ≥ 0.075 ppm, red. **(c)** CSP map of reduced Y48*p*CMF C*c* upon addition of reduced Cc_1 at a 1:1 ratio. Residues are colored according to the $\Delta\delta$avg categories, as indicated in (**b**). Proline and non-assigned residues are in gray. **(d)** ITC measurements of the Y48*p*CMF C*c*-Cc_1 and Y48*p*CMF C*c*-C*c*O complexes in their reduced states. Experimental data were fitted to a 2:1 binding model. Thermograms are shown in the upper panels, and binding isotherms, in the lower panel.

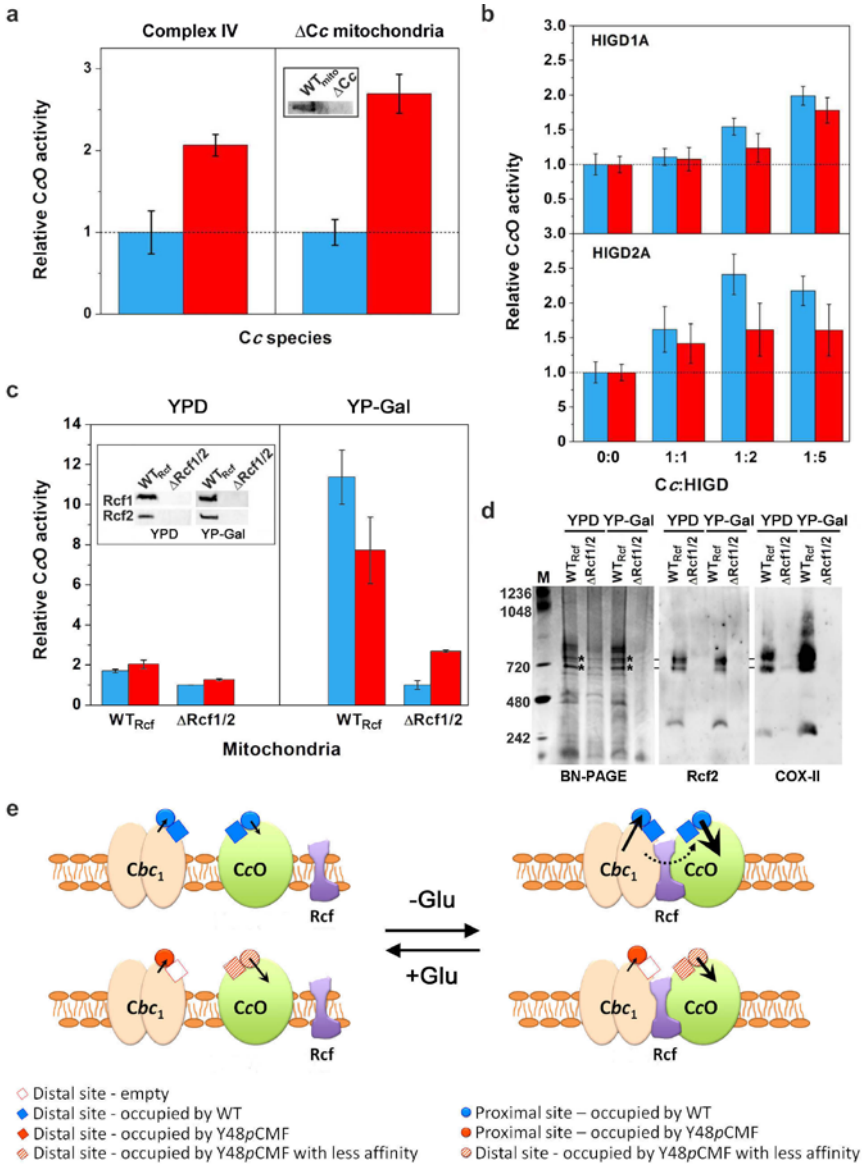

Figure 5. C*c*O activity with WT or Y48*p*CMF C*c* as the electron donor. **(a)** C*c*O activity of isolated complex IV and of mitochondria lacking C*c* (ΔC*c*) upon addition of exogenous WT (blue bars) or Y48*p*CMF C*c* (red bars). Western blot results confirmed the lack of endogenous C*c* in ΔC*c* mitochondria (see *inset*). **(b)** *In vitro* modulation of C*c*O activity by HIGD1A and HIGD2A. WT C*c* (blue bars) or Y48*p*CMF C*c* (red bars), along with HIGD1A or HIGD2A at the indicated ratios, were added to isolated complex IV. (**c**) Effect of the modulators Rcf1 and Rcf2 on the C*c*O activity

of mitochondria isolated from yeasts grown in YPD or YP-Gal media with either WT C*c* (blue bars) or Y48*p*CMF C*c* (red bars). All data represent the mean ±SD of three independent experiments. In all cases, C*c*O activity was detected only upon addition of exogenous C*c* but not with endogenous C*c*. *Inset*, Western blots of WT_{Rcf} mitochondria (lane 1) and mitochondria lacking Rcf1 and Rcf2 (∆Rcf1/2) (lane 2). **(d)** Blue-native gel (BN-PAGE) and western blots of mitochondria from WT_{Rcf} and ∆Rcf1/2 strains, using antibodies against Rcf2 and COX-II. Bands submitted to tryptic digestion (Figure. S7d) are highlighted by asterisks. **(e)** Scheme of the interactions within the electron transport chain involving C*cb*$_1$, C*c*O, Rcf proteins and WT or Y48*p*CMF C*c*, as a function of glucose (Glu) availability. The Rcf proteins facilitate the interaction between C*cb*$_1$ and C*c*O to form OxPhos supercomplexes, mainly under glucose deprivation (*right*). Thickness of solid arrows refers to the electron transfer rate at the C*c*-binding proximal sites of C*bc*$_1$ and C*c*O by WT or Y48*p*CMF C*c*—the longer and thicker the arrow, the more efficient the electron transfer. Dashed line highlights the channeling of WT C*c* molecules.

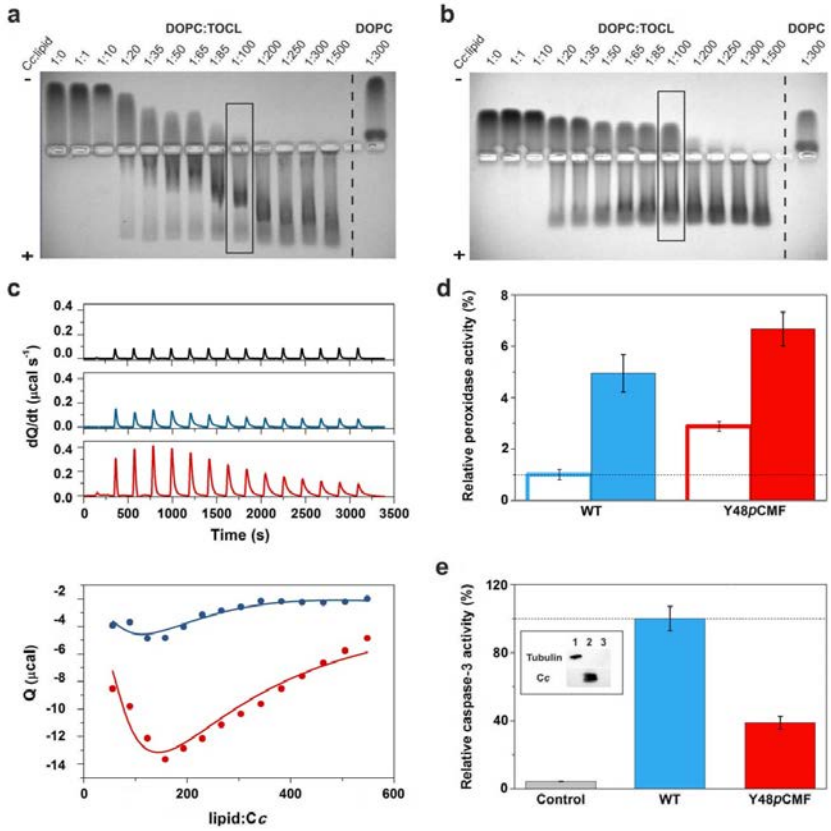

Figure 6. Liposome-binding assays with caspase-3 activity induced by WT and Y48*p*CMF C*c*. **(a**,**b)** Electrophoretic mobility shift assay (EMSA) of C*c* in the presence of increasing concentrations of lipids. DOPC:TOCL (4:1) or DOPC liposomes were incubated with WT (**a**) or Y48*p*CMF (**b**) C*c* in 25 mM HEPES buffer (pH 7.4). Note that free C*c* species moved to the cathode, whereas liposome-bound C*c* migrated to the anode. Samples were loaded onto a 0.8% agarose gel, and gels were stained with Coomassie Brilliant Blue. Lanes marked by rectangles correspond to the C*c*:lipid ratio at which the peroxidase activity was determined (see below). **(c)** Calorimetric assays for lipid binding to C*c*. Upper, ITC thermograms, corresponding to titrations of DOPC:TOCL 4:1 liposomes in phosphate buffer (black), WT C*c* (blue) or Y48*p*CMF C*c* (red). Lower, binding isotherms with WT C*c* (blue dots) or Y48*p*CMF C*c* (red dots). Continuous lines represent the best fits to a sequential binding, as

computed with the Nanoanalyze software (TA instruments) with a stoichiometry of 30 molecules of lipid per molecule of C*c*. **(d)** Relative peroxidase activities of WT C*c* (blue) or Y48*p*CMF C*c* (red) in the presence of liposomes containing DOPC (empty bars) or DOPC:TOCL (4:1) (filled bars). **(e)** Relative caspase-3 activity in HEK293 cell extracts devoid of endogenous C*c* upon addition of exogenous WT C*c* (blue) or Y48*p*CMF C*c* (red). A lack of caspase auto-activation was verified in a run without the addition of C*c* (gray). Western blots confirmed the lack of endogenous C*c* in cytoplasmic cell extracts after immunoblotting with anti α-tubulin (cytosolic marker) and anti-C*c* antibodies (see *inset*). Lane 1, cytoplasmic cell extracts; lane 2, C*c*; lane 3, BSA as a negative control.

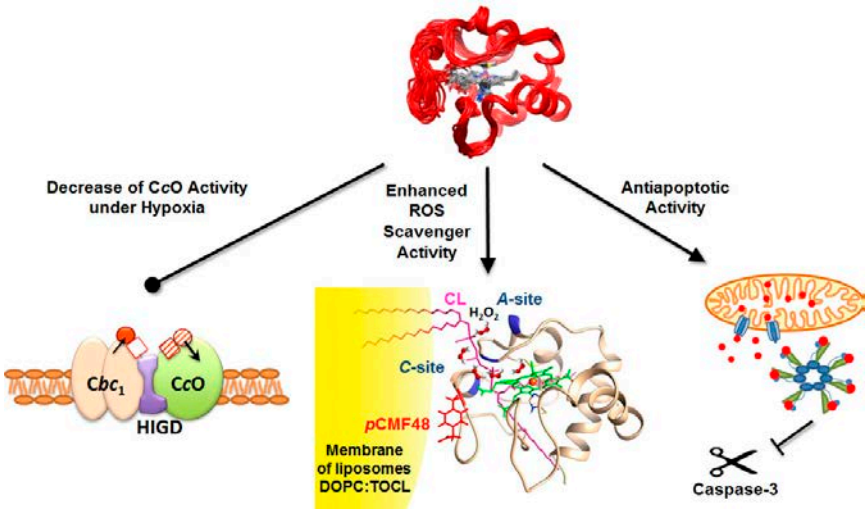

Figure 7. Schematic diagram illustrating the changes induced in cell function by phosphomimic Y48*p*CMF C*c*. The negative charge at position 48 decreases C*c*O activity by disrupting C*c* channeling in OxPhos supercomplexes (*left*), enhances the reactive oxygen species (ROS) scavenger activity by increasing the peroxidase activity of CL-bound C*c* (*middle*) and promotes the anti-apoptotic function of Y48*p*CMF C*c* by inhibiting its ability to activate the caspase-3 cascade (*right*).

Structural Basis of Mitochondrial Dysfunction in Response to Cytochrome *c* Phosphorylation at Tyrosine 48

Supporting Information

Blas Moreno-Beltrán*[,1], Alejandra Guerra-Castellano*[,1], Antonio Díaz-Quintana[1],
Rebecca Del Conte[2], Sofía M. García-Mauriño[1], Sofía Díaz-Moreno[3], Katiuska González-Arzola[1], Carlos Santos-Ocaña[4], Adrián Velázquez-Campoy[5], Miguel A. De la Rosa[1], Paola Turano[2] and Irene Díaz-Moreno[1,#]

[1]Instituto de Investigaciones Químicas, cicCartuja, Universidad de Sevilla – CSIC, Avda. Américo Vespucio 49, 41092 Seville (Spain).
[2]Magnetic Resonance Center (CERM) – Department of Chemistry, University of Florence, Via Luigi Sacconi 6, 50019 Sesto Fiorentino, Florence (Italy).
[3]Diamond Light Source Ltd., Harwell Science and Innovation Campus, Didcot, Oxfordshire OX11 0DE (United Kingdom).
[4]Centro Andaluz de Biología del Desarrollo, Universidad Pablo de Olavide – CSIC, and CIBERER Instituto de Salud Carlos III, Carretera de Utrera km. 1, 41013 Seville (Spain).
[5]Institute of Biocomputation and Physics of Complex Systems (BIFI), Joint Unit BIFI-IQFR (CSIC), Universidad de Zaragoza, Mariano Esquillor s/n, 50018 Zaragoza (Spain); Aragon Institute for Health Research (IIS Aragon), Avda. San Juan Bosco 13, 50009 Zaragoza, Spain; Fundacion ARAID, Government of Aragon, Maria de Luna 11, 50018 Zaragoza (Spain).
*These authors contribute equally to the work.

[#]Correspondence should be addressed to I. D.-M. (idiazmoreno@us.es)
Telephone number: +34 954489513; Fax number: +34 954460065

SUPPLEMENTARY METHODS

Protein expression and purification

Uniformly ^{13}C,^{15}N-labeled, ^{15}N-labeled and unlabeled samples of the Y48*p*CMF variant species of cytochrome *c* (C*c*)—in which tyrosine 48 was replaced by *p*-carboxymethyl-L-phenylalanine (*p*CMF)—were expressed using the evolved tRNA synthetase technique and purified as previously described (Xie *et al*., 2007; Guerra-Castellano *et al*., 2015). For isotopic labelling, ^{15}N-labeled ammonium chloride and ^{13}C-labeled glucose were added to minimal cell culture media to express the ^{13}C,^{15}N-labeled protein samples, whereas only ^{15}N-labeled ammonium chloride was added to media for ^{15}N-labeled protein samples. Unlabeled *p*CMF and δ-aminolevulinic acid were added to a final concentration of 1 mM each after cell culture induction. Cultures were induced with IPTG and arabinose at 1 mM and 0.02% final concentrations, respectively. Tryptic digestion and MALDI-TOF analyses confirmed the molecular mass and the substitution of tyrosine by *p*CMF. Uniformly ^{15}N-labeled and unlabeled samples of wild-type (WT) C*c* were expressed and purified as reported previously (Moreno-Beltrán *et al*., 2015). Protein concentration was determined by visible spectrophotometry, using an extinction coefficient of 29 mM^{-1} cm^{-1} for reduced Y48*p*CMF and WT C*c.* For NMR experiments, pure C*c* samples were first dialyzed against 10 mM sodium phosphate (pH 6.3), and afterwards concentrated in Millipore 3 K Nominal Molecular Weight Limit (NMWL) centricons until a final C*c* concentration of 0.7 mM.

Plant cytochrome c_1 (Cc_1) was obtained as described (Moreno-Beltrán *et al*., 2014). Bovine cytochrome *c* oxidase (C*c*O) was purchased from Sigma; before use, the buffer was exchanged to 10 mM sodium phosphate buffer (pH 7.4), supplemented with 0.2% (w/v) *n*-dodecyl-β-D-maltoside (DDM) and 5 mM sodium dithionite, using Millipore 3K NMWL centricons, as reported previously (Moreno-Beltrán *et al*., 2015).

Hypoxia-inducible domain family members 1A and 2A (HIGD1A and HIGD2A, respectively) were expressed by cell-free protein synthesis using

a continuous exchange reaction (dialysis mode; ratio 1:10), with a 6 mL final volume. Briefly, 10 μg mL^{-1} of either HIGD1A- or HIGD2A-coding DNA in the pIVEX2.4d plasmid were added to the reaction mixture, which consisted of 1 mM amino acid mix, 0.8 mM ribonucleotides (guanosine-, uracyl- and cytidine- triphosphate), 1.2 mM adenosine triphosphate, 55 mM HEPES buffer (pH 7.5), 68 μM folinic acid, 0.64 mM cyclic adenosinemonophosphate, 3.4 mM dithiothreitol, 27.5 mM ammonium acetate, 2 mM spermidine, 80 mM creatine phosphate, 208 mM potassium glutamate, 16 mM magnesium acetate, 250 μg mL^{-1} of creatine kinase, 27 μg mL^{-1} of T7 RNA polymerase, 0.175 μg mL^{-1} of tRNA and 0.4 mL of S30 *Escherichia coli* (*E. coli*) bacterial extract. DDM detergent was added to a final concentration of 0.4% (w/v). For the feeding mix in the external tank (60 mL), the same conditions were used but omitting DNA, creatine kinase, T7 RNA polymerase, tRNA and S30 *E. coli* bacterial extract. Incubation was carried out at 23°C with agitation for 16 h. The His-tagged forms of HIGD1A and HIGD2A were then purified by nickel affinity chromatography. The final yield was 125 μg of protein per mL of reaction in both cases. Before using the HIGD proteins, the buffers were exchanged to 10 mM sodium phosphate buffer (pH 7.4) with 0.2% (w/v) DDM.

Circular dichroism

Circular dichroism (CD) spectra were recorded on a JASCO J-815 spectropolarimeter, equipped with a Peltier temperature system, in a 1-mm quartz cuvette. CD intensities were presented in terms of molar ellipticity [θ_{molar}], based on molar protein concentration (Kelly *et al.*, 2005). Secondary structural elements of reduced WT and Y48*p*CMF C*c* were analyzed by recording their respective far-UV CD spectra (185–250 nm) at 25°C. The samples contained 3 μM hemeprotein in 5 mm sodium phosphate buffer (pH 6.3), supplemented with 10 mM ascorbic acid. Twenty scans were averaged and analyzed for each sample, using the CDPro software package (Sreerama and Woody, 2000; Greenfield, 2007) SMP50 and SP37A were used as reference sets. CLSTR option was employed for comparison with a set of proteins with similar folds.

Nuclear magnetic resonance experiments

Nuclear magnetic resonance (NMR) spectra of fresh 0.6 mM ^{13}C,^{15}N-labeled Y48*p*CMF C*c* samples, in 90% buffer and 10% D_2O, were recorded at 25°C on Bruker Avance spectrometers operating at 950, 700 and 500 MHz ^{1}H frequencies. A standard set of triple-resonance experiments, necessary for the full assignment of backbone and side-chain resonances, were acquired at 700 MHz ^{1}H frequency, whereas 2D and 3D NOESY experiments required for structure determination were acquired at 950 MHz ^{1}H frequency. Recorded NMR experiments for determination of backbone resonances were 2D ^{1}H-^{15}N heteronuclear single-quantum correlation (HSQC), 2D ^{1}H-^{13}C HSQC, 3D HNCA, 3D HNCACB, 3D CACB(CO)NH, 3D HN(CA)CO and 3D HNCO, and specific experiments for determination of side-chain resonances were 3D HCCHTOCSY and 3D HBHA(CO)NH (Zuiderweg *et al*., 1988; Grzesiek and Bax, 1993; Kay *et al*., 1993). Additional 2D COSY and aromatic 2D ^{1}H-^{13}C HSQC spectra of an unlabeled sample of Y48*p*CMF C*c* were acquired for the assignment of aromatic residues. Therefore, the ^{1}H-^{13}C HSQC spectrum was recorded in natural abundance of ^{13}C. Water suppression was achieved in all mentioned spectra by WATERGATE (Piotto *et al*., 1991) 1D ^{1}H spectra were launched before and after each spectrum to check the state of the sample, and especially the redox state of the hemeprotein.

The following NOESY experiments were acquired: 2D ^{1}H-^{15}N NOESY, 3D ^{1}H-^{15}N NOESY-HSQC and 3D ^{1}H-^{13}C NOESY-HSQC spectra in the aliphatic region (Marion *et al*., 1989a; Marion *et al*., 1989b; Zuiderweg *et al.*, 1989). Mixing times were 100 ms for all NOESY experiments, recorded on a ^{15}N-labeled sample, with the exception of the 3D ^{1}H-^{13}C NOESY-HSQC, which was acquired on a ^{13}C,^{15}N-labeled sample. An additional 2D ^{1}H-^{15}N EXSY spectrum was launched for assignment of heme resonances using a partially oxidized ^{15}N-labeled sample. WATERGATE suppression was used. 1D ^{1}H spectra were again launched to check the state of the samples.

^{15}N relaxation R_1 (=1/T_1), R_2 (=1/T_2) and {^{1}H}-^{15}N NOE parameters (also known as HetNOE) were obtained from standard experiments recorded at 500 MHz ^{1}H frequency and 25°C (Kay *et al.*, 1989) on ^{15}N-labeled

samples of the Y48*p*CMF and WT C*c* species. R_1 and R_2 values were obtained using 10 delays, of 1, 2.5, 10, 35, 70, 200, 380, 550, 740 and 3000 ms for R_1 experiments, and 16.96, 33.92, 67.84, 101.76, 135.68, 186.56, 237.44, 271.36, 305.28 and 356.16 ms for R_2 experiments. To determine HetNOE values, spectra were recorded in the presence or absence of a proton presaturation period. HetNOE, R_1 and R_2 values from residues in well-defined regions were used to estimate the comprehensive ^{15}N relaxation parameters (Blackledge *et al.*, 1998; Dosset *et al.*, 2000). The R_1/R_2 ratio was used to estimate the rotational correlation time (τ_c) of the protein constructs using TENSOR2 software (Dosset *et al.*, 2000). Internal mobility was also calculated by an isotropic model-free analysis via TENSOR2 routines (Dosset *et al.*, 2000). Amide hydrogen exchange experiments were also carried out on these ^{15}N-labeled samples of the Y48*p*CMF and WT C*c* species. For this purpose, 2D ^{1}H-^{15}N HSQC experiments were run using C*c* samples in 95% buffer and 5% D_2O, or 100% D_2O.

NMR data processing was carried out using the Bruker TopSpin software package. The assignments of 2D and 3D spectra were performed manually with the help of the CARA and SPARKY software packages (Keller, 2004; Goddar and Kneller, 2001). A list of NOEs of reduced yeast C*c* was used as a reference (Baistrocchi *et al*., 1996). Final reviews of peak assignments and integrations of peak volumes were executed by the XEASY software (Bartels *et al*., 1991). ^{15}N relaxation parameters were analyzed using CARA routines (Keller, 2004).

NMR titrations of 100 μM ^{15}N-labeled, reduced Y48*p*CMF C*c* with aliquots of unlabeled, reduced plant cytochrome c_1 (Cc_1) were performed at 25ºC and recorded on a Bruker Avance 700 MHz. Titrations were performed in 5 mM sodium phosphate (pH 6.3) with 10% D_2O. Each titration step was prepared in an independent NMR tube (Shigemi) up to a 0.28 mL final volume. The pH of the samples was checked before and after recording each spectrum. The Chemical-Shift Perturbations (CSP) were monitored in a series of ^{1}H-^{15}N HSQC experiments. The data were processed using Bruker TopSpin and analyzed with SPARKY (Goddar and

Kneller, 2001). CSP titration curves were analyzed with Origin 7 (OriginLab, http://www.originlab.com), using a two-parameter non-linear least squares fit with two-site binding model, as previously described (Moreno-Beltrán *et al*., 2015; Moreno-Beltrán *et al*., 2014).

Distance geometry calculations

Volumes of cross-peaks between assigned resonances were obtained using the integration routines of the XEASY program. Elliptical integration was applied. NOESY cross-peak intensities were converted into upper limits of inter-atomic distances by CYANA (Güntert *et al*., 1997). The heme group, axial ligands and two Cys residues covalently linked to the porphyrin ring were treated as in previous computations (Bartalesi *et al*., 2003). Upper and lower distance limits were imposed to build up the heme group. Upper (1.90 Å) and lower (1.70 Å) distance limits from the α-carbons of thioethers 2 and 4 of the heme moiety to the S_γ of cysteines 14 and 17, respectively, were used in the computations to covalently link the heme moiety to the cysteine residues. An upper distance limit of 2.50 Å and a lower distance limit of 2.20 Å between the S_δ of Met80 and the heme iron atom were also introduced. The orientations of Met80 and His18 side-chains were defined only by experimental NOE constraints.

A residue containing the heme moiety was added to the standard CYANA library. In addition, the non-standard amino acid *p*CMF was built and added to the CYANA library. Several cycles of structure calculation were carried out in order to recalibrate the NOE distance constraints. CYANA calculations were performed following the procedure and with the parameters used for the determination of other *c*-type cytochromes (Baistrocchi *et al*., 1996; Banci *et al*., 1997; Assfalg *et al*., 2002). Initially, 200 structures were calculated. In each calculation, violated constraints were analyzed for the 20 best structures with respect to the target function. After consecutive rounds of review and refinement of violated constraints, a final CYANA computation was performed in which no consistent violations were determined. The final average value of the target function was equal to 0.73 ± 018.

Molecular dynamics simulations

NMR-restrained Molecular Dynamics (RMD) computations were performed by the AMBER 12.1 package and using the AMBER-2003 force field on a selection of the 20-best structures derived from the CYANA calculations (Duan *et al*., 2003; Case *et al*., 2006). Distance constraints were introduced by the DIS_RST module of Amber 12.1. Simulations were performed under periodic boundary conditions using an orthorhombic cell geometry (with the minimum distance between protein and cell faces initially set to 10 Å) and particle mesh Ewald (PME) electrostatics with a Ewald summation cut off of 9Å. The structures were solvated with extended simple point charge model (SPC) water molecules, and Cl^- counterions were added to neutralize the net charge of the full systems. Afterwards, solvent and counterions were subjected to 2500 steps of steepest descent minimization followed by 500 ps NPT-MD computations using isotropic molecule position scaling and a pressure relaxation time of 2 ps at 298 K. Once the systems were NMR-restrained energy minimized (REM), the resulting data were submitted to RMD computations for 5 ns at 298 K. The temperature was regulated using a Langevin thermostat with a collision frequency of 5 ps^{-1} (Andersen, 1980). Finally, structures from RMD were energy minimized for 5000 steps. The SHAKE algorithm was used to constrain bonds involving hydrogen atoms (Ryckaert *et al*., 1977). The PTRAJ module of AMBER was used for trajectory analyses. Force field parameters for the heme group were taken from a previous work (Autenrieth *et al*., 2004). The Met80 residue was non-bonded to the iron atom and a constraint was applied instead. Molecular graphics were performed with UCSF Chimera (Pettersen *et al*., 2004). Final minimized structures were validated by the Protein Structure Validation Software suite (PSVS) (Bhattacharya *et al*., 2007), the iCING server (Doreleijers *et al.*, 2012) and the Protein Data Bank (PDB) validation suite. In addition, a non-restrained MD computation of 20 ns was launched to check the stability of the resulting conformers. A non-restrained MD computation of 20 ns was also launched on the NMR structure of WT C*c*. S^2 parameters values

per residue were obtained from the non-restrained computations performed for both C*c* species.

Finally, NMR assignments and PDB coordinates for the Y48*p*CMF C*c* were deposited in the Biological Magnetic Resonance Data Bank (BMRB) and PDB databases. BMRB and PDB entries for the Y48*p*CMF C*c* are 25660 and 2N3Y, respectively.

X-ray absorption spectroscopy

X-ray absorption spectroscopy (XAS) experiments were carried out at Diamond Light Source (UK), operating at 3 GeV and 300 mA ring current. The Fe K-edge (7112 eV) was measured at beamline I20-scanning, comprising a four-bounce Si(111) crystal monochromator. Two Rh-coated mirrors working at 5.0 mrad were used for high-energy harmonics rejection. The spectra were recorded in fluorescence mode, using a 36-element monolithic Ge detector (Canberra). An iron foil was simultaneously recorded in transmission mode using ionization chamber detectors to be used as internal calibration. To avert radiation damage, X-rays were attenuated with a 1.5-mm thick carbon foil. In addition, samples were measured at cryogenic temperatures using a liquid nitrogen cryojet (Oxford Instrument). Each datapoint was collected using a 1 s acquisition time, and 36 scans were averaged. Samples were measured in plastic capillary cells. 350 μM C*c* samples were prepared in 10 mM sodium phosphate buffer (pH 5.8).

Spectra averaging, background subtraction and amplitude normalization required to obtain the extended X-ray absorption fine structure (EXAFS) signals (k) were performed using the Athena (version 0.9.024) code (Ravel and Newville, 2005). The best fit to the data was performed by using the Artemis program (version 0.9.024) (Ravel and Newville, 2005). Scattering paths were computed using FEFF 6.0. Initial atomic coordinates of the heme moiety were taken from the crystallographic structure of the WT form (PDB: 3zcf) (Rajagopal *et al.*, 20013). Neither the initial coordinates from this structure nor those from the NMR structure (PDB: 1j3s) (Jeng *et al*., 2002) yielded acceptable fits.

Still, the distances coming out from these fits were used as input to screen 10^4 coordinates from each MD computation (Guerra-Castellano *et al*., 2015). The snapshots with the smallest sum of quadratic distance differences with respect to the EXAFS fit-derived distances were selected iteratively.

Isothermal titration calorimetry

Interactions of the human C*c* species with plant Cc_1, at their reduced and oxidized states were analyzed by isothermal titration calorimetry (ITC) using an Auto-ITC200 microcalorimeter (MicroCal) at 25°C. The reference cell was filled with distilled water. The experiments consisted of 2 μL injections of 0.4 mM C*c* solution in 10 mM sodium phosphate buffer (at pH 5.8, 7.4 and 8.5) into the sample cell, initially containing 20 μM Cc_1 solution in the same buffer. All solutions were degassed before titration. Titrant was injected at appropriate time intervals to ensure that the thermal power signal returned to the baseline prior to the next injection. To achieve a homogeneous mixing in the cell, the stirring speed was kept constant at 1000 rpm. The data, specifically the heat-per-injection normalized per mol of injectant *versus* molar ratio, were analyzed with Origin 7 (OriginLab) using a two-site binding model with a distinct affinity for each site, as recently reported for the plant C*c*-Cc_1 complex (Moreno-Beltrán *et al*., 2014). In addition, the titration of reduced bovine C*c*O (3.85 μM) with the reduced C*c* species (0.10 mM) was performed in 10 mM sodium phosphate buffer (pH 7.4), supplemented with 0.2% (w/v) *n*-dodecyl-β-D-maltoside and 5 mM sodium dithionite, as described previously (Moreno-Beltrán *et al*., 2015). Calibration and performance tests of the calorimeter were carried out by conducting Ca^{+2}-EDTA titrations with the solutions provided by the manufacturer.

Calorimetric liposome binding assays were carried out in a low-volume Nano-ITC (TA instruments, Inc.). All titrations were performed in 25 mM HEPES buffer (pH 7.4). A 6 μM C*c* solution was titrated with a suspension of unilamellar vesicles. Stirring was set to 350 rpm. Unilamellar vesicles

contained 1,2-dioleoyl-*sn*-glycero-3-phosphocholine (DOPC) either alone or with 1,1'2,2'-tetraoleoylcardiolipin (TOCL) at a 4:1 ratio. Total lipid concentration in the syringe was 8.9 mM. DOPC unilamellar vesicles (7.9 mM) were used for control experiments. Data processing and analyses were carried out with the Nanoanalyze software (TA Instruments).

Cytochrome *c* oxidase assays

The ability of C*c* species to act as electron donors for cytochrome *c* oxidase (C*c*O) activity was tested in isolated complex IV and in mitochondria from *Saccharomyces cerevisiae*. Two yeast cell strains were used for mitochondria extraction, namely WT (BY4741; MATa; ura3Δ0; leu2Δ0; his3Δ1; met15Δ0) (WT_{mito}) and C*c*-deficient Y06846 (BY4741; MATa; ura3Δ0; leu2Δ0; his3Δ1; met15Δ0; YJR048w::kanMX4) (Δ*Cc*) strains. Two other yeast cell strains were likewise used for mitochondria extraction, namely WT (W303-1A; mata leu2 trp1 ura3 his3 ade2) (WT_{Rcf}) and Rcf-deficient RCF1::HIS3 RCF2::KAN (W303-1A; mata leu2 trp1 ura3 ade2) (ΔRcf1/2) strains. WT_{mito} and Δ*Cc* cells were grown in YPD medium (1% yeast extract, 2% peptone and 2% glucose), whereas WT_{Rcf} and ΔRcf1/2 cells were grown in YPD medium or YP-0.5% lactate medium supplemented with 2% galactose (YP-Gal), as described previously (Strogolova *et al*., 2012), to obtain mitochondria-enriched cells. In all cases, crude mitochondria were isolated as previously described (Padilla-López *et al*., 2009) and stored at –80ºC in 0.6 M sorbitol, 20 mM K-MES buffer (pH 6.0). C*c*O activity was measured spectrophotometrically (Beckman DU® 650 spectrophotometer) using the commercial C*c*O activity kit from Sigma®, according to the manufacturer's instructions. In experiments with HIGD1A/2A proteins, the reaction mixtures were incubated at 25ºC for 30 min before running the assay.

Liposome preparation and binding experiments

In order to analyze the interaction of the C*c* species with cardiolipin (CL), small unilamellar liposomes were prepared by sonication in 25 mM

HEPES buffer (pH 7.4). Liposomes contained either DOPC and TOCL (4:1 ratio) or DOPC alone (manufactured by Avanti Polar Lipids®). C*c*:liposome binding assays were performed by incubating the C*c* species with DOPC or TOCL/DOPC liposomes at different ratios (protein:lipids) for 1 h in 25 mM HEPES buffer (pH 7.4). The complexes were analyzed by electrophoretic mobility shift assay (EMSA). The samples were applied onto 0.8% agarose gel, and the electrophoresis was run for 90 min at 50 V in non-denaturing 35 mM HEPES buffer (pH 7.4). Gels were stained for protein detection with 0.25% Coomassie Brilliant Blue R-250 in 45% methanol and 10% acetic acid.

Peroxidase assays

Peroxidase assays of C*c*:liposomes were performed as previously described with minor modifications (Belikova *et al*., 2006). TOCL/DOPC liposomes were incubated for 1 h at room temperature with C*c* (1 μM) in a 1:100 ratio (w/w) (protein:lipid) in 20 mM HEPES buffer (pH 7.4). After incubation, and immediately before starting the measurement, 2′,7′-dichlorofluorescin diacetate (H_2DCF) and H_2O_2 were added to the samples at 5 μM and 100 μM final concentrations, respectively. Increases in DCF fluorescence at 522 nm were recorded along 30 min upon excitation at 502 nm, with 5-nm slits, in a Cary Eclipse (Varian) fluorescence spectrophotometer. Basal peroxidase activity of C*c* in CL-free liposomes was used as control.

Caspase activation assays

In vitro activation of caspases was achieved as described previously with minor modifications (Rodríguez-Roldán *et al*., 2008). Human embryonic kidney 293 (HEK 293) cytoplasmic cell extract (100 μg), prepared as described previously (Pecina *et al*., 2010), was incubated for 60 min at 37°C, in a total volume of 25 μL, with 25 mM KCl, 0.2 mM DTT, 0.2 mM dATP and human WT or Y48*p*CMF C*c* at a final concentration of 8 μM. After incubation, 180 μL of buffer A (10 mM HEPES buffer (pH 7.0) with 50 mM NaCl, 40 mM β-glycerophosphate, 2 mM $MgCl_2$, 5 mM EGTA, 0.1 mg mL^{-1} bovine serum albumin, and 0.1% (w/v) CHAPS),

supplemented with 10 μM of acetyl-Asp-Glu-Val-Asp-7-amino-4-methylcoumarin (Ac-DEVD-AMC; a fluorescent substrate specific for caspases 3/7), was added to the reaction mixture. Fluorescence increases resulting from Ac-DEVD-AMC cleavage was rapidly determined in a Cary Eclipse (Varian) fluorescence spectrophotometer (optical slits of 2.5 nm), using an excitation wavelength of 360 nm and an emission wavelength of 460 nm. Data were the averages of at least three independent experiments.

Blue-native gel electrophoresis of protein complexes from yeast mitochondria

Fresh mitochondria (400 μg of protein) isolated from yeast cell extracts were permeabilized in 40 μL of solubilization buffer (30 mM HEPES buffer (pH 7.4), with 150 mM KOH-acetate, 10% glycerol and 1 mM PMSF) plus digitonin at a 4:1 (w:w) ratio of digitonin:protein. Samples were incubated on ice for 30 min, centrifuged for 30 s, and loaded onto NativePAGE Novex 3–12% Bis-Tris protein gel (1.0 mm, 15-well; Thermo Fisher Scientific, cat. No. BN2012BX10), following the manufacturer's instructions.

Antibodies

Mouse monoclonal anti-His_6 and anti-α-tubulin were obtained from Sigma-Aldrich (catalog numbers 11922416001 and T8328, respectively). Secondary horseradish peroxidase (HRP)-conjugated anti-mouse IgG was obtained from Sigma-Aldrich (catalog number A4416). Rabbit antibody against yeast C*c*, and mouse antibody again yeast COX II, were a gift from Dr. Carlos Santos-Ocaña. Rabbit antibodies against the C-terminal domains of yeast Rcf1 and Rcf2 were kindly provided by Prof. Peter Rehling. Rabbit antiserum against yeast Cc_1 was a gift from Prof. Nikolaus Pfanner. Rabbit anti-human C*c* serum was obtained by immunizing male

rabbits with full-length recombinant C*c* suspended in a 0.85% NaCl solution. Secondary horseradish peroxidase (HRP)–conjugated anti-rabbit IgG was obtained from Sigma-Aldrich (catalog number A0545).

Western blot analysis

For immunoblot detection of yeast C*c*, Rcf1 and Rcf2 in mitochondria and human C*c* and α-tubulin in cytoplasmic fractions of HEK293 cells, protein quantification was first assessed using the Bradford protein assay (Bradford, 1976). For immunodetection of Cc_1, COX II, Rcf1 and Rcf2 inside the respiratory supercomplexes, mitochondrial content were obtained after permeabilization and protein quantification by the Bradford protein assay (Bradford, 1976). For cytoplasmic cell extracts and mitochondria samples, 10–20 μg of proteins were resolved by β-dodecyl sulphate–polyacrylamide gel electrophoresis (SDS-PAGE). For supercomplexes analysis, 20-μg protein samples were loaded onto NativePAGE Novex 3–12% Bis-Tris protein gels (1.0 mm, 15-well; Thermo Fisher Scientific, catalog number BN2012BX10), which were further transferred to polyvinylidene fluoride (PVDF) membranes (EMD Millipore) using a Mini Trans-Blot electrophoretic transfer cell (Bio-Rad). Membranes were blocked in 5% nonfat dry milk in PBS with Tween-20 (TPBS) for cytoplasmic extracts and mitochondria, and in only TBS for supercomplex analyses. Immunoblots were performed with primary antibodies, and then HRP-conjugated secondary antibodies were used for detection. The immunoreactive bands were detected using Amersham ECL Plus Western Blotting Detection Reagents (GE Healthcare Life Sciences).

SUPPLEMENTARY TABLES

Supplementary Table 1. **NMR experiments performed on reduced Y48*p*CMF C*c***

	Experiments	Magnetic Field
Backbone assignment	2D ^{1}H-^{15}N HSQC, 2D ^{1}H-^{13}C HSQC, 3D HNCA, 3D HNCACB, 3D CBCA(CO)NH, 3D HN(CA)CO and 3D HNCO.	700 MHz
Side-chain assignment	2D ^{1}H-^{13}C HSQC, 2D COSY, 3D HBHA(CO)NH and 3D HCCH-TOCSY.	700 MHz
	Aromatic 2D ^{1}H-^{13}C HSQC	500 MHz
Mobility analysis	^{15}N R_1, ^{15}N R_2 and steady-state {^{1}H}-^{15}N NOE	500 MHz
Distance constraints	2D ^{1}H-^{1}H NOESY, 3D ^{1}H-^{15}N NOESY-HSQC, 3D ^{1}H-^{13}C NOESY-HSQC	950 MHz
Heme assignments & constraints	2D COSY, 2D ^{1}H-^{15}N NOESY and ^{1}H-^{15}N EXSY	950 MHz
Amide hydrogen exchange	2D ^{1}H-^{15}N HSQC	700 MHz
Biomolecular interactions	2D ^{1}H-^{15}N HSQC	700 MHz

Supplementary Table 2. Comprehensive ^{15}N relaxation parameters of the WT and Y48*p*CMF C*c* species

	WT C*c*	Y48*p*CMF C*c*	Difference
R_1 (s^{-1})	2.26 ± 0.08	2.15 ± 0.07	0.11
R_2 (s^{-1})	8.53 ± 0.46	9.14 ± 0.48	0.61
R_2 / R_1	3.77 ± 0.23	4.25 ± 0.23	0.48
NOE ratio	0.80 ± 0.03	0.80 ± 0.02	0.00
τ_c (ns)	6.33 ± 0.02	6.96 ± 0.02	0.63

Supplementary Table 3. Equilibrium and thermodynamic parameters for the interaction of WT and Y48*p*CMF C*c* at the two binding sites of C*c*$_1$, as determined by ITC

	***Proximal* site**				***Distal* site**				
Protein couple	K_{D1} (μM)	ΔH_1 (kcal/mol)	$-T\Delta S_1$ (kcal/mol)	ΔG_1 (kcal/mol)	K_{D2} (μM)	ΔH_2 (kcal/mol)	$-T\Delta S_2$ (kcal/mol)	ΔG_2 (kcal/mol)	***n***
C*c* WT$_{red}$/C*c*$_{1red}$[a,1]	11.5	11.7	–18.40	–6.70	54.0	10.5	–16.30	–5.80	2
C*c* Y48*p*CMF$_{red}$/C*c*$_{1red}$[a]	5.1	–1.8	–5.42	–7.22	230.0	4.4	–9.36	–4.96	2
C*c* WT$_{ox}$/C*c*$_{1ox}$[b]	1.9	6.2	–14.00	–7.80	110.0	1.1	–6.50	–5.40	2
C*c* Y48*p*CMF$_{ox}$/C*c*$_{1ox}$[b]	1.8	8.2	–16.03	–7.83	71.0	3.3	–8.96	–5.66	2
C*c* WT$_{ox}$/C*c*$_{1ox}$[c]	50.0	4.3	–10.16	–5.86	140.0	0.8	–6.05	–5.25	2
C*c* Y48*p*CMF$_{ox}$/C*c*$_{1ox}$[c]	12.0	1.4	–8.11	–6.71	140.0	1.3	–6.55	–5.25	2

Relative errors: K_D, 20%; ΔH and $-T\Delta S$, 5%; ΔG 2%

1 = Moreno-Beltrán *et al*., 2015

[a] = pH 7.4

[b] = pH 5.8

[c] = pH 8.5

Supplementary Table 4. Equilibrium and thermodynamic parameters for the interaction of WT and Y48*p*CMF C*c* at the two binding sites of bovine C*c*O, as determined by ITC

	***Proximal* site**				***Distal* site**				
Protein couple	K_{D1} (μM)	ΔH_1 (kcal/mol)	$-T\Delta S_1$ (kcal/mol)	ΔG_1 (kcal/mol)	K_{D2} (μM)	ΔH_2 (kcal/mol)	$-T\Delta S_2$ (kcal/mol)	ΔG_2 (kcal/mol)	***n***
C*c* WT_{red}/C*c*O_{red}[1]	0.03	–6.6	–3.7	–10.3	0.30	–5.4	–3.5	–8.9	2
C*c* Y48*p*CMF_{red}/C*c*O_{red}	2.10	–6.3	–1.4	–7.7	7.00	–30.0	23.0	–7.0	2

Relative errors: K_D, 20%; ΔH and $-T\Delta S$, 5%; ΔG, 2%

[1] = Moreno-Beltrán *et al*., 2015.

SUPPLEMENTARY FIGURES

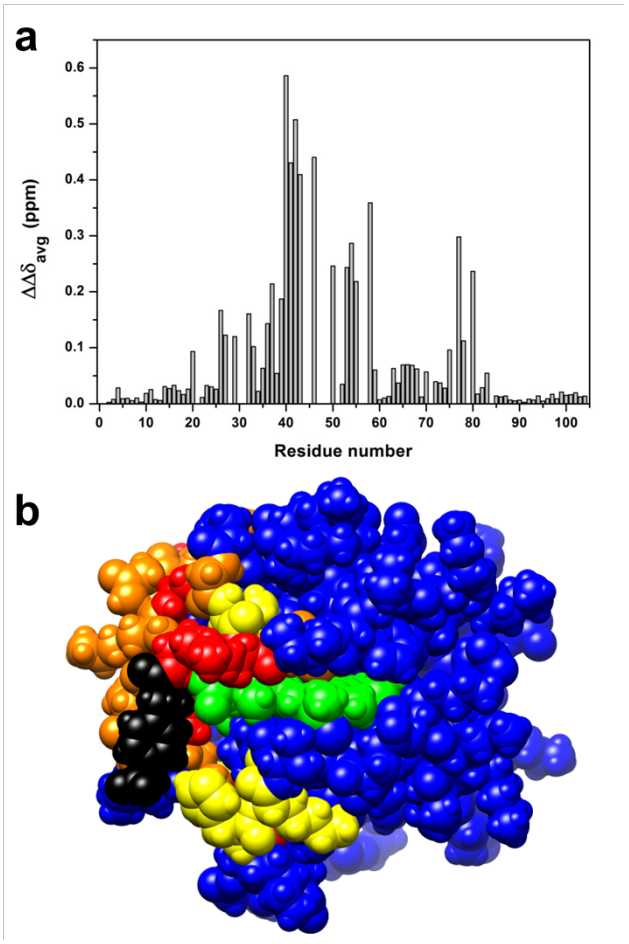

Supplementary Figure 1. Chemical-shift differences between WT and Y48*p*CMF C*c*. **(a)** Plot of the chemical-shift differences between both C*c* species for backbone amides along their primary sequence. **(b)** The chemical shift differences are mapped on the Y48*p*CMF C*c* surface according to the degree of change. Residues are colored in yellow if the chemical-shift difference ranged between 0.1 and 0.2 ppm, and in red if the difference was greater than 0.2 ppm. Residues with undetectable backbone amide resonances in the ^{1}H-^{15}N HSQC spectrum of Y48*p*CMF C*c* but detectable in WT C*c* are colored in orange. *p*CMF48 and the heme group are given in black and green, respectively. Unaffected, unassigned and proline residues are in blue.

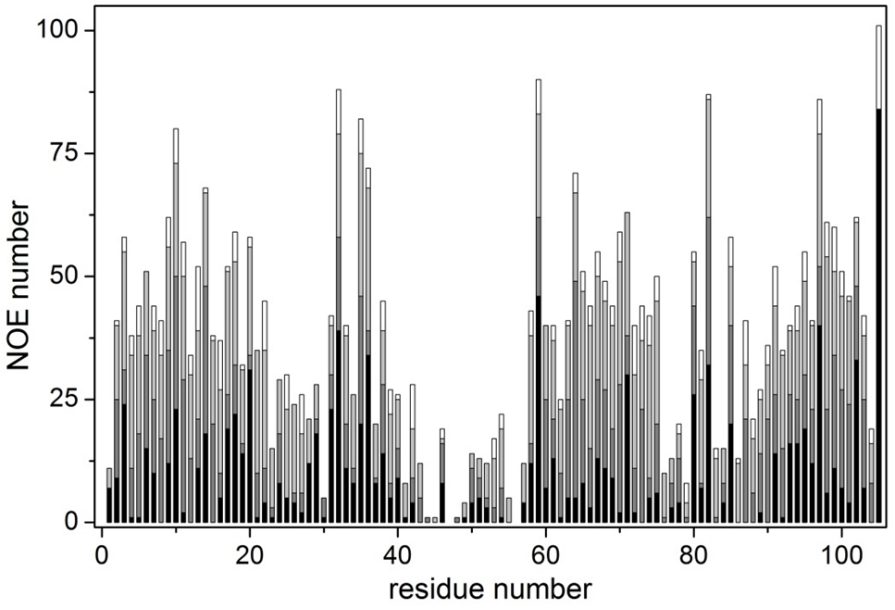

Supplementary Figure 2. Number of experimental meaningful NOEs per residue used for the structure calculation of Y48*p*CMF C*c*. The color code for the NOE bars is: intra-residue, white; sequential, light gray; medium, gray; and long range, black. Residue 105 corresponds to the heme group.

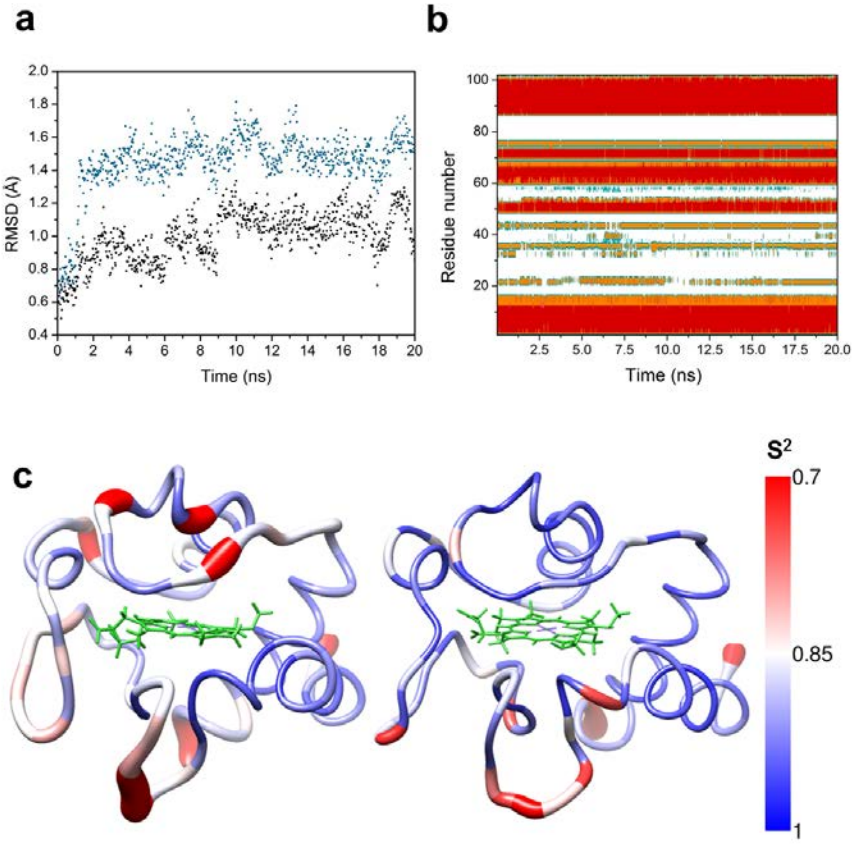

Supplementary Figure 3. Molecular Dynamics simulations for the Y48*p*CMF variant and WT form of C*c*. **(a)** A non-restrained MD computation was performed to check the stability of conformers derived from the NMR structure of Y48*p*CMF C*c*. RMSD values are plotted along the full 20 ns trajectory, considering either residues away from the mutation surroundings (black) or the whole protein sequence (blue). **(b)** Time evolution of secondary structural elements along the MD trajectory represented in (**a**). The color code is as follows: α-helix, red; π-helix, orange; extended β-brand, blue; β-bridge, cyan; turn, yellow; and coil, white. **(c)** Comparison of S^2 order parameter values for Y48pCMF and WT C*c* obtained from MD computations. S^2 order parameter values per residue for Y48*p*CMF (*left*) and WT (*right*) C*c* are represented on their respective NMR ribbon structures using a blue-red scale (color key is shown). Heme atoms are displayed in green. Internal mobility of alpha carbon atoms was calculated with the Amber software.

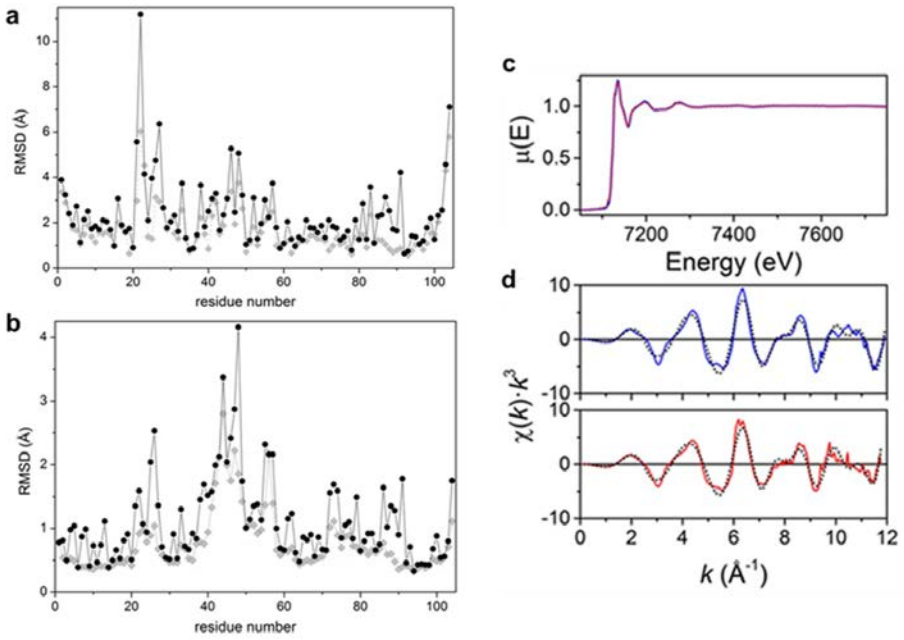

Supplementary Figure 4. **(a)** Per residue RMSD values between the first conformer of the NMR solution structures of WT C*c* (PDB ID: 1J3S) (Jeng *et al*., 2002) and the refined lowest-TF Y48*p*CMF C*c*. Backbone and heavy atoms are represented as gray triangles and black circles, respectively. RMSD calculations were performed with the MOLMOL software (Koradi *et al*., 1996). **(b)** Global RMSD values per residue of the best 20 conformers of Y48*p*CMF C*c* with respect to the mean structure. The color code is as in (**a**). **(c)** Normalized X-ray Absorption Spectra (XAS) of WT (blue line) and Y48*p*CMF (red dots) C*c*. **(d)** Extended absorption fine structure (EXAFS) waves for WT C*c* (blue) and Y48*p*CMF C*c* (red). Black dots correspond to the best fits summarized in Figure 2 and Table 1.

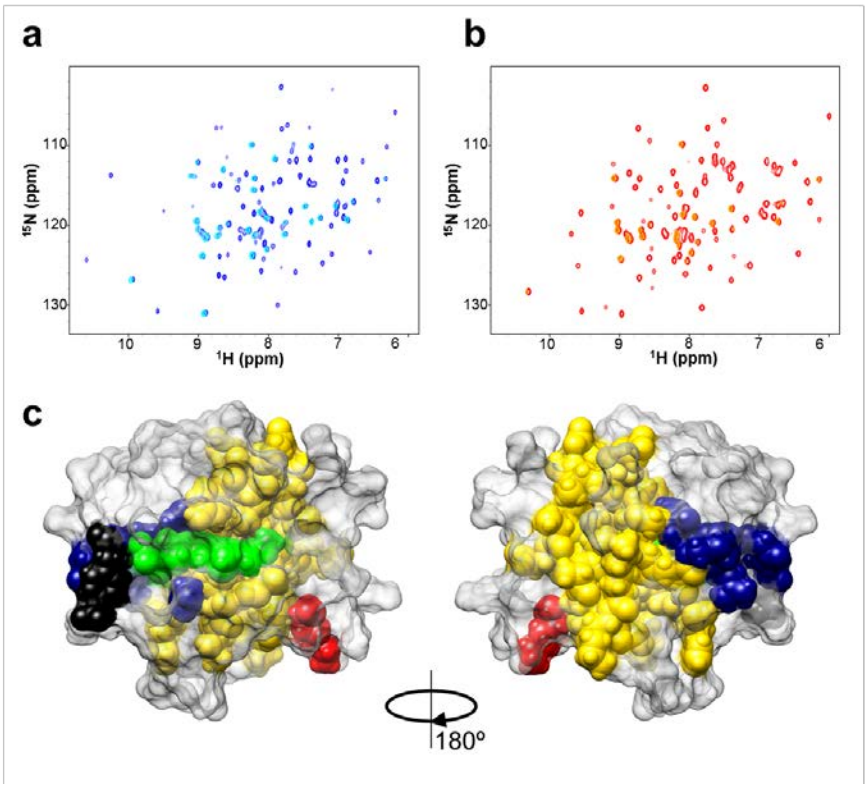

Supplementary Figure 5. Amide-hydrogen exchange experiments with WT and Y48*p*CMF C*c*. **(a)** ^{1}H-^{15}N HSQC spectrum of WT C*c* recorded either in 95% H_2O and 5% D_2O (blue) or in 100% D_2O (cyan). **(b)** ^{1}H-^{15}N HSQC spectrum of Y48*p*CMF C*c* recorded either in 95% H_2O and 5% D_2O (red) or in 100% D_2O (gold). **(c)** Residues protected from amide-hydrogen exchange in both C*c* species are displayed in gold, those protected only in Y48*p*CMF C*c*, in red, and those protected only in WT C*c*, in blue. *p*CMF48 and the heme group are in black and green, respectively. The representation is projected on the Y48*p*CMF C*c* structure, whose surface is light gray.

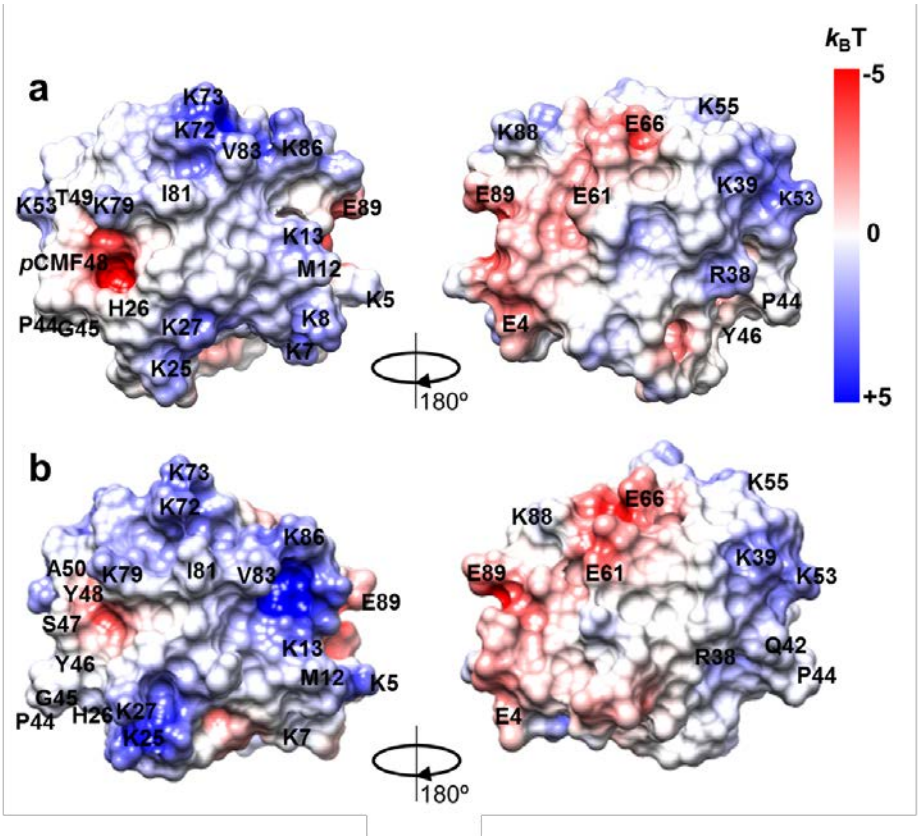

Supplementary Figure 6. **(a**, **b)** Surface electrostatic potentials of WT (**a**) and Y48*p*CMF (**b**) C*c* molecules. Negatively and positively charged regions are depicted in red and blue, respectively. Simulations were performed with the DelPhi program (Nicholls and Honig, 1991) aided by Chimera (Pettersen *et al*., 2004), assuming an ionic strength of 250 mM. The color scale ranges from –5 (red) to +5 (blue) k_BT. Some residues were labelled to better show the orientation of both C*c* species. The PDB file 1J3S was used for the WT C*c* structure.

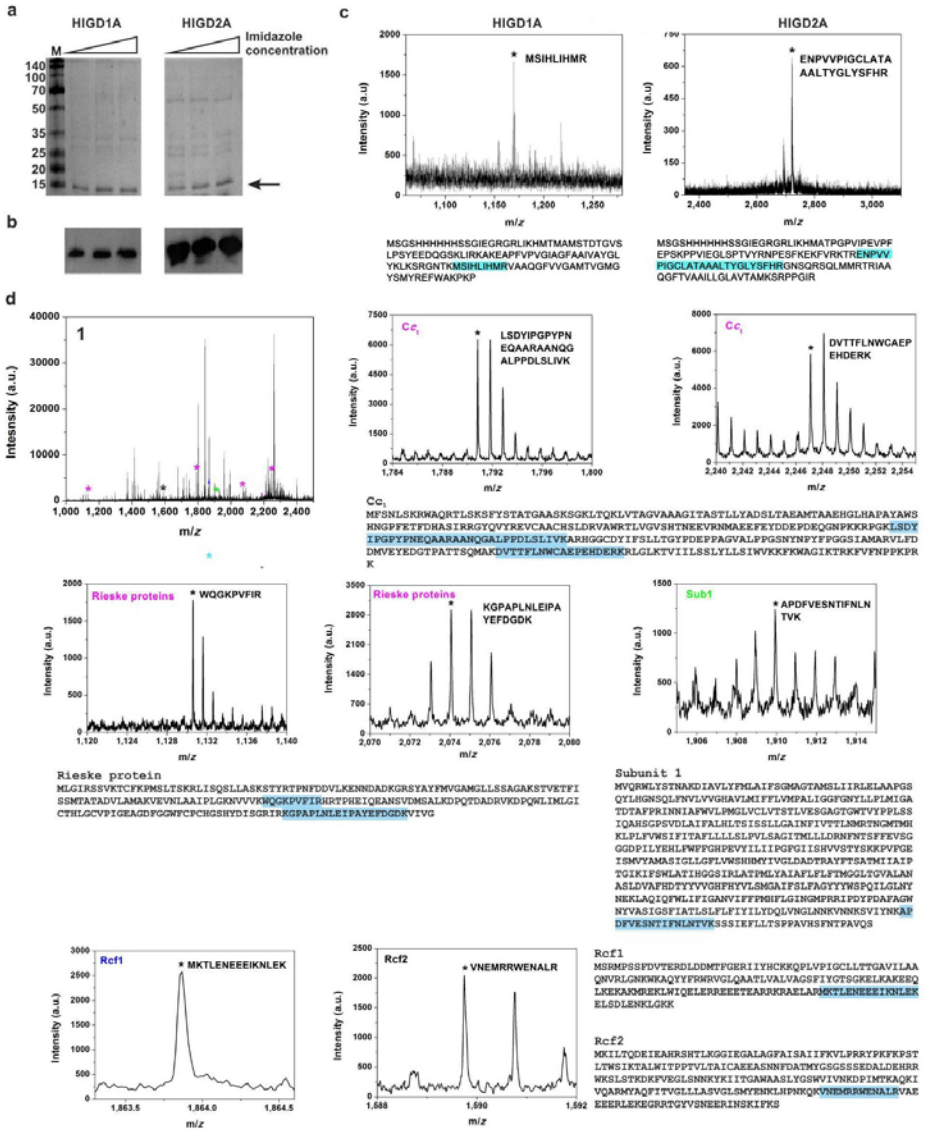

Supplementary Figure 7. HIGD proteins. **(a)** SDS-PAGE of purified HIGD1A and HIGD2A His-tagged proteins after applying an imidazole gradient. M, molecular weight markers. The arrow points to the bands corresponding to HIGD proteins. **(b)** Western blot analysis using an antibody against His-tag to identify HIGD1A and HIGD2A following Ni-column purification. **(c)** Trypsin digestion of HIGD proteins followed by matrix-assisted laser desorption ionization with time-of-light (MALDI-TOF) analysis. **(d)** Tryptic digestion of proteins from BN-PAGE

bands followed by MALDI-TOF/TOF and highlighted by asterisks in Figure 5d. Specifically, the data presented here correspond to the upper band in YP-Gal in Figure 5d. The expected tryptic masses clearly matched the calculated values, with 0.5 Da tolerance. The sequence coverage of these fragments is shaded in cyan.

REFERENCES

Andersen HC. 1980. Molecular dynamics simulations at constant pressure and/or temperature. *J Chem Phys* **24:** 1999-2012. doi:10.1063/1.439486.

Assfalg M, Bertini I, Turano P, Bruschi M, Durand MC, Giudici-Orticoni MT and Dolla A. 2002. A quick solution structure determination of the fully oxidized double mutant K9-10A cytochrome c_7 from *Desulfuromonas acetoxidans* and mechanistic implications. *J Biomol NMR* **22:** 107-22. doi:10.1023/A:1014202405862.

Autenrieth F, Tajkhorshid E, Baudry J and Luthey-Schulten Z. 2004. Classical force field parameters for the heme prosthetic group of cytochrome *c*. *J Comput Chem* **25:** 1613-22. doi:10.1002/jcc.20079.

Baistrocchi P, Banci L, Bertini I and Turano P. 1996. Three-dimensional solution structure of *Saccharomyces cerevisiae* reduced iso-1-cytochrome *c*. *Biochemistry* **35:** 13788-96. **doi:**10.1021/bi961110e.

Banci L, Bertini I, Bren KL, Gray HB, Sompornpisut P and Turano P. 1997. Solution structure of oxidized *Saccharomyces cerevisiae* iso-1-cytochrome *c*. *Biochemistry* **36**: 8992-9001. **doi:**10.1021/bi963025c.

Bartalesi I, Bertini I and Rosato A. 2003. Structure and dynamics of reduced *Bacillus pasteurii* cytochrome *c*: oxidation state depedent properties and implications for electron transfer processes. *Biochemistry* **42**: 739-45. doi**:**10.1021/bi0266028.

Bartels C, Xia TH, Billeter M, Guntert P and Wuthrich K. 1995. The program XEASY for computer-supported NMR spectral analysis of biological acromolecules. *J Biomol NMR* **6**: 1-10. doi:10.1007/BF00417486.

Bradford MM. 1976. A rapid and sensitive method for the quantitation of microgram quantities of protein utilizing the principle of protein-dye binding. *Anal Biochem* **72**: 248-54. doi:10.1016/0003-2697(76)90527-3.

Belikova NA, Vladimirov YA, Osipov AN, Kapralov AA, Tyurin VA, Potapovich MV, Basova LV, Peterson J, Kurnikov IV and Kagan VE. 2006. Peroxidase activity and structural transitions of cytochrome *c* bound to cardiolipin-containing membranes. *Biochemistry* **45**: 4998-5009. **doi:**10.1021/bi0525573.

Bhattacharya A, Tejero R and Montelione GT. 2007. Evaluating protein structures determined by structural genomics consortia. *Proteins* **66**: 778-95. doi:10.1002/prot.21165.

Blackledge M, Cordier F, Dosset P and Marion D. 1998. Precision and uncertainty in the characterization of rotational diffusion from heteronuclear relaxation data. *J Am Chem Soc* **120**: 4538-39. **doi:**10.1021/ja9742646.

Case DA, Darden TA, Cheatham III TE, Simmerling CL, Wang J, Duke RE, Luo R, Merz KM, Pearlman DA, Crowley M, Walker RC, Zhang W, Wang B, Hayik S, Roitberg A, Seabra G, Wong KF, Paesani F, Wu X, Brozell S, Tsui V, Gohlke H, Yang L, Tan C, Mongan J, Hornak V, Cui G, Beroza P, Mathews DH, Schafmeister CEAF, Ross WS and Kollman PA. 2006. AMBER 9 University of California, San Francisco.

Doreleijers JF, Sousa da Silva AW, Krieger E, Nabuurs SB, Spronk CA, Stevens TJ, Vranken WF, Vriend G and Vuister GW. 2012. CING: an integrated residue-based structure validation program suite. *J Biomol NMR* **54**: 267-83. doi: 10.1007/s10858-012-9669-7.

Dosset P, Hus JC, Blackledge M and Marion D. 2000. Efficient analysis of macromolecular rotational diffusion from heteronuclear relaxation data. *J Biomol NMR* **16**: 23-8. doi:10.1023/A:1008305808620.

Duan Y, Wu C, Chowdhury S, Lee MC, Xiong G, Zhang W, Yang R, Cieplak P, Luo R, Lee T, Caldwell J, Wang J and Kollman P. 2003. A point-charge force field for molecular mechanics simulations of proteins based on condensed-phase quantum mechanical calculations. *J Comput Chem* **24**: 1999-2012. doi:10.1002/jcc.10349.

Goddar TD and Kneller DG. 2001. SPARKY 3, University of California, San Francisco, CA, USA.

Greenfield NJ. 2007. Using circular dichroism spectra to estimate protein secondary structure. *Nat Protoc* **1**: 2876-90. doi:10.1038/nprot.2006.202.

Guerra-Castellano A, Díaz-Quintana A, Moreno-Beltrán B, López-Prados J, Nieto PM, Meister W, Staffa J, Teixeira M, Hildebrandt P, De la Rosa MA and Díaz-Moreno I. 2015. Mimicking tyrosine phosphorylation in human cytochrome *c* by the evolved tRNA synthetase technique. *Chem Eur J* **21**: 15004-12. doi:10.1002/chem.201502019.

Grzesiek S and Bax A. 1993. Amino acid type determination in the sequential assignment procedure of uniformly $^{13}C/^{15}N$-enriched proteins. *J Biomol NMR* **3**: 185-204. doi:10.1007/BF00178261.

Güntert P, Mumenthaler C and Wüthrich K. 1997. Torsion angle dynamics for NMR structure calculation with the new program Dyana1. *J Mol Biol* **273**: 283-98. doi:10.1006/jmbi.1997.1284.

Jeng WY, Chen CY, Chang HC and Chuang WJ. 2002. Expression and characterization of recombinant human cytochrome *c* in *E. coli*. *J Bioenerg Biomembr* **34**: 423-31. doi:10.1023/A:1022561924392.

Kay LE, Torchia DA and Bax A. 1989. Backbone dynamics of proteins as studied by ^{15}N inverse detected heteronuclear NMR spectroscopy: application to staphylococcal nuclease. *Biochemistry* **28**: 8972-9. **doi:**10.1021/bi00449a003.

Kay LE, Xu G, Singer AU, Muhandiram DR and Forman-Kay JD. 1993. A gradient-enhanced HCCH-TOCSY experiment for recording side-chain ^{1}H and ^{13}C correlation in H_2O samples of proteins. *J Magn Reson* **101**: 333-7.

Keller R. 2004. *The computer aided resonance assignment tutorial 1st edn (Cantina Verlag*.).

Kelly SM, Jess TJ and Price NC. 2005. How to study proteins by circular dichroism. *Biochim Biophys Acta – Proteins Proteomics* **1751**: 119-39. doi:10.1016/j.bbapap.2005.06.005.

Koradi R, Billeter M and Wüthrich K. 1996. MOLMOL: a program for display and analysis of macromolecular structures. *J Mol Graph* **51**: 29-32.

Marion D, Driscoll PC, Kay LE, Wingfield PT, Bax A, Gronenborn AM, Clore GM. 1989a. Overcoming the overlap problem in the assignment of ^{1}H NMR spectra of larger proteins by use of three-dimensional heteronuclear ^{1}H-^{15}N Hartmann-Hahn-multiple quantum coherence and nuclear Overhauser-multiple quantum coherence spectroscopy: application to interleukin 1β. *Biochemistry* **28**: 6150-6.

Marion D, Kay LE, Sparks SW, Torchia DA and Bax A. 1989b. Three-dimensional heteronuclear NMR of nitrogen-^{15} labeled proteins. *J Am Chem Soc* **111**: 1515-7. **doi:**10.1021/ja00186a066.

Moreno-Beltrán B, Díaz-Quintana A, González-Arzola K, Velázquez-Campoy A, De la Rosa MA and Díaz-Moreno I. 2014. Cytochrome c_1 exhibits two binding sites for cytochrome *c* in plants. *Biochim Biophys Acta – Bioenerg* **1837**: 1717-29. doi:10.1016/j.bbabio.2014.07.017.

Moreno-Beltrán B, Díaz-Moreno I, González-Arzola K, Guerra-Castellano A, Velázquez-Campoy A, De la Rosa MA and Díaz-Quintana A. 2015. Respiratory complexes III and IV can each bind two molecules of cytochrome *c* at low ionic strength. *FEBS Lett* **589**: 476-83. doi:10.1016/j.febslet.2015.01.004.

Nicholls A and Honig B. 1991. A rapid finite difference algorithm, utilizing successive overrelaxation to solve the Poisson–Boltzmann equation. *J Comput Chem* **12**: 435-45. doi:10.1002/jcc.540120405.

Padilla-López S. Jiménez-Hidalgo M, Martín-Montalvo A, Clarke CF, Navas P and Santos-Ocaña C. 2009. Genetic evidence for the requirement of the endocytic pathway in the uptake of coenzyme Q6 in *Saccharomyces cerevisiae*. *Biochim Biophys Acta – Biomemb* **1788**: 1238-48. doi:10.1016/j.bbamem.2009.03.018.

Pecina P, Borisenko GG, Belikova NA, Tyurina YY, Pecinova A, Lee I, Samhan-Arias AK, Przyklenk K, Kagan VE and Hüttemann M. 2010. Phosphomimetic substitution of cytochrome *c* tyrosine 48 decreases respiration and binding to cardiolipin and abolishes ability to trigger downstream caspase activation. *Biochemistry* **49**: 6705-14. doi:10.1021/bi100486s.

Pettersen EF, Goddard TD, Huang CC, Couch GS, Greenblatt DM, Meng EC and Ferrin TE. 2004. UCSF Chimera - A visualization system for exploratory research and analysis. *J Comput Chem* **25**: 1605-12. doi:10.1002/jcc.20084.

Piotto M, Saudek V and Sklenar V. 1991. Gradient-tailored excitation for single-quantum NMR spectroscopy of aqueous solutions. *J Biomol NMR* **2**: 661-5. doi:10.1007/BF02192855.

Rajagopal BS, Edzuma AN, Hough MA, Blundell KL, Kagan VE, Kapralov AA, Fraser LA, Butt JN, Silkstone GG, Wilson MT, Svistunenko DA and Worrall JA. 2013. The hydrogen-peroxide-induced radical behaviour in human cytochrome *c*-phospholipid complexes: implications for the enhanced pro-apoptotic activity of the G41S mutant. *Biochem J* **456**: 441-52. doi: 10.1042/BJ20130758.

Ravel B and Newville M. 2005. ATHENA, ARTEMIS, HEPHAESTUS: data analysis for X-ray absorption spectroscopy using IFEFFIT. *J Synchrotron Rad* **12**: 537-41.

Rodríguez-Roldán V, García-Heredia JM, Navarro JA, De la Rosa MA and Hervás M. 2008. Effect of nitration on the physicochemical and kinetic features of wild-type and monotyrosine mutants of human respiratory cytochrome *c*. *Biochemistry* **47**: 12371-9. doi: 10.1021/bi800910v.

Ryckaert JP, Ciccotti G and Berendsen HJC. 1977. Numerical integration of the cartesian equations of motion of a system with constraints: Molecular dynamics of *n*-Alkanes. *J Comp Phys* **23**: 327-41. doi:10.1016/0021-9991(77)90098-5

Sreerama N and Woody RM. 2000. Estimation of protein secondary structure from circular dichroism spectra: comparison of CONTIN, SELCON, and CDSSTR

methods with an expanded reference set. *Anal Biochem* **282**: 252-60. doi:10.1006/abio.2000.4880.

Strogolova V, Furness A, Robb-McGrath M, Garlich J and Stuart RA. 2012. Rcf1 and Rcf2, members of the hypoxia-induced gene 1 protein family, are critical components of the mitochondrial cytochrome bc_1-cytochrome *c* oxidase supercomplex. *Mol Cell. Biol* **32**: 1363-73. doi:10.1128/MCB.06369-11.

Xie J, Supekova L and Schultz PG. 2007. A genetically encoded metabolically stable analogue of phosphotyrosine in *Escherichia coli*. *ACS Chem Biol* **2**: 474-8. doi:10.1021/cb700083w.

Zuiderweg ER and Fesik SW. 1988. Heteronuclear 3-dimensional NMR spectroscopy. A strategy for the simplification of homonuclear two-dimensional NMR spectra. *J Magn Reson* **78**: 588-93. doi:10.1016/0022-2364(88)90144-8.

Zuiderweg ER and Fesik SW. 1989. Heteronuclear three-dimensional NMR spectroscopy of the inflammatory protein C5a. *Biochemistry* **28**: 2387-91. **doi:**10.1021/bi00432a008.

12. APPENDIX III

Cytochrome *c* with a phosphomimetic mutation at position 97 retains its structural features but has modified functionality

Alejandra Guerra-Castellano, Antonio Díaz-Quintana,
Sofía M. García-Mauriño, Miguel A. De la Rosa and Irene Díaz-Moreno*

Instituto de Investigaciones Químicas (IIQ) – Centro de Investigaciones Científicas Isla de la Cartuja (cicCartuja), Universidad de Sevilla – Consejo Superior de Investigaciones Científicas (CSIC), Avda. Américo Vespucio 49, Sevilla 41092, Spain

***Corresponding author:**
Email: idiazmoreno@us.es
Telephone number: +34 954489513; Fax number: +34 954460065

Abstract

Cytochrome *c* (C*c*) is phosphorylated at tyrosine 97 in the post-ischemic brain by neuroprotective insulin treatment. Here we characterize a phosphomimetic, phosphatase-resistant C*c* mutant, which was recombinantly generated by site-specific incorporation of *p*-carboxymethyl-L-phenylalanine at position 97 using an evolved aminoacyl-tRNA synthetase. The mutant C*c* was not significantly affected in its overall folding and heme environment but had a decreased thermal stability. COX activity increased 5-fold in isolated complex IV in the presence of HIGD1A and the mutant C*c*, but decreased by half in mitochondrial supercomplexes from hypoxia-induced yeast with the phosphomimetic mutant, as compared to wild-type C*c*. The peroxidase activity of mutant C*c*, as well as its capacity to bind cardiolipin and activate caspases, are likewise investigated. This phosphomimetic C*c* could potentially have therapeutic applications for acute diseases, such as brain ischemia.

Keywords: caspase activity; cytochrome *c*; electron transport chain; liposomes binding; peroxidase activity; phosphorylation

Abbreviations:

Ac-DEVD-AMC	acetyl-Asp-Glu-Val-Asp-7-amino-4-methylcoumarin
Apaf1	apoptosis protease activation factor 1
βDDM	*n*-dodecyl β-D-maltoside
CD	circular dichroism
CHAPS	3-[(3-cholamidopropyl)dimethylammonio]-1-propanesulfonate
CL	cardiolipin
COX	cytochrome *c* oxidase
Cbc_1	cytochrome bc_1 complex
C*c*	cytochrome *c*
Cc_1	cytochrome c_1
DOPC	1,2-dioleoyl-sn-glycero-3-phosphocholine
EMSA	electrophoretic mobility shift assay
ETC	electron transfer chain
H_2DCF	dichlorofluorescein diacetate
HEK	human embryonic kidney
HIG1	hypoxia-induced gene 1
HIGD1A	HIG hypoxia inducible domain family member 1A
HIGD2A	HIG hypoxia inducible domain family member 2A
MD	molecular dynamics
MES	2-(N-morpholino)ethanesulfonic acid, 4-morpholineethanesulfonic acid
PCD	programmed cell death
*p*CMF	*p*-carboxymethyl-L-phenylalanine
OxPhos	oxidative phosphorylation
Rcf1	respiratory supercomplex factor 1
Rcf2	respiratory supercomplex factor 2
ROS/RNS	reactive oxygen/nitrogen species
T_m	midpoint melting temperature
TOCL	1,1′2,2′-tetraoleoylcardiolipin
WT	wild-type

Highlights

- Replacing Tyr97 with *p*CMF97 generated a C*c* mutant that retained its overall structure and heme properties
- The Y97*p*CMF C*c* mutant enhanced the HIGD1A-dependent COX activity *in vitro*
- Under hypoxia conditions, the COX action triggered by Y97*p*CMF was decreased to half of that triggered by WT C*c*
- The Y97*p*CMF mutation slightly decreased caspase cascade activity

1. Introduction

One post-translational modification known to regulate proteins is phosphorylation, which is modulated by kinases and phosphatases, affecting for instance the functionality of proteins in redox signaling (Monteiro and Sterm, 1996; Liaudet *et al*., 2009; Corcoran and Cotter, 2013). This is particularly important in mitochondria, which are the main source of reactive oxygen/nitrogen species (ROS/RNS) in the cell (Turrens, 2000).

Cytochrome *c* (C*c*) is a small soluble hemeprotein localized in the mitochondrial intermembrane space. It is an essential component of the electron transfer chain (ETC), which transfers electrons from the cytochrome bc_1 complex (Cbc_1) to cytochrome *c* oxidase (COX). The yeast respiratory supercomplex factors (Rcfs) are modulators that stabilize both membrane-embedded Cbc_1 and COX complexes within respiratory supercomplexes (Strogolova *et al*., 2012; Vukotic *et al*., 2012). Rcf1 (formerly Aim31) and Rcf2 (formerly Aim38) are members of the hypoxia-induced gene 1 (HIG1) protein family. Rcf1 is required for yeast growth under hypoxia and is directly involved in the association of Cbc_1 and COX, which form a stable supercomplex. Rcf1 is a conserved subunit and has two human orthologues, the hypoxia inducible domain family members 1A and 2A (HIGD1A and HIGD2A, respectively). However, Rcf2 is yeast-specific, in which it is necessary for the oligomerization of a subclass of COX into respirasomes (Strogolova *et al*., 2012; Vukotic *et al*., 2012).

Under nitro-oxidative stress conditions, C*c* acts as a programmed cell death (PCD) inductor (Ow *et al*., 2008). During the start of apoptosis, a population of tightly mitochondrial membrane–bound C*c* triggers phospholipid peroxidation, affecting in particular cardiolipin (CL) (Tuominem *et al*., 2002; Kagan *et al*., 2005; Belikova *et al*., 2006; Kapralov *et al*., 2011).

CL-adducted C*c* undergoes a profound tertiary conformational rearrangement that creates an entry channel for H_2O_2 molecules, which explains how C*c* enhances its peroxidase activity (Jemmerson *et al*., 1999; Vladimirov *et al*., 2006; Pandiscia and Schweitzer-stenner, 2005). It has been

proposed that C*c*-CL conjugates are sufficient for formation of mitochondrial pores, which then release the hemeprotein into the cytosol during apoptosis (Iverson and Orrenius, 2004; Gonzalvez and Gottlieb, 2007; Bergstrom *et al*., 2013).

Extramitochondrial C*c* binds to the apoptosis protease activation factor 1 (Apaf1), thereby eliciting the apoptosome platform assembly and activating the caspase cascade (Zou *et al*., 1999; Desagher and Martinou, 2000). Recent data indicate that the apoptotic network involving C*c* is complex, and that C*c* targets several proteins that are functionally equivalent in humans and plants (Martínez-Fábregas *et al*., 2013; Martínez-Fábregas *et al*., 2014a; Martínez-Fábregas *et al*., 2014b). In human cells, C*c* reaches the cell nucleus upon DNA damage and sequesters SET/TAF1β, a histone chaperone that remodels chromatin (González-Arzola *et al*., 2015).

The two major targets of oxidative phosphorylation (OxPhos) that control signaling are C*c* and COX. C*c* can undergo several post-translational modifications, including nitration or phosphorylation of tyrosine residues (Lee *et al*., 2006; Yu *et al*., 2008; Souza *et al*., 2008; García-Heredia *et al*., 2010; Díaz-Moreno *et al*., 2011; Ly *et al*., 2012; Capdevila *et al*., 2015). These two mutually-exclusive modifications can alter how C*c* binds to its physiological partners, in either the mitochondria or cytosol, but these effects are highly dependent on which tyrosine is modified (reviewed in ref. Díaz-Moreno *et al*., 2011). In addition to tyrosine residues, C*c* can also be phosphorylated at Thr28 and Ser47, as detected in human skeletal muscle. Recent data obtained with phosphomimic mutants suggest that phosphorylation of these residues enhances electron transport (Zhao *et al*., 2011; Guerra-Castellano *et al*., 2016).

Tyr97 phosphorylation has been correlated with several pathologies, including ischemia. Indeed, it has been proposed that Tyr97 of C*c* is targeted for phosphorylation during the insulin-induced neuroprotection response following an ischemic injury (Sanderson *et al*., 2013). A possible mechanism could be that Tyr97-phosphorylation of C*c* impairs its electron shuttling to COX (Lee *et al*., 2006). In addition, although the HIGD1A membrane protein positively regulates

the activity between COX and wild-type (WT) C*c*, it is unknown how it reacts with phosphorylated C*c* (Hayasi *et al*., 2015).

Research on tyrosine phosphorylation in C*c* has normally resorted to using Tyr-to-Glu mutations (Pecina *et al*., 2010; García-Heredia *et al*., 2011), to overcome the difficulties of obtaining enough phosphorylated C*c* for biophysical and functional studies if the specific C*c*-phosphorylating kinase is unknown (Kadenbach and Urban, 1968). However, the Tyr-to-Glu substitution leads to a substantial decrease in the residue volume and the loss of an aromatic ring. Therefore, we used the tRNA-evolved technique to include the non-canonical *p*-carboxymethyl-L-phenylalanine (*p*CMF) amino acid at position 97, as previously reported for Tyr48 (Guerra-Castellano *et al*., 2015). Thus, this non-canonical amino acid can be used to synthesize stable analogues of a wide array of phosphoproteins, allowing it to be used when specific kinase is unknown or the yield of phosphoprotein is very low. In addition, *p*CMF provides a dependable analogue of a phosphorylated tyrosine that can be used to study signal transduction pathways. The resulting Y97*p*CMF C*c* mutant maintained its overall folding and heme moiety. However, we found that this post-translational modification of C*c* affected the OxPhos process: on the one hand, Y97*p*CMF C*c* enhanced the HIGD1A-dependent COX activity *in vitro*; on the other, the electron donation rate to COX by Y97*p*CMF was decreased to half of that of WT C*c* in mitochondria isolated from yeast grown under hypoxia. Thus, the COX-driven oxidation rate of C*c* is controlled by phosphorylation to maintain low levels of apoptotic-inducing ROS/RNS. Y97*p*CMF C*c* is also an inefficient caspase activator, thereby avoiding inducing apoptosis. Altogether, our findings can help shed light on the role of phosphorylated C*c* in insulin-stimulated post-ischemic neuroprotection.

2. Materials and methods

2.1. Site-directed mutagenesis, protein expression and purification of recombinant proteins

Y97*p*CMF C*c* was expressed and purified as previously described (Guerra-Castellano *et al*., 2015) using the evolved tRNA synthetase technique (Xie *et al*., 2007). Detailed descriptions of the DNA constructs, protein expression and protein purification are provided in Supporting Information.

The HIGD1A protein was expressed by cell-free protein synthesis in continuous exchange (dialysis mode; ratio 1:10) following our recently established protocol [data not shown]. The His-tagged form of HIGD1A was purified by nickel affinity chromatography according to earlier protocols. The final yield was 125 μg protein·mL^{-1} of reaction. The protein was exchanged to a final 10 mM sodium phosphate buffer (pH 7.4) with 0.2% *n*-dodecyl β-D-maltoside (βDDM).

2.2. Circular dichroism spectroscopy

Circular dichroism (CD) spectra were recorded using a Jasco® J-815 spectropolarimeter equipped with a Peltier temperature-control system. CD intensities are presented in terms of molar ellipticity [θ_{molar}] using molar protein concentration (Kelly *et al*., 2005). The secondary structure analyses were carried out by recording far-UV CD spectra (185–250 nm) at 25°C in a 1-mm quartz cuvette. Samples contained 3 μM protein in 10 mM sodium phosphate (pH 6.5), supplemented with 10 μM potassium ferricyanide. For each sample, 20 scans were averaged and analyzed using the CDpro software package with the SMP50 and SP37A reference set, as well as with the CLSTR option to compare with a set of proteins with similar folds (Sreeema and Woody, 2000; Greenfield, 2007).

The coordination of the heme iron atom to the S_{δ} atom of Met80—the sixth axial ligand of heme group—was analyzed by visible (B-band) recording visible CD spectra (300–600 nm) at 25°C in a 10-mm quartz cuvette. Samples

contained 30 μM protein in 10 mM sodium phosphate (pH 6.5), supplemented with 100 μM potassium ferricyanide.

Thermal unfolding was monitored between 20°C and 105°C (with a heating rate of 1 °C/min) by recording the CD signal at far-UV in a 10-mm quartz cuvette. For these assays, the oxidized C*c* species were at 3 μM final concentration in 10 mM sodium phosphate (pH 6.5), supplemented with 10 μM potassium ferricyanide. Changes in the tertiary structure of the protein upon temperature increases were additionally monitored by fluorescence-detected CD following the increment of the intensity for the 270 nm excitation signal due to the exposure of Trp59 to the solvent (Blauer *et al*., 1993). The sample mixture contained 30 μM C*c* in 10 mM sodium phosphate (pH 6.5) and 100 μM potassium ferricyanide. The experimental data were processed by a principal component analysis (Johnson *et al*., 2002) as described (Guerra-Castellano *et al*., 2015). This strategy eliminates the noise that appears with the single-wavelength analysis and allows the distinction of processes involving different attributes.

2.3. Electronic absorption spectroscopy

The coordination of the heme group of C*c* was analyzed by monitoring the absorption changes at 699 nm, indicative of the heme Fe-Met80(S_δ) bond (Ranjbar and Gill, 2009). Electronic absorption spectra were recorded in the 630–740 nm range, using a Jasco® V-650 spectrophotometer in a 1-mL quartz cuvette with a path length of 10 mm (García-Heredia *et al*., 2010). Samples contained 0.2 mM oxidized C*c* in 50 mM Tris-HCl (pH 7.4), supplemented with 0.2 mM potassium ferricyanide. For pH titration studies, the pH of each sample was adjusted to the reported values by adding aliquots of 0.1–0.5 M NaOH or 0.1–0.5 M HCl.

2.4. Cytochrome *c* oxidase measurements

Whether human C*c* species is able to restore bovine COX activity was first tested using both isolated hemeproteins in the presence or absence of the HIGD1A membrane protein. Secondly, COX activity was measured *in*

mitochondria from the following *Saccharomyces cerevisiae* yeast strains: WT (W303-1A mata leu2 trp1 ura3 his3 ade2), RCF1::HIS3 (ΔRcf1) strain (W303-1A mata leu2 trp1 ura3 ade2), RCF2::KAN (ΔRcf2) strain (W303-1B matα leu2 trp1 ura3 his3 ade2) or RCF1::HIS3 RCF2::KAN (ΔRcf1/Rcf2) strain (W303-1A mata leu2 trp1 ura3 ade2), all of which were provided by Dr. Rosemary A. Stuart (Klingler College of Arts and Sciences, Marquette University, Milwaukee). All yeast strains were grown in YP–0.5% lactate medium supplemented with 2% galactose (YPL-Gal) as described previously to obtain mitochondria-enriched cells grown in hypoxia-like conditions [5]. Crude mitochondria were then isolated as previously described and stored at –80°C in 0.6 M sorbitol, 20 mM 2-(N-morpholino)ethanesulfonic acid, 4-morpholineethanesulfonic acid (MES)/KOH (pH 6) (Padilla-López *et al*., 2009). To permeate the outer mitochondrial membrane and allow exogenous WT and Y97*p*CMF C*c* (to a final concentration of 6.9 μM) to enter into the organelle, βDDM detergent was used following previously-reported protocols (Musatov *et al*, 2000). *In vitro* and *in mitochondria* COX activity was measured spectrophotometrically (Jasco® V-650 spectrophotometer) using a COX activity kit (Sigma®) according to the manufacturer's instructions. No signal of C*c* oxidation was obtained in these assays, showing that it was necessary to add exogenous C*c* to test the COX activity (data not shown). For measurements involving HIGD1A, WT or Y97*p*CMF C*c* and HIGD1A proteins were incubated with COX at 25ºC for 30 min before each assay. The slopes of the 550-nm absorbance for at least three independent experiments were correlated with a value of COX activity.

2.5. Liposome preparation and binding to cytochrome *c*

To analyze the interaction of C*c* with cardiolipin (CL), small unilamellar liposomes were formed by sonication in 25 mM HEPES buffer (pH 7.4). Liposomes were prepared from 1,2-dioleoyl-sn-glycero-3-phosphocholine (DOPC) and 1,1'2,2'-tetraoleoylcardiolipin (TOCL) (4:1 ratio) or DOPC alone (manufactured by Avanti Polar Lipids®).

C*c*:CL binding assays were performed as previously described (Guerra-Castellano *et al*., 2016). C*c* and liposomes were incubated at different ratios for

1 h in 25 mM HEPES buffer (pH 7.4). The samples were applied to a 0.8% agarose gel for electrophoresis for 90 min at 50 mV in non-denaturing 35 mM HEPES buffer (pH 7.4). Gels were stained for protein detection with 0.25% Coomassie Brilliant Blue R-250 in 45% methanol and 10% acetic acid.

2.6. Peroxidase assays

Peroxidase assays of C*c* were carried out as reported previously (Belikova *et al*., 2006). DOPC:TOCL liposomes were incubated for 1 h at room temperature with C*c* in a ratio 1:100 (w/w) (C*c*:lipids) in 20 mM HEPES buffer (pH 7.4). After the incubation, and immediately before starting measurements, 5 μM 2′,7′-dichlorofluorescein diacetate (H_2DCF) and 100 μM hydrogen peroxide were added to the samples. DCF fluorescence increment was measured for 30 min using an excitation wavelength of 502 nm and emission of 522 nm (with a slit of 5 nm in both cases) in a Cary Eclipse (Varian) fluorescence spectrophotometer, estimating the peroxidase activity as the slope of fluorescence increment. To test the basal peroxidase activity of C*c*, control assays without liposomes were also performed.

2.7. Caspase activation assays

In vitro activation of caspases was achieved as formerly described with slight changes (Dutton and Wilson, 1974). Cytoplasmic cell fractions devoid of endogenous C*c* from human embryonic kidney 293 (HEK 293) were obtained as previously described with minor modifications (Pecina *et al*., 2010). Detailed descriptions of cell culture, subcellular fractioning and caspase-3 activation assays are provided in Supporting Information.

3. Results and Discussion

3.1. The Tyr97*p*CMF mutation preserves the physicochemical properties of wild-type cytochrome *c* species

In order to mimic the phosphorylation of C*c* at position 97, we substituted Tyr97 with the non-canonical amino acid *p*CMF, using the evolved tRNA synthetase method (Ryu and Schultz, 2006) as described previously (Guerra-Castellano *et al*, 2015). This substitution simulates the charge and the volume of a phosphotyrosine residue better than a glutamic acid substitution.

To confirm that the non-canonical amino acid *p*CMF was successfully introduced at position 97 of the protein (**Figure 1A**), the Y97*p*CMF mutant was purified to homogeneity, and its molecular mass was compared to that of WT C*c* by MALDI-TOF (**Figure S1** in Supporting Information). The molecular mass of the phosphomimetic protein was increased by 41 Da as compared to WT, consistent with the expected substitution. We checked whether the amino acid replacement affected the secondary structure and heme environment by CD spectroscopy in the far-UV and visible region, respectively. We demonstrated that the overall secondary structure and heme properties of Y97*p*CMF C*c* are conserved, being similar to the WT species (**Figure 1B**, **C**).

At physiological pH values, the heme iron ion is hexacoordinated, with His18 and Met80 as axial ligands. In contrast, at least five distinct conformations of the oxidized form can exist in pH ranges from 1 to 12, which have altered heme axial coordination and/or in protein folding (Boffi *et al*., 2001). The so-called alkaline transition is the transformation from the physiological state III into state IV with increased pH and involves the replacement of Met80 as an axial ligand by Lys72, Lys73 or Lys79 (Wilson and Greenwood, 1996; Assfalg *et al*., 2003; Ying *et al*., 2009). In addition, the alkaline transition has been related to a change in the C*c* cell location, which is essential for its role in PCD (Godoy *et al*., 2009). To analyze the Fe-Met80(S_δ) bond changes caused by pH, we monitored the charge-transfer band at 699 nm (Fig. 1D), which disappears concomitantly with the alkaline transition (Schejter

and George, 1964). The estimated pK_a values for the WT and the Y97*p*CMF C*c* species were similar to each other, as well as to that reported for the Y97E mutant (García-Heredia *et al*., 2011). Thus, the pK_a of the alkaline transition is unaltered by the phosphomimetic mutation at residue 97. The presence of the 699-nm absorption band data in the Y97*p*CMF mutant contrasts with the shift towards 687 nm that is characteristic of Tyr97-phosphorylated C*c* (P-Y97), which is attributed to structural changes in the catalytic heme crevice (Lee *et al.*, 2006). Indeed, a similar intensity of the 699-nm band is observed for both the WT and the Y97*p*CMF C*c* species (**Figure 1D**). However, a prominent 650-nm band appeared in the spectrum of the Y97*p*CMF mutant, which is related to ferric high-spin heme iron (Chen *et al*., 1994; Pereira *et al*, 1997).

3.2. Thermal stability of the Y97pCMF cytochrome *c* mutant

The thermal stability of C*c* mainly depends on residues localized in the heme core (Cys14, Cys17, His18 and Met80) and in the N- and C-terminal α-helices (Gly6 and Phe10, and Leu94 and Tyr97, respectively). All of these residues are known as "key residues" of C*c* and are highly conserved (Zaidi *et al*., 2014). Remarkably, the N-terminal helix packs with an "extended" C-terminal helix or non-canonical "ridges and grooves" pattern (Chotia *et al.*, 1985) by a weak polar interaction, establishing a conserved structural motif shared by prokaryotic and eukaryotic C*c* (Pielak *et al*., 1995). The assembly of this helix-helix motif constitutes an early event in C*c* folding (Ptitsyn, 1998).

Most mutations in Tyr97 performed to date destabilize the structure of C*c*, as exemplified by the Y97E, Y97N and Y97I mutants. Nevertheless, the Y97F substitution increases thermal stability of the hemeprotein (García-Heredia *et al*., 2011; Pielak *et al*., 1995)]. We therefore recorded the denaturation of the Y97*p*CMF mutant along temperature ramps by far-UV CD together with simultaneous total fluorescence measurements. Data fitted to a two-state model (Lumry and Eyring, 1954). While the midpoint melting temperature (T_m) of the Y97*p*CMF mutant was slightly lower than that calculated for WT C*c* (**Table 1**), it was significantly higher than the T_m of Y97E (García-Heredia *et al*., 2011). In fact, the *p*CMF non-canonical amino acid contributed to keeping the

volume of a phosphotyrosine inside the folding core, making it a more appropriate phosphomimetic substitution than the Y97E mutation.

We also monitored the heme moiety environment along the temperature ramps by Vis CD. In contrast to the WT C*c*, which shows two transitions (Guerra-Castellano *et al*, 2015), the Y97pCMF data fit into a two-state model. In addition, the T_m of Y97*p*CMF was lower than the T_m of the second transition (T_{m2}) of WT C*c* (**Table 1**).

Altogether, these data indicate that there is a slight destabilization in the overall structure of Y97*p*CMF mutant as compared to the WT C*c*. Such thermal changes can be explained by alterations in the folding core formed by residues Phe10, Leu94 and Tyr97 upon phosphorylation, along with polar interactions between the N-terminal and C-terminal helices. Nevertheless, mimicking tyrosine phosphorylation in C*c* by including the non-canonical amino acid *p*CMF at a specific sequence position is a smarter solution than a Tyr $\rightarrow$Glu substitution, since *p*CMF emulates not only the charge but also the volume of a phosphotyrosine.

3.3. COX activity modulated by Y97*p*CMF cytochrome *c* and respiratory supercomplex factors

The ability of Y97*p*CMF C*c* to reduce COX was measured in the absence (**Figure 2A**) or presence of HIGD1A (Fig. 2B), which is a pro-survival membrane protein that acts as a positive modulator of COX (Hayasi *et al*., 2015). The measured COX activities were slightly higher with the Y97*p*CMF mutant as compared to the WT C*c* (with an increase of about 30%) (**Figure 2A**). This contrasts with previous measurements on respiration kinetics of WT and phosphorylated C*c* (Lee *et al*., 2006), in which COX was also phosphorylated, allowing a rapid adjustment of OxPhos components and their function. COX activity hardly increased upon HIGD1A addition but increased significantly when HIGD1A was added in the presence of Y97*p*CMF C*c* (**Figure 2B**). Hence, C*c* phosphorylation and HIGD1A might cooperatively modulate COX performance.

The HIGD1A-mediated regulation of COX activity was further tested in a cellular context using isolated mitochondria from yeast cells grown on YPL-Gal medium and incubated with either exogenous WT C*c* or Y97*p*CMF C*c*, after the outer mitochondrial membrane had been permeabilized. Under such hypoxia-like stress conditions, Rcf1—a yeast orthologue of human HIGD1A—and Rcf2 stabilize the Cbc_1-COX supercomplex (Strogolova *et al*., 2012; Vukotic *et al*., 2012; Chen *et al*., 2012). Hence, we used mitochondria obtained from a ΔRcf1/2 yeast strain in next COX assays; the absence of Rcf1 and Rcf2 proteins was corroborated by western blots. Regardless whether WT or Y97*p*CMF C*c* was added, the endogenous COX activity was strongly impaired in these mitochondria (**Figure 2C**). A single deletion of either Rcf1 or Rcf2 partially affected the COX activity levels, indicating a cooperative effect when the two membrane proteins Rcf1 and Rcf2 were present (**Figure 2C**). Interestingly, WT C*c* exhibited more COX activity than the Y97pCMF mutant, both in the presence of Rcf2 alone (ΔRcf1 strain) or together with Rcf1 (WT strain). Therefore, in mitochondria isolated from yeast undergoing hypoxic stress and incubated with exogenous Y97*p*CMF C*c*, the Rcf-mediated ETC flux is less accelerated. This may help to prevent hyperpolarization of the mitochondrial membrane and subsequent ROS/RNS production. In a similar manner, phosphorylation of Tyr97 in C*c*, which is triggered in the brain upon ischemic injury by the insulin-induced neuroprotection response (Sanderson *et al*., 2013), may aid to avoid cellular damage and guarantee cell survival during hypoxia in the brain.

3.4. Peroxidase activity and cardiolipin binding of the Y97*p*CMF phosphomutant

Recently, Sanderson and co-workers described the relation between C*c* phosphorylation at Tyr97 and the decrease in neuronal death under ischemia (Sanderson *et al*., 2013). The onset of PCD is triggered by the ability of the hemeprotein to leave mitochondria after binding to CL, which enhances the peroxidase activity of C*c* (Pandiscia and Schweitzer-Stenner, 2015). Therefore, a plausible hypothesis is that the decrease in neuronal ischemic death may be due to a less efficient release of phosphorylated C*c* to the cytosol, concomitantly with its role as PCD inductor. Hence, we examined the binding of

C*c* species to liposomes containing DOPC:TOCL (4:1) or DOPC by electrophoretic mobility shift assays (EMSA) in native agarose gels (**Figure 3A**). EMSA data revealed that Y97*p*CMF and WT C*c* had similar affinities for DOPC:TOCL membranes. Likewise, both C*c* species presented weak affinities for DOPC liposomes.

We also measured the peroxidase activity of C*c* that was either free or bound to DOPC:TOCL vesicles at a 1:100 ratio (C*c*:lipid). The peroxidase activity of C*c* species rose in the presence of liposomes, although no differences in activity were observed between the Y97*p*CMF and WT C*c* forms (**Figure 3B**).

3.5. Activation of caspase cascade by the Y97*p*CMF C*c* mutant

After mitochondrial membrane permeation during apoptosis, cytosolic C*c* interacts with Apaf1 to assemble the caspase-activation platform, the so-called apoptosome. In the context of brain ischemic damage, inhibition of both the C*c*-Apaf1 interaction and caspase-3 cleavage constitutes a potent neuroprotective strategy (Namura *et al*., 1998; Cao *et al*., 2004). Using HEK293 cytoplasmic cell extracts devoid of C*c*, we analyzed the caspase-3 activation by WT and Y97*p*CMF species (see inset, **Figure 4**). The presence of a negative charge at position 97 decreased caspase-3 cleavage by about 26% with respect to WT C*c* (**Figure 4**). These findings perfectly agree with our previous results on Y97E and Y97F C*c* mutants as well as with the nitrated mono-Tyr97 C*c*, which has a caspase activation slightly lower than that of the WT (García-Heredia *et al*., 2010; García-Heredia *et al*., 2011). Interestingly, none of these C*c* species disrupted the C*c*/Apaf1 complex assembly, and this is also expected for the Y97*p*CMF form. However, the formation of a non-functional apoptosome upon post-translational modifications of C*c* cannot be excluded (García-Heredia *et al*., 2010; García-Heredia *et al*., 2011; García-Heredia *et al*., 2010; García-Heredia *et al*., 2012). In summary, Y97*p*CMF C*c* acts as an inefficient caspase activator that would not induce apoptosis during post-ischemic neuroprotection.

This work shows the potential for designing a drug based on the *p*CMF molecule—a stable analogue of the phosphotyrosine that is resistant to

phosphatase hydrolysis and keeps C*c* in its phosphorylated state, which could have therapeutic applications for acute diseases, such as brain ischemia.

Acknowledgements

This work was supported by Ministry of Economy and Competitiveness (BFU2015-71017/BMC MINECO/FEDER, EU), Ramon Areces Foundation (2015-2017), European Social Fund 2007-2013, Andalusian Government (CVI-BIO198), grant JaePre_2011_01248 awarded to AGC, Biointeractomics platform (cicCartuja, Seville) and TA Instruments. This work also used the platforms of the Grenoble INSTRUCT centre (ISBG; UMS 3518 CNRS-CEA-UJF-EMBL) with support from FRISBI (ANR-10-INSB-05-02) and GRAL (ANR-10-LABX-49-01) within the Grenoble Partnership for Structural Biology (PSB). We thank Professor P. G. Schultz (Scripps Research Institute, California) for generously providing us with the plasmid pEVOL/pCMF/tRNA, Dr. Rosemary A. Stuart (Klingler College of Arts and Sciences, Marquette University, Milwaukee) for generously providing us with the *Saccharomyces cerevisiae* strains of WT (W303-1A mata leu2 trp1 ura3 his3 ade2), RCF1::HIS3 (Δrcf1) (W303-1A mata leu2 trp1 ura3 ade2), RCF2::KAN (Δrcf2) (W303-1B matα leu2 trp1 ura3 his3 ade2), and RCF1::HIS3 RCF2::KAN (Δrcf1 Δrcf2) (W303-1A mata leu2 trp1 ura3 ade2) and Prof. Peter Rehling for the antibodies αRcf1 and αRcf2.

6. References

Assfalg M, Bertini I, Dolfi A, Turano P, Mauk AG, Rosell FI and Gray HB (2003) Structural model for an alkaline form of ferricytochrome *c. J Am Chem Soc* **125**, 2913-2922.

Belikova NA, Vladimirov YA, Osipov AN, Kapralov AA, Tyurin VA, Potapovich MV, Basova LV, Peterson J, Kurnikov IV and Kagan VE (2006) Peroxidase activity and structural transitions of cytochrome *c* bound to cardiolipin-containing membranes. *Biochemistry* **45**, 4998-5009.

Bergstrom CL, Beales PA, Lv Y, Vanderlick TK and Groves JT (2013) Cytochrome *c* causes pore formation in cardiolipin-containing membranes. *Proc Natl Acad Sci USA* **110**, 6269-6274.

Blauer G, Sreerama N and Woody RW (1993) Optical activity of hemeproteins in the Soret region. Circular dichroism of the heme undecapeptide of cytochrome *c* in aqueous solution. *Biochemistry* **32**, 6674-6679.

Boffi F, Bonincontro A, Cinelli S, Congiu Castellano A, De Francesco A, Della Longa S, Girasole M and Onori G (2001) pH-Dependent local structure of ferricytochrome *c* studied by x-ray absorption spectroscopy. *Biophys J* **80**, 1473-149.

Cao G, Xiao M, Sun F, Xiao X, Pei W, Li J, Graham SH, Simon RP and Chen J (2004) Cloning of a novel Apaf-1-interacting protein: a potent suppressor of apoptosis and ischemic neuronal cell death. *J Neurosci* **24**, 6189-6201.

Capdevila DA, Oviedo Rouco S, Tomasina F, Tortora V, Demicheli V, Radi R and Murgida DH (2015) Active site structure and peroxidase activity of oxidatively modified cytochrome *c* species in complexes with cardiolipin. *Biochemistry* **54**, 7491-504.

Chen L, Pereira MM, Teixeira M, Xavier AV and Le Gall J (1994) Isolation and characterization of a high molecular weight cytochrome from the sulfate reducing bacterium *Desulfovibrio gigas*. *FEBS Lett* **347**, 295-299.

Chen YC, Taylor EB, Dephoure N, Heo JM, Tonhato A, Papandreou I, Nath N, Denko NC, Gygi SP and Rutter J (2012) Identification of a protein mediating respiratory supercomplex stability. *Cell Metab* **15**, 348-360.

Chotia C, Levitt M and Robertson D (1985) Helix to helix packing in proteins. *J Mol Biol* **145**, 215-250.

Corcoran A and Cotter TG (2013) Redox regulation of protein kinases. *FEBS J* **280**, 1944-1965.

Desagher S and Martinou JC (2000) Mitochondria as the central control point of apoptosis. *Trends Cell Biol* **10**, 369-377.

Díaz-Moreno I, García-Heredia JM, Díaz-Quintana A, Teixeira M and De la Rosa MA (2011) Nitration of tyrosines 46 and 48 induces the specific degradation of cytochrome *c* upon change of the heme iron state to high-spin. *Biochim Biophys Acta – Bioenerg* **1807**, 1616-1623. a

Díaz-Moreno I, García-Heredia JM, Díaz-Quintana A and De la Rosa MA (2011) Cytochrome *c* signalosome in mitochondria. *Eur Biophys J* **40**, 1301-1315. B

Dutton PL and Wilson DF (1974) Redox potentiometry in mitochondrial and photosynthetic bioenergetics. *Biochim Biophys Acta – Bioenerg* **346**, 165-212.

García-Heredia JM, Díaz-Moreno I, Nieto PM, Orzáez M, Kocanis S, Teixeira M, Pérez-Payá E, Díaz-Quintana A and De la Rosa MA (2010) Nitration of tyrosine 74 prevents human cytochrome *c* to play a key role in apoptosis signaling by blocking caspase-9 activation. *Biochim Biophys Acta – Bioenerg* **1797**, 981-993.

García-Heredia JM, Díaz-Quintana A, Salzano M, Orzáez M, Pérez-Payá E, Teixeira M, De la Rosa MA and Díaz-Moreno I (2011) Tyrosine phosphorylation turns alkaline transition into a biologically relevant process and makes human cytochrome *c* behave as an anti-apoptotic switch. *J Biol Inorg Chem* **16**, 1155-1168.

García-Heredia JM, Díaz-Moreno I, Díaz-Quintana A, Orzáez M, Navarro JA, Hervás M and De la Rosa MA (2012) Specific nitration of tyrosines 46 and 48 makes cytochrome *c* assemble a non-functional apoptosome. *FEBS Lett* **586**, 154-158.

Godoy LC, Muñoz-Pinedo C, Castro L, Cardaci S, Schonhoff CM, King M, Tórtora V, Marín M, Miao Q, Jiang JF, Kapralov A, Jemmerson R, Silkstone GG, Patel JN, Evans JE, Wilson MT, Green DR, Kagan VE, Radi R and Mannick JB (2009) Disruption of the M80-Fe ligation stimulates the translocation of cytochrome *c* to the cytoplasm and nucleus in nonapoptotic cells. *Proc Natl Acad Sci USA* **106**, 2653-2658.

González-Arzola K, Díaz-Moreno I, Cano-González A, Díaz-Quintana A, Velázquez-Campoy A, Moreno-Beltrán B, López-Rivas A and De la Rosa MA (2015) Structural basis for inhibition of the histone chaperone activity of SET/TAF-Iβ by cytochrome *c*. *Proc Natl Acad Sci USA* **112**, 9908-9913.

Gonzalvez F and Gottlieb E (2007) Cardiolipin: setting the beat of apoptosis. *Apoptosis* **12**, 877-885.

Guerra-Castellano A, Díaz-Quintana A, Moreno-Beltrán B, López-Prados J, Nieto PM, Meister W, Staffa J, Teixeira M, Hildebrandt P, De la Rosa MA and Díaz-Moreno I (2015) Mimicking tyrosine phosphorylation in human cytochrome *c* by the evolved tRNA synthetase technique. *Chem Eur J* **21**, 15004-15012.

Guerra-Castellano A, Díaz-Moreno I, Velázquez-Campoy A, De la Rosa MA and Díaz-Quintana A (2016) Structural and functional characterization of phosphomimetic mutants of cytochrome *c* at threonine 28 and serine 47. *Biochim Biophys Acta – Bioenerg* **1857**, 387-395.

Greenfield NJ (2007) Using circular dichroism spectra to estimate protein secondary structure. *Nat Protoc* **1**, 2876-2890.

Hayashi T, Asano Y, Shintani Y, Aoyama H, Kioka H, Tsukamoto O, Hikita M, Shinzawa-Itoh K, Takafuji K, Higo S, Kato H, Yamazaki S, Matsuoka K, Nakano A, Asanuma H, Asakura M, Minamino T, Goto Y, Ogura T, Kitakaze M, Komuro I, Sakata Y, Tsukihara T, Yoshikawa S and Takashima S (2015) Higd1a is a positive regulator of cytochrome *c* oxidase. *Proc Natl Acad Sci USA* **112**, 1553-1558.

Iverson SL and Orrenius S (2004) The cardiolipin–cytochrome *c* interaction and the mitochondrial regulation of apoptosis. *Arch Biochem Biophys* **423**, 37-46.

Jemmerson R, Liu J, Hausauer D, Lam KP, Mondino A and Nelson RDA (1999) A conformational change in cytochrome *c* of apoptotic and necrotic cells is detected by monoclonal antibody binding and mimicked by association of the native antigen with synthetic phospholipid vesicles. *Biochemistry* **38**, 3599-3609.

Johnson GW, Ehrlich R and Full W (2002) Principal components analysis and receptor models in environmental forensics, in *Introduction to environmental forensics* (Eds.: Murphy BL and Morrison RD), Academic Press, San Diego, pp. 461–515.

Kadenbach B and Urban PF (1968) Application of a quantitative chromatographic method of purification in the study of the biosynthesis of cytochrome *c*. *Fresen Z Anal Chem* **243**, 542-554.

Kagan VE, Tyurin VA, Jiang J, Tyurina YY, Ritov VB, Amoscato AA, Osipov AN, Belikova NA, Kapralov AA, Kini V, Vlasova II, Zhao Q, Zou M, Di P, Svistunenko DA, Kurnikov IV and Borisenko GG (2005) Cytochrome *c* acts as a cardiolipin oxygenase required for release of proapoptotic factors. *Nat Chem Biol* **1**, 223-232.

Kapralov AA, Yanamala N, Tyurina YY, Castro L, Arias AS, Vladimirov YA, Maeda A, Weitz AA, Peterson J, Mylnikov D, Demicheli V, Tortora V, Klein-Seetharaman J, Radi R and Kagan VE (2011) Topography of tyrosine residues and their involvement in peroxidation of polyunsaturated cardiolipin in cytochrome *c*/cardiolipin peroxidase complexes. *Biochim Biophys Acta – Biomembr* **1080**, 2147-2155.

Kelly SM, Jess TJ and Price NC (2005) How to study proteins by circular dichroism. *Biochim Biophys Acta – Proteins Proteom* **1751**, 119-139.

Lee I, Salomon AR, Yu K, Doan JW, Grossman LI and Hüttemann M (2006) New prospects for an old enzyme: mammalian cytochrome *c* is tyrosine-phosphorylated *in vivo*. *Biochemistry* **45**, 9121-9128.

Liaudet L, Vassalli G and Pacher P (2009) Role of peroxynitrite in the redox regulation of cell signal transduction pathways. *Front Biosci* **14**, 4809-4814.

Ly HK, Utesch T, Díaz-Moreno I, García-Heredia JM, De La Rosa MA and Hildebrandt P (2012) Perturbation of the redox site structure of cytochrome *c* variants upon tyrosine nitration. *J Phys Chem B* **116**, 5694-5702.

Lumry R and Eyring H (1954) Conformation changes of proteins. *J. Phys. Chem.* **58**, 110-120.

Martínez-Fábregas J, Díaz-Moreno I, González-Arzola K, Janocha S, Navarro JA, Hervás M, Bernhardt R, Díaz-Quintana A and De la Rosa MA (2013) New *Arabidopsis thaliana* cytochrome *c* partners: a look into the elusive role of cytochrome *c* in programmed cell death in plants. *Mol Cell Proteomics* **12**, 3666-3676.

Martínez-Fábregas J, Díaz-Moreno I, González-Arzola K, Janocha S, Navarro JA, Hervás M, Bernhardt R, Velázquez-Campoy A, Díaz-Quintana A and De la Rosa MA (2014) Structural and functional analysis of novel human cytochrome *c* targets in apoptosis. *Mol Cell Proteomics* **13**, 1439-1456. a

Martínez-Fábregas J, Díaz-Moreno I, González-Arzola K, Díaz-Quintana A and De la Rosa MA (2014) A common signalosome for programmed cell death in humans and plants. *Cell Death Dis* **5**, e1314. b

Monteiro HP and Stern A (1996) Redox modulation of tyrosine phosphorylation-dependent signal transduction pathways. *Free Radic Biol Med* **21**, 323-333.

Musatov A, Ortega-Lopez J and Robinson NC (2000) Detergent-solubilized bovine cytochrome *c* oxidase: Dimerization depends on the amphiphilic environment. *Biochemistry* **39**, 12996-13004.

Namura S, Zhu J, Fink K, Endres M, Srinivasan A, Tomaselli KJ, Yuan J and Moskowitz MA (1998) Activation and cleavage of caspase-3 in apoptosis induced by experimental cerebral ischemia. *J Neurosci* **18**, 3659-3668.

Ow Y-LP, Green DR, Hao Z and Mak TW (2008) Cytochrome *c*: functions beyond respiration. *Nat Rev Mol Cell Biol* **9**, 532-542.

Padilla-López S, Jiménez-Hidalgo M, Martín-Montalvo A, Clarke CF, Navas P and Santos-Ocaña C (2009) Genetic evidence for the requirement of the endocytic pathway in the uptake of coenzyme Q6 in *Saccharomyces cerevisiae*. *Biochim Biophys Acta – Biomembranes* **1788**, 1238-1248.

Pandiscia LA and Schweitzer-Stenner R (2015) Coexistence of native-like and non-native cytochrome *c* on anionic liposomes with different cardiolipin content. *J Phys Chem B* **119**, 12846-12859.

Pecina P, Borisenko GG, Belikova NA, Tyurina YY, Pecinova AA, Lee I, Samhan-Arias AK, Przyklenk K, Kagan VE and Hüttemann M (2010) Phosphomimetic substitution of cytochrome *c* tyrosine 48 decreases respiration and binding to cardiolipin and abolishes ability to trigger downstream caspase activation. *Biochemistry* **49**, 6705-6714.

Pereira IAC, Le Gall J, Xavier AV and Teixeira M (1997) The membrane-bound high-molecular-mass cytochromes *c* from *Desulfovibrio gigas* and *Desulfovibrio vulgaris* Hildenborough; EPR and Mössbauer studies. *J Biol Inorg Chem* **2**, 23-31.

Pielak GJ, Auld DS, Beasley JR, Betz SF, Cohen DS, Doyle DF, Finger SA, Fredericks ZL, Hilgen-Willis S, Saunders AJ and Trojak SJ (1995) Protein thermal denaturation, side-chain models, and evolution: amino acid substitutions at a conserved helix-helix interface. *Biochemistry* **34**, 3268-3276.

Ptitsyn OB (1998) Protein folding and protein evolution: common folding nucleus in different subfamilies of *c*-type cytochromes? *J Mol Biol* **278**, 655-666.

Ranjbar B and Gill P. (2009) Circular dichroism techniques: biomolecular and nanostructural analyses - A review. *Chem Biol Drug Des* **74**, 101-120.

Ryu Y and Schultz PG (2006) Efficient incorporation of unnatural amino acids into proteins in *Escherichia coli*. *Nat Methods* **3**, 263-265.

Sanderson TH, Mahapatra G, Pecina P, Ji Q, Yu K, Sinkler C, Varughese A, Kumar R, Bukowski MJ, Tousignant RN, Salomon AR, Lee I and Hüttemann M (2013) Cytochrome *c* is tyrosine 97 phosphorylated by neuroprotective insulin treatment. *PLoS One* **8**, e78627.

Schejter A and George P (1964) The 695-mμ band of ferricytochrome *c* and its relationship to protein conformation. *Biochemistry* **3**, 1045-1049.

Schweitzer-Stenner R (2008) Internal electric field in cytochrome *c* explored by visible electronic circular dichroism spectroscopy. *J Phys Chem B* **112**, 10358-10366.

Souza JM, Castro L, Cassina AM, Batthyány C and Radi R (2008) Nitrocytochrome *c*: synthesis, purification, and functional studies. *Methods Enzymol* **441**, 197-215.

Sreerama N and Woody RM (2000) Estimation of protein secondary structure from CD spectra: comparison of CONTIN, SELCON and CDSSTR methods with an expanded reference set. *Anal Biochem* **282**, 252-260.

Strogolova V, Furness A, Robb-McGrath M, Garlich J and Stuart RA (2012) Rcf1 and Rcf2, members of the hypoxia-induced gene 1 protein family, are critical components of the mitochondrial cytochrome bc_1-cytochrome *c* oxidase supercomplex. *Mol Cell Biol* **32**, 1363-1673.

Tuominen EKJ, Wallace CJA and Kinnunen PKJ (2002) Phospholipid cytochrome *c* interaction. Evidence for the extended lipid anchorage. *J Biol Chem* **277**, 8822–8826.

Turrens JF (2003) Mitochondrial formation of reactive oxygen species. *J Physiol* **552**, 335-344.

Vladimirov YA, Proskurnina EV, Izmailov DY, Novikov AA, Brusnichkin AV, Osipov AN and Kagan VE (2006) Cardiolipin activates cytochrome *c* peroxidase activity since it facilitates H_2O_2 access to heme. *Biochemistry* **71**, 998-1005.

Vukotic M, Oeljeklaus S, Wiese S, Vögtle FN, Meisinger C, Meyer HE, Zieseniss A, Katschinski DM, Jans DC, Jakobs S, Warscheid B, Rehling P and Deckers M. (2012) Rcf1 mediates cytochrome oxidase assembly and respirasome formation, revealing heterogeneity of the enzyme complex. *Cell Metab* **15**, 336-347.

Wilson MT and Greenwood C (1996) *Cytochrome c: a multidisciplinary approach* (Eds: Scott RA and Mauk AG) University Science Books, Sausilito, pp. 611-634.

Xie J, Supekova L and Schultz PG (2007) A genetically encoded metabolically stable analogue of phosphotyrosine in *Escherichia coli*. *ACS Chem Biol* **2**, 474-478.

Ying T, Zhong F, Xie J, Feng Y, Wang ZH, Huang ZX and Tan X (2009) Evolutionary alkaline transition in human cytochrome *c*. *J Bioenerg Biomembr* **41**, 251-257.

Yu H, Lee I, Salomon AR, Yu K and Hüttemann M (2008) Mammalian liver cytochrome *c* is tyrosine-48 phosphorylated *in vivo*, inhibiting mitochondrial respiration. *Biochim Biophys Acta – Bioenerg* **1777**, 1066-1071.

Zaidi S, Hassan MI, Islam A and Ahmad F (2014) The role of key residues in structure, function, and stability of cytochrome-*c*. *Cell Mol Life Sci* **71**, 229-255.

Zhao X, León IR, Bak S, Mogensen M, Wrzesinski K, Højlund K and Jensen ON (2011) Phosphoproteome analysis of functional mitochondria isolated from resting human muscle reveals extensive phosphorylation of inner membrane protein complexes and enzymes, *Mol Cell Proteomics* **10**, M110.000299.

Zou H, Li Y, Liu X and Wang X. (1999) An APAF-1·cytochrome *c* multimeric complex is a functional apoptosome that activates procaspase-9. *J Biol Chem* **274**, 11549-11556.

Figures

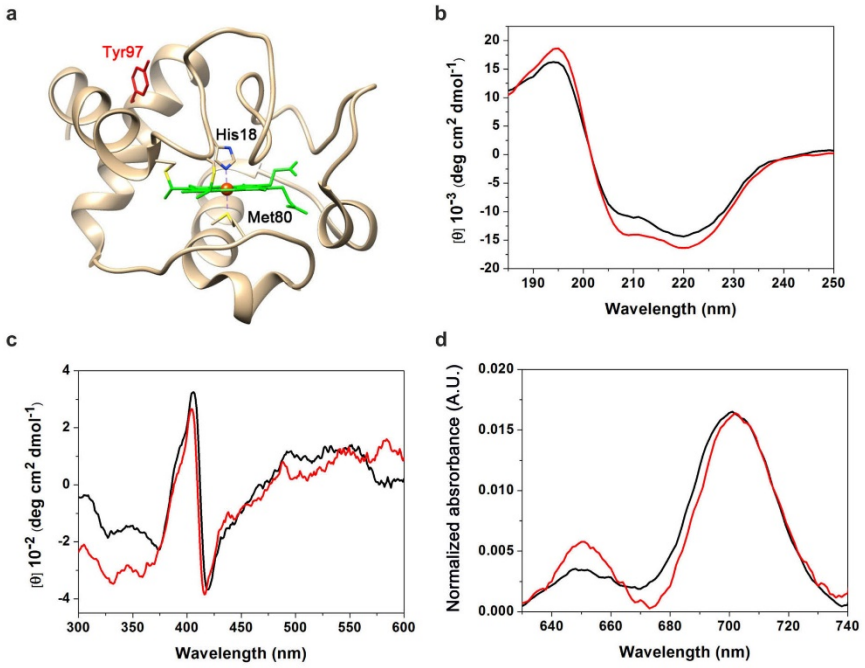

Figure 1. The Y97*p*CMF C*c* mutant. (A) Ribbon representation of the solution NMR structure of human C*c* (PDB code 1J3S). The Tyr97 residue is colored in red. The heme group is in green, with its Fe atom in red. The two axial ligands of heme group (His18 and Met80) are also shown. Far-UV CD (B), visible CD (C) and visible absorption spectra (D) of WT (blue lines) and Y97*p*CMF (red lines) C*c* species are shown. All measurements were recorded on oxidized hemeprotein samples.

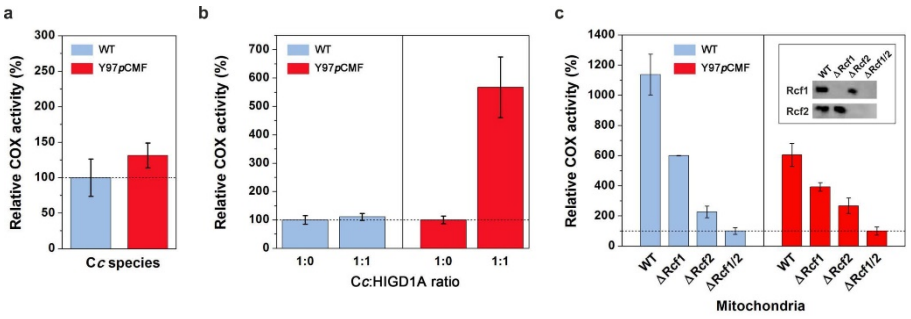

Figure 2. COX activity in the presence of WT or Y97*p*CMF C*c*. (A) Activity of exogenous COX in the presence of WT (blue) or Y97*p*CMF (red) C*c*. COX activity data were normalized with respect to WT C*c* data. (B) Modulation of COX activity by the HIGD1A membrane protein in the presence of either WT (blue) or Y97*p*CMF (red) C*c*. The 1:0 bars represent the exogenous COX activity without HIGD1A. Data were normalized to the C*c*:HIGD1A ratios 1:0 for each C*c* form. (C) Effect of the modulators Rcf1 and Rcf2 on COX activity in yeast mitochondria in the presence of either WT (blue) or Y48*p*CMF (red) C*c*. Endogenous COX activity measurements from WT and Y97*p*CMF C*c* were normalized with respect to those obtained by mitochondria isolated from ΔRcf1/2 yeast strains. *Inset:* Western blots of WT mitochondria (lane 1), Rcf1-deficient mitochondria (lane 2), Rcf2-deficient mitochondria (lane 3) and Rcf1- and Rcf2-deficient mitochondria (lane 4). All mitochondria were purified from yeast grown under hypoxic-like conditions. Data represent the mean ± SD of three individual experiments.

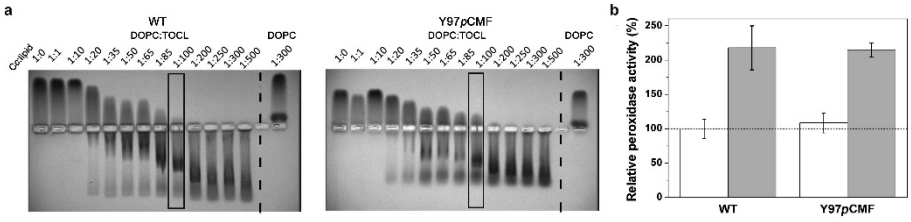

Figure 3. Liposome-binding assays and peroxidase activity of WT and Y97*p*CMF C*c* species. (A) EMSA of the C*c* species in the presence of increasing concentrations of lipids. DOPC:TOCL (4:1) or DOPC liposomes were incubated with WT or Y97*p*CMF C*c* in 25 mM HEPES buffer (pH 7.4). Samples were analyzed on 0.8% agarose gels stained with Coomassie Brilliant Blue. Open squares highlight the C*c*:lipid ratio (1:100 w/w) at which the peroxidase activity was measured. (B) Relative peroxidase activity of C*c* species that was either free (white) or bound to the DOPC:TOCL (4:1) mixture (gray). Data represent the mean ± SD of three individual experiments and are normalized to the results with relative peroxidase activity of free WT C*c*.

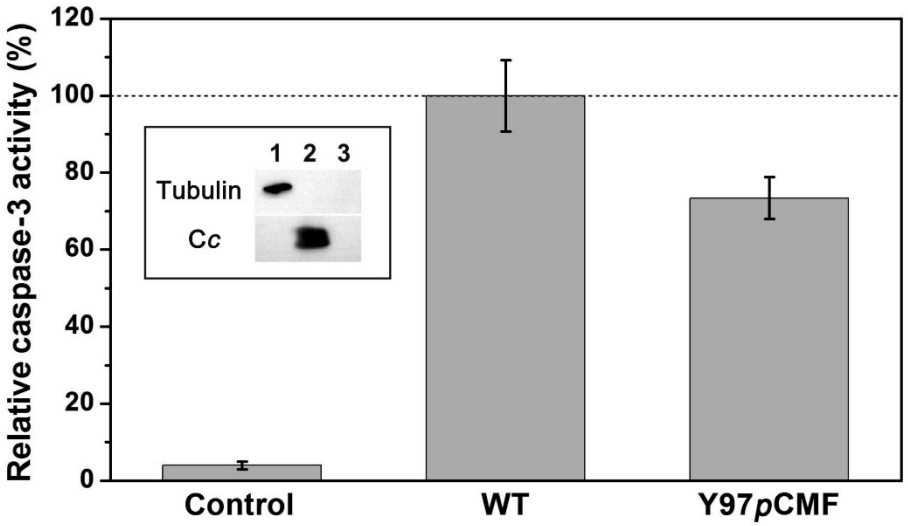

Figure 4. Caspase-3 activity of WT and Y97*p*CMF C*c* species. Relative caspase-3 activities in HEK293 cytoplasmic cell extracts devoid of endogenous C*c* were measured upon addition of exogenous WT or Y97*p*CMF C*c*. Caspase auto-activation, without addition of exogenous C*c*, was also tested (control bar). Data represent the mean ± SD of three individual experiments and are normalized with respect to WT C*c* results. *Inset*: Western blots confirmed the lack of endogenous C*c* in the cytoplasmic cell extracts, by immunoblotting with anti-tubulin (cytosolic marker) and anti-C*c* antibodies. Lane 1, cytoplasmic cell extracts; lane 2, purified C*c*; and lane 3, BSA, as a negative control.

Table 1. Midpoint melting temperature (T_m,°C) of C*c* species

	Far-UV CD (220 nm)	Visible CD (419 nm)	Fluorescence (270 nm)
WT	88.6 ± 1.9	Tm_1: 43.9 ± 2.0 Tm_2: 85.1 ± 2.3	86.3 ± 1.4
Y97*p*CMF	82.2 ± 0.3	76.6 ± 4.9	82.6 ± 1.6

Supporting Information

Cytochrome *c* with a phosphomimetic mutation at position 97 retains its structural features but has modified functionality

Alejandra Guerra-Castellano, Antonio Díaz-Quintana, Sofía M García-Mauriño, Miguel A. De la Rosa and Irene Díaz-Moreno*

Instituto de Investigaciones Químicas (IIQ) – Centro de Investigaciones Científicas Isla de la Cartuja (cicCartuja), Universidad de Sevilla – Consejo Superior de Investigaciones Científicas (CSIC), Avda. Américo Vespucio 49, Sevilla 41092, Spain

Supporting Figures

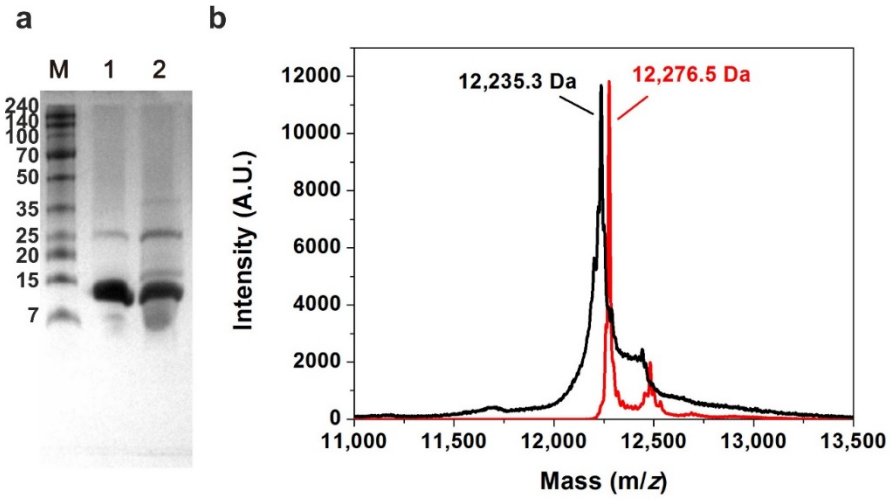

Supporting Figure S1. Protein expression of the Y97*p*CMF C*c* species. (A) SDS-PAGE of purified WT and Y97*p*CMF C*c*. About 10 μg of WT (lane 1) and Y97*p*CMF (lane 2) C*c* proteins was loaded onto a 12% SDS-PAGE gel. M: Molecular weight marker. (B) MALDI-TOF spectra of WT and Y97*p*CMF C*c* species. The molecular mass of WT C*c* (black line) is 12,235.3 Da, whereas that of Y97*p*CMF species (red line) is 12,276.5 Da. The molecular weight of the Y97*p*CMF C*c* is consistent with the substitution of a tyrosine for *p*CMF.

Supporting Materials and methods

Site-directed mutagenesis, protein expression and purification of recombinant proteins

AMBER mutation was performed on a pBTR1 plasmid (pC*c*WT) comprising the CYCS gene-coding for human C*c*, along with the CYC3 gene of the yeast C*c* heme lyase. CYC3 is required for the proper maturation of human C*c*. Notably, the CYCS and CYC3 genes lack topogenic sequences, thereby avoiding the export of the gene products to periplasm, the location of endogenous *c*-type cytochromes in *Escherichia coli* (*E. coli*). Thus, the resulting proteins were located in the bacterial cytoplasm. The selectable marker of pC*c*WT was a cassette that conferred ampicillin resistance to cells containing this plasmid (Olteanu *et al*., 2003). pC*c*WT was mutated by replacing the TAT triplet corresponding to Tyr97 by TAG, the amber stop signal. The primers for PCR were pBTR1 Y97amber fw (5′-CYT CTGATCGCGTAGCTGAAAAAGG-3′) and pBTR1 Y97amber rv (5′-CYT CTTTTTCAGCTACGCGATCAGG-3′). For this purpose, one-step mutagenic PCR with Accusure® DNA Polymerase (Bioline) was used following the manufacturer's instructions. *E. coli* DH5α was used as a host in all cloning procedures. Plasmid DNA was transferred to the *E. coli* strain following a standard heat-shock transformation method. In all cloning procedures involving PCR amplification, the sequences of the amplified fragments were checked with the aid of a commercial sequencing service (StabVida, Caparica, Portugal). The new plasmid, containing the mutated sequences, was named pC*c*Y97AMBER.

The *p*CMF and δ-aminolevulinic acid compounds were added at a final concentration of 1 mM after cell culture induction. IPTG and arabinose were used to induce the cultures at 1 mM and 0.02% final concentrations, respectively. Tryptic digestion and MALDI-TOF analyses confirmed the molecular mass and the tyrosine substitution by *p*CMF. Protein concentration was determined by Vis spectrophotometry, using an extinction coefficient of 29 mM^{-1} cm^{-1} for reduced Y97*p*CMF C*c* (Guerra-Castellano *et al*., 2015).

Caspase activation assays

Human embryonic kidney 293 (HEK 293) cells were cultured in Dulbecco's modified Eagle's medium supplemented with 10% heat-inactivated fetal bovine serum, 2 mM L-glutamine, 100 $U \cdot mL^{-1}$ penicillin and 100 $\mu g \cdot mL^{-1}$ streptomycin, and maintained at 37°C in a humidified 5% CO_2 atmosphere. For subcellular fractioning, cells were treated with trypsin and collected by centrifugation (2,000 g for 5 min). Pellets were washed twice with PBS and once with cell extract buffer (CEB, 20 mM HEPES [pH 7.5], 10 mM KCl, 1.5 mM $MgCl_2$, 1 mM EDTA, 1 mM EGTA, 1 mM dithiothreitol, 100 μM PMSF). After these washes, cells were again collected by centrifugation (2,000 g for 5 min), and pellets were resuspended with two volumes of CEB and transferred to a Dounce homogenizer. The cell solution was incubated for 15 min at 4°C. Subsequently, cells were disrupted by 30 strokes with a tight pestle. Lysates were centrifuged at 15,000 g for 15 min at 4 ºC to remove nuclei and organelles. Protein concentration of the extracts was measured using the Bradford protein assay (Bio-Rad, Hercules, CA). 100 μg of cytoplasmic cell fractions were incubated with 1 μM of reduced C*c* species for 60 min at 37°C in a total volume of 25 μL with 25 mM KCl, 0.2 mM DTT and 0.2 mM dATP. Then, 180 μL of buffer A (10 mM HEPES [pH 7.0] with 50 mM NaCl, 40 mM β-glycerophosphate, 2 mM $MgCl_2$, 5 mM EGTA, 0.1 $mg \cdot mL^{-1}$ bovine serum albumin and 0.1% [w/v] 3-[(3-cholamidopropyl)dimethylammonio]-1-propanesulfonate [CHAPS]) supplemented with 10 μM of acetyl-Asp-Glu-Val-Asp-7-amino-4-methylcoumarin (Ac-DEVD-AMC) (a fluorescent substrate specific for caspases 3/7) was added to the reaction mixture and measured afterwards. The increase in fluorescence resulting from Ac-DEVD-AMC cleavage was determined in a Cary Eclipse (Varian) fluorescence spectrophotometer (optical slits of 5 nm), using an excitation wavelength of 360 nm and an emission wavelength of 460 nm. Experimental data derive from the average of at least three independent experiments.

Supporting references

Guerra-Castellano A, Díaz-Quintana A, Moreno-Beltrán B, López-Prados J, Nieto PM, Meister W, Staffa J, Teixeira M, Hildebrandt P, De la Rosa MA *et al*. (2015) Mimicking tyrosine phosphorylation in human cytochrome *c* by the evolved tRNA synthetase technique. *Chem Eur J* **21**, 15004-15012.

Olteanu A, Patel CN, Dedmon MM, Kennedy S, Linhoff MW, Minder CM, Potts PR, Deshmukh M and Pielak GJ (2003) Stability and apoptotic activity of recombinant human cytochrome *c*. *Biochem Biophys Res Commun* **312**, 733-740.


GOBIERNO
DE ESPAÑA
MINISTERIO
DE ECONOMÍA
Y COMPETITIVIDAD

CSIC
CONSEJO SUPERIOR DE INVESTIGACIONES CIENTÍFICAS

FUNDACION RAMON
ARECES

JUNTA DE ANDALUCIA

cicCartuja

UNIVERSIDAD DE SEVILLA

FEDER